OFFICIAL JOURNAL OF THE SCIENTIFIC SOCIETY OF ANATOMISTS, HISTOLOGISTS, EMBRYOLOGISTS AND TOPOGRAPHIC ANATOMISTS OF UKRAINE

DOI: 10.31393
ISSN 1818-1295
eISSN 2616-6194

ВІСНИК МОРФОЛОГІЇ
REPORTS OF MORPHOLOGY

Vol. 29, №2, 2023

Scientific peer-reviewed journal in the fields of normal and pathological anatomy, histology, cytology and embryology, topographical anatomy and operative surgery, biomedical anthropology, ecology, molecular biology, biology of development

Published since 1993
Periodicity: 4 times a year

Vinnytsya · 2023

ВІСНИК МОРФОЛОГІЇ - REPORTS OF MORPHOLOGY

Founded by the "Scientific Society of Anatomists, Histologists, Embryologists, and Topographic Anatomists of Ukraine" and National Pyrogov Memorial Medical University, Vinnytsya in 1993

Certificate of state registration КВ №9310 from 02.11.2004

Professional scientific publication of Ukraine in the field of medical sciences in specialties 221, 222, 228, 229
According to the list of professional scientific publications of Ukraine, approved by the order of the Ministry of Education and Science of Ukraine No. 1188 of 24.09.2020
Professional scientific publication of Ukraine in the field of biological sciences in specialty 091
According to the list of professional scientific publications of Ukraine, approved by the order of the Ministry of Education and Science of Ukraine No. 1471 of 26.11.2020

Approved by the Academic Council of National Pyrogov Memorial Medical University, Vinnytsya, protocol №8 from 25.05.2023.

Indexation: CrossRef, Index Copernicus, Google Schoolar Metrics, National Library of Ukraine Vernadsky

Address editors and publisher:
Pyrogov Str. 56,
Vinnytsya, Ukraine - 21018
Tel.: +38 (0432) 553959
E-mail: nila@vnmu.edu.ua

Computer page-proofs - Klopotovska L.O.
Translator - Gunas V.I.
Technical support - Levenchuk S.S.
Scientific editing - editorship

The site of the magazine - https://morphology-journal.com

CONTENT

DOI: 10.31393/morphology-journal-2023-29(2)-01 Reports of Morphology, Vol. 29, №2, Pages 5-11

ISSN 1818-1295 eISSN 2616-6194

REPORTS OF MORPHOLOGY

Official Journal of the Scientific Society of Anatomists, Histologists, Embryologists and Topographic Anatomists of Ukraine

journal homepage: https://morphology-journal.com

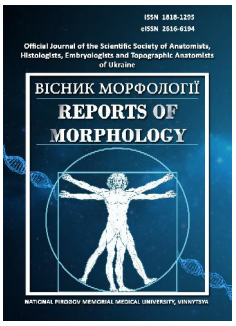

Determination of cephalometric parameters according to the COGS method, related to the profile of the soft tissues of the face depending on the types of faces in Ukrainian young men and young women with an orthognathic bite

Nesterenko Ye. A., Shinkaruk-Dykovytska M. M., Muntian V. L., Prokopenko S. V., Kyrychenko V. I.
National Pirogov Memorial Medical University, Vinnytsia, Ukraine

ARTICLE INFO
Received: 12 January 2023
Accepted: 14 February 2023

UDC: 616.714.1-071.3(477)

CORRESPONDING AUTHOR
e-mail: tikhonova_123@ukr.net
Nesterenko Ye. A.

CONFLICT OF INTEREST
The authors have no conflicts of interest to declare.

FUNDING
Not applicable.

The use of cephalometric analysis of lateral teleroentgenograms allows orthodontists, maxillofacial surgeons and other related specialists to organize a patient's treatment plan. However, for the full application of this method, it is necessary to determine in advance which indicators for it can be considered the norm, and which are already a pathology. The purpose of the study is to establish the peculiarities of cephalometric parameters according to the COGS method, related to the profile of the soft tissues of the face, in Ukrainian young men and young women with an orthognathic bite with different facial types. 46 young men and 72 young women who belonged to the residents of Ukraine of the Caucasian race in three generations and had an orthognathic bite were subjected to cephalometry according to the COGS method of indicators related to the profile of the soft tissues of the face. The face type was determined according to Garson's morphological index. Statistical processing of the obtained results was carried out in the license package "Statistica 6.0" using non-parametric estimation methods. Among Ukrainian young women with different types of faces, the following reliable or trends of differences in teleroentgenometric indicators related to the profile of soft tissues of the face according to the COGS method were established: young women with a very wide face have smaller values of the Gl'-Sn-Pog' angle and the Sn-Gn'/H-Gn' ratio (compared to the middle and narrow faces) and the angle Cotg-Sn-Ls and the distance Ls-(Sn-Pog') (compared to the middle face); young women with a wide face have larger values of the Ls-(Sn-Pog') distance and smaller values of the Stms-I distance (compared to the average face type); women with a narrow face have larger values of the Gl'-Sn distance and the Gl'-Sn/Sn-Me' ratio (compared to the medium face), the Sn-Gn'/H-Gn' ratio (compared to the wide face) and smaller values of the distance Sm-(Li-Pog') (compared to the wide face). Among Ukrainian young men with different types of faces, the following reliable or trends of differences in teleroentgenometric indicators related to the profile of soft tissues of the face according to the COGS method were established: representatives with a very wide face have larger values of the Gl'-Pog' distance (compared to an average face) and smaller values of Sn-Gn'/H-Gn' ratio and Stms-I distance (compared to the average face); representatives with a wide face have larger values of the Sn-Stms/Stmi-Me ratio (compared to the average face) and smaller values of the Gl'-Sn/Sn-Me' ratio (compared to the average face); representatives with a narrow face have larger values of the Gl'-Sn/Sn-Me' ratio (compared to very wide and wide faces). Minor manifestations of sexual dimorphism of cephalometric parameters determined by the COGS method related to the profile of the soft tissues of the face were also established between young men and young women with different facial types.

Keywords: *teleradiography, cephalometry according to the COGS method, cephalometry, indicators of the profile of soft tissues of the face, young men, young women, orthognathic bite, facial types, gender differences.*

Introduction

Bite pathology is one of the most common in orthodontist practice. The results of the examination of almost 2,000 schoolchildren from Saudi Arabia revealed that 1,219 of them have a molar ratio of class I, 326 - class II and 154 -

class III. Among the most common signs of malocclusion, the authors noted bulging teeth, an increase in the space between the teeth, overbite, crossbite, front open bite [2]. Another common pathology is the presence of supernumerary teeth. According to the literature, this pathology occurs in 0.3-0.8 % of people with non-permanent and 1.5-3.5 % of people with permanent dentition. It is also noted that this pathology occurs more often among men than women (the ratio of patients is 2:1, respectively) and more often on the upper jaw than the lower [3]. Manifestations of sexual and age-related dimorphism were also found when studying the prevalence of impacted teeth [16]. Agenesis of teeth occurs in 2.2-10.1 % of people and has a pronounced ethnic heterogeneity of distribution. It is most common among the white population of Australia, where it is found in 6.3 %, the least common among the white population of North America - 3.9 % [5].

The cost of orthodontic treatment varies considerably depending on the method used and the country. In Finland, the average cost of providing orthodontic care to children and adolescents varies between 517-926 euros, in Great Britain it is 36-2941 euros [18].

The prevalence and diversity of orthodontic pathology, the high cost of its treatment have led to the rapid development of instrumental methods for both diagnosis and treatment of this pathology. One of the methods of treatment planning is cephalometric analysis, which became widespread and recognized in the first half of the 20th century [20, 23].

The accuracy of cephalometric analysis of lateral teleroentgenograms is extremely high. Thus, when compared with direct craniometric measurement, the error is less than 1 mm. In general, when comparing the data, the Co-Gn, Go-Me, Co-ANS indicators had higher values in direct craniometry, while all other indicators had lower values [7]. Currently, scientific and technical progress allows, in addition, to use computer tomography data for cephalometric analysis. Nevertheless, the use of traditional lateral teleroentgenograms is almost in no way inferior in terms of informativeness and accuracy to data obtained by analyzing computer tomography data [13].

However, this method requires appropriate clinical research to be implemented in the practice of orthodontists.

The purpose of the study is to establish the peculiarities of cephalometric parameters according to the COGS method, related to the profile of the soft tissues of the face, in Ukrainian young men and young women with an orthognathic bite with different facial types.

Materials and methods

46 young men (YM) (aged 17 to 21) and 72 young women (YW) (aged 16 to 20) underwent a cephalometric study of lateral teleroentgenograms obtained using a Veraviewepocs 3D Morita dental cone-beam tomograph. All young men and women applied to the private dental clinic "Vinintermed" for a diagnostic examination, belonged in three generations to residents of Ukraine of the Caucasian race and had a physiological bite that was as close as possible to the orthognathic one. Committee on Bioethics of National Pirogov Memorial Medical University, Vinnytsya (protocol № 8 From 30.09.2021) found that the studies do not contradict the basic bioethical standards of the Declaration of Helsinki, the Council of Europe Convention on Human Rights and Biomedicine (1977), the relevant WHO regulations and laws of Ukraine.

Cephalometry was performed according to the COGS method [6]. The OnyxCeph³™ software, version 3DPro, from Image Instruments GmbH, Germany (software license №URSQ-1799) was used for this analysis. The face type YM and YW is determined, respectively, by the value of Garson's morphological index [19].

The main cephalometric points and measurements according to the COGS method, including indicators of the structures of the *soft profile* of the face (Fig. 1):

Gl'-Sn-Pog' (facial convexity angle, convex) - the angle formed by the lines Gl'-Sn and Sn-Pog' (°);

Gl'-Sn (maxillary prognathism) - distance from the point Gl' to point Sn, which is measured parallel to the horizontal line HR-Line (mm);

Gl'-Pog' (mandibular prognathism) - distance from the point Gl' to point Pog', which is measured parallel to the horizontal line HR-Line (mm);

Sn-Gn'-C (lower face - neck angle, lower face - throat angle) - the angle formed by the lines Sn-Pog' and Me'-C(H) (°).

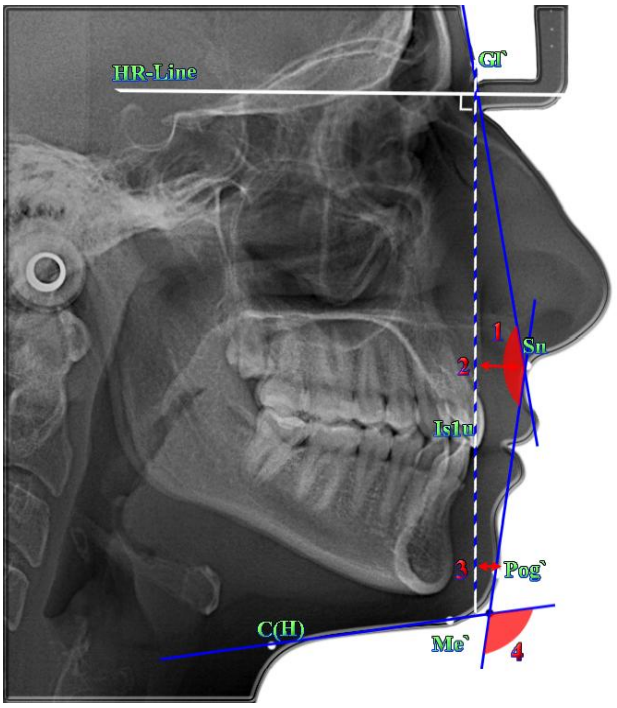

Fig. 1. Indicators of soft facial profile structures using the COGS method, characterizing the shape of the facial profile: 1 - angle **Gl'-Sn-Pog'**; 2 - distance **Gl'-Sn**; 3 - distance **Gl'-Pog'**; 4 - angle **Sn-Gn'-C**.

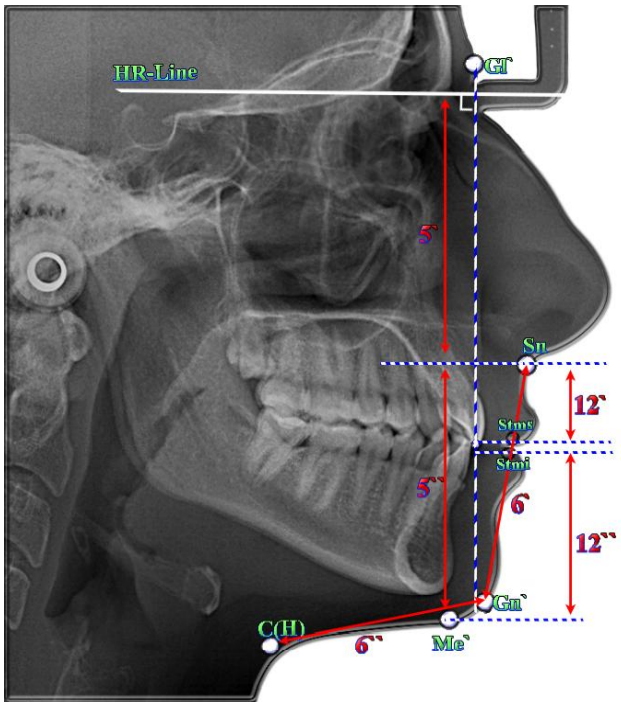

Fig. 2. Calculated indicators of soft facial profile structures using the COGS method, characterizing the *shape of the facial profile*: 5 - ratio **Gl'-Sn(5')/Sn-Me'(5'')**; 6 - ratio **Sn-Gn'(6')/C-Gn'(6'')**; and the position and *shape of the lips*: 12 - ratio **Sn-Stms(12')/Stmi-Me'(12'')**.

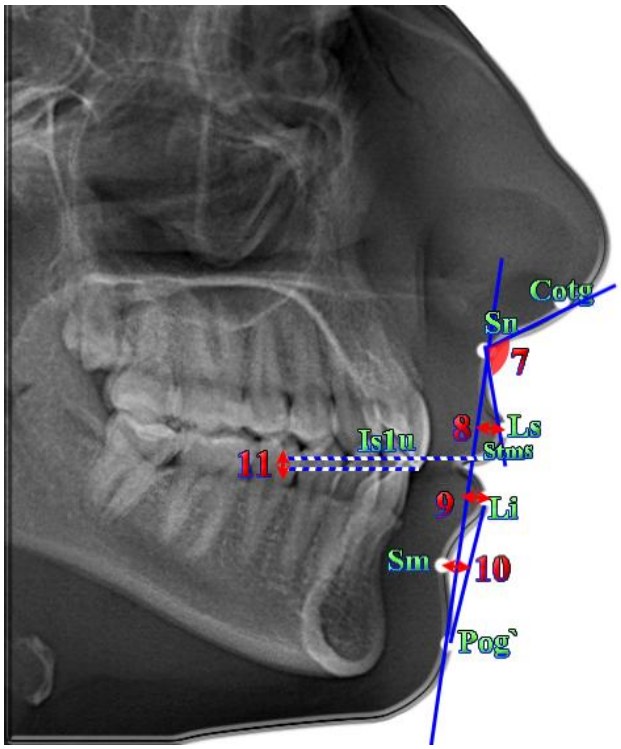

Fig. 3. Indicators of the structures of the soft profile of the face according to the COGS method, characterizing the position and shape of the lips: 7 - angle **Cotg-Sn-Ls**; 8 - distance **Ls-(Sn-Pog')**; 9 - distance **Li-(Sn-Pog')**; 10 - distance **Sm-(Li-Pog')**; 11 - distance **Stms-I**.

Calculated indicators of *soft facial profile* structures according to the COGS method, characterizing the *shape of the facial profile and the position and shape of the lips* (Fig. 2):

Gl'-Sn/Sn-Me' - vertical height ratio, vertical Facial Profile;

Sn-Gn'/C-Gn' - lower vertical height-depth ratio;

Sn-Stms/Stmi-Me' (vertical lip-chin ratio) - ratio of distances Sn-Stms and Stmi-Me' (%).

Indicators of the structures of the *soft profile* of the face according to the COGS method, characterizing the *position and shape of the lips* (Fig. 3):

Cotg-Sn-Ls (nasolabial angle) - the angle formed by the lines Cotg-Sn and Sn-Ls (°);

Ls-(Sn-Pog') (upper lip protrusion) - distance from the point Ls to line Sn-Pog' (mm);

Li-(Sn-Pog') (lower lip protrusion) - distance from the point Li to line Sn-Pog' (mm);

Sm-(Li-Pog') (mentolabial sulcus) - distance from the point Sm to line Li-Pog' (mm);

Stms-I (maxillary incisor exposure) - distance from the point Stms to point Is1u (mm).

Statistical processing of the results was carried out in the license package "Statistica 6.0" using non-parametric estimation methods. Mean values and standard deviation were determined. The significance of the difference in values between independent quantitative values was determined using the Mann-Whitney U-test.

Results

The following distribution of young people according to the value of the Garson index was established: YM - 5 with a very wide face, 22 with a wide face, 11 with an average face, 8 with a narrow face; YW - 25 very wide face, 25 wide face, 10 medium face, 12 narrow face.

Tables 1 and 2 present the results of teleroentgenometric values according to the COGS method, related to the profile of the soft tissues of the face in boys or girls with an orthognathic bite with different types of faces.

Also, between YM and YW with different types of faces, the following gender differences in the indicators related to the profile of soft tissues of the face were established, namely, larger values:

in YM, larger values of the distance Gl'-Sn (with wide, $p<0.05$ and the average face, $p=0.057$), the distance Gl'-Pog' (with the average face, $p=0.062$), as well as the angle Sn-Gn'-C (with wide face $p<0.05$);

in YW larger values are the Sm-(Li-Pog') and Stms-I distances (with a very wide face, $p=0.059$, $p=0.089$), Sm-(Li-Pog') distances (with a wide face, $p<0.001$ and medium face, $p<0.05$), the Cotg-Sn-Ls angle (with a narrow face, $p=0.083$) and the Gl'-Sn/Sn-Me' ratio (with a wide face, $p<0.05$).

Discussion

When comparing Ukrainian YM or YW with an orthognathic bite with different facial types of indicators

Table 1. The value of COGS teleroentgenometric indicators related to the profile of facial soft tissues in YM with different types of face (M±σ).

Indicator	Face type				p_{1-2}	p_{1-3}	p_{1-4}	p_{2-3}	p_{2-4}	p_{3-4}
	Very Wide (1)	Wide (2)	Average (3)	Narrow (4)						
Angle Gl'-Sn-Pog'	12.00±6.44	13.73±6.03	13.09±6.01	9.875±6.468	>0.05	>0.05	>0.05	>0.05	>0.05	>0.05
Distance Gl'-Sn	9.800±5.630	7.367±4.541	6.546±3.804	5.125±3.871	>0.05	>0.05	>0.05	>0.05	>0.05	>0.05
Distance Gl'-Pog'	7.800±8.927	0.591±9.303	-0.546±5.989	-0.125±5.693	>0.05	**=0.070**	>0.05	>0.05	>0.05	>0.05
Ratio Gl'-Sn/Sn-Me'	93.40±13.16	95.77±8.29	100.9±6.5	106.6±7.6	>0.05	>0.05	**=0.057**	**=0.076**	**<0.01**	>0.05
Angle Sn-Gn'-C	110.4±11.1	112.4±8.2	108.6±11.0	109.4±7.1	>0.05	>0.05	>0.05	>0.05	>0.05	>0.05
Ratio Sn-Gn'/H-Gn'	102.6±19.0	120.4±24.6	125.6±24.2	117.0±16.0	>0.05	**=0.070**	>0.05	>0.05	>0.05	>0.05
Angle Cotg-Sn-Ls	104.0±9.4	105.4±10.1	106.9±13.8	99.13±11.54	>0.05	>0.05	>0.05	>0.05	>0.05	>0.05
Distance Ls-(Sn-Pog')	3.200±1.483	3.318±1.912	2.818±1.471	3.750±1.581	>0.05	>0.05	>0.05	>0.05	>0.05	>0.05
Distance Li-(Sn-Pog')	1.400±2.074	2.091±1.974	1.636±1.748	2.375±1.685	>0.05	>0.05	>0.05	>0.05	>0.05	>0.05
Distance Sm-(Li-Pog')	-6.200±1.304	-5.864±0.941	-5.727±0.905	-6.000±1.195	>0.05	>0.05	>0.05	>0.05	>0.05	>0.05
Ratio Sn-Stms/Stmi-Me	46.40±3.85	46.91±6.93	42.91±4.18	44.50±3.46	>0.05	>0.05	>0.05	**=0.079**	>0.05	>0.05
Distance Stms-I	1.600±1.140	2.136±1.754	2.818±1.079	2.625±1.302	>0.05	**=0.089**	>0.05	>0.05	>0.05	>0.05

Notes: here and in the following table, M±σ - sample mean ± standard deviation; $p_{(1-2,\ 1-3,\ 1-4,\ 2-3,\ 2-4,\ 3-4)}$ - the validity of the differences in scores between the corresponding face types in YM or YW.

Table 2. The value of COGS teleroentgenometric indicators related to the profile of facial soft tissues in YW with different facial types (M±σ).

Indicator	Face type				p_{1-2}	p_{1-3}	p_{1-4}	p_{2-3}	p_{2-4}	p_{3-4}
	Very Wide (1)	Wide (2)	Average (3)	Narrow (4)						
Angle Gl'-Sn-Pog'	8.880±5.718	11.56±5.90	13.00±4.62	13.75±4.45	>0.05	**<0.05**	**<0.05**	>0.05	>0.05	>0.05
Distance Gl'-Sn	5.320±3.750	4.440±3.583	3.330±3.057	6.250±3.223	>0.05	>0.05	>0.05	>0.05	>0.05	**<0.05**
Distance Gl'-Pog'	2.000±5.781	-2.240±5.555	-5.300±4.347	-1.417±5.107	>0.05	**<0.01**	>0.05	>0.05	>0.05	**=0.070**
Ratio Gl'-Sn/Sn-Me'	103.4±10.4	102.7±12.4	99.70±10.63	108.2±9.2	>0.05	>0.05	>0.05	>0.05	>0.05	**=0.081**
Angle Sn-Gn'-C	103.2±9.6	104.6±9.2	105.2±7.1	106.5±7.3	>0.05	>0.05	>0.05	>0.05	>0.05	>0.05
Ratio Sn-Gn'/H-Gn'	105.6±17.7	112.8±21.9	123.9±31.2	121.6±11.6	>0.05	**<0.05**	<0.01	>0.05	**=0.077**	>0.05
Angle Cotg-Sn-Ls	104.0±8.5	105.7±8.3	110.8±8.4	108.0±11.7	>0.05	**=0.074**	>0.05	>0.05	>0.05	>0.05
Distance Ls-(Sn-Pog')	2.120±1.641	3.200±1.414	2.200±1.476	3.000±1.859	>0.05	>0.05	>0.05	**=0.086**	>0.05	>0.05
Distance Li-(Sn-Pog')	1.160±2.115	2.080±1.913	2.500±1.509	2.250±1.603	>0.05	**=0.093**	>0.05	>0.05	>0.05	>0.05
Distance Sm-(Li-Pog')	-5.000±1.041	-4.120±2.205	-4.600±0.966	-5.250±1.138	>0.05	>0.05	>0.05	>0.05	**<0.05**	>0.05
Ratio Sn-Stms/Stmi-Me	43.68±3.85	47.60±5.67	45.40±5.36	46.50±4.72	>0.05	>0.05	>0.05	>0.05	>0.05	>0.05
Distance Stms-I	2.600±0.957	2.360±1.411	3.400±1.350	2.667±1.670	>0.05	>0.05	>0.05	**=0.065**	>0.05	>0.05

related to the profile of facial soft tissues according to the COGS method, more pronounced differences are established between YW with different facial types, namely (see Table 2):

in YW with a *very wide face*, significantly smaller values or trends of the Gl'-Sn-Pog' angle and the Sn-Gn'/H-Gn' ratio (compared to the medium and narrow face types), the Cotg-Sn-Ls angle, and Ls-(Sn-Pog') distances (compared to the average face type);

in YW with a *wide face*, there is a tendency for larger Ls-(Sn-Pog') distance values (compared to the average face type) and a tendency for smaller Stms-I distance values (compared to the average face type);

YW with *narrow face* have significantly greater, or trends toward, greater values of Gl'-Sn distance (compared to medium face type), Sn-Gn'/H-Gn' ratio (compared to wide face type), Gl'-Sn/Sn-Me' ratio (compared to the medium face type), as well as a significantly smaller value of the Sm-(Li-Pog') distance (compared to the wide face type).

Between Ukrainian YM with different types of faces, a significantly smaller number of reliable, or trends, indicators of differences related to the profile of the soft tissues of the face according to the COGS method were established (see Table 1):

in YM with a *very wide face*, there is a tendency towards larger values of the Gl'-Pog' distance (compared to the

average face type) and a tendency towards smaller values of the Sn-Gn'/H-Gn' ratio and the Stms-I distance (compared to average face type);

in *broad-faced* YM, a tendency towards higher Sn-Stms/Stmi-Me ratio values (compared to the average face type) and a tendency towards lower values of the Gl'-Sn/Sn-Me' ratio (compared to the average face type);

in YM with a *narrow face*, significantly higher, or a trend towards higher values of the value of the ratio of Gl'-Sn/Sn-Me' (compared to very wide and wide face types).

Minor manifestations of sexual dimorphism of indicators related to the profile of the soft tissues of the face were also established, namely: larger values, in most cases in YM with wide and medium face types - values of Gl'-Sn distances, Gl'-Pog' distances (only with an average face type), Sn-Gn'-C angle (only with a wide face type); and in YW - values of Sm-(Li-Pog') and Stms-I distances (with very wide face type), Sm-(Li-Pog') distance (with wide and medium face types), Cotg-Sn-Ls angle (with narrow face type) and Gl'-Sn/Sn-Me' ratio (with wide face type).

COGS analysis is an excellent tool that is actively used for the assessment and planning of orthodontic treatment, which involves various types of surgical interventions, such as osteotomies, genioplasty and other interventions on the maxillo-dental apparatus [8, 11, 12, 15].

In a previous study, we analyzed COGS cephalometric parameters that characterize the position of individual teeth in boys and girls with an orthognathic bite and different facial types. As a result, pronounced manifestations of sexual dimorphism were found for both linear and angular indicators, namely, YW have higher values of the OP-HP angle, and YM have higher values of most linear dimensions [14].

Indeed, taking into account as many parameters as possible is important when conducting cephalometric studies. Yes, the type of face affects the position of the hyoid bone. Significant differences were found for SNB, ANB and NSH indicators in different groups [1].

It is also important to take into account the age of the examined persons. Bergman R. T. with co-authors [4] investigated changes in the soft tissue structures of the face of persons aged 6 to 18 years using COGS analysis. In particular, with age, such indicators as the lower face height, the thickness of the upper and lower lips, the length of the upper lip and the lower lip-chin length increase, the interlabial gap and the contour of the furrow of the lower jaw decrease. Some indicators do not change with age: the angle of the face profile, the nasolabial angle, the upper and lower protrusion of the lips.

The existence of sex differences in terms of indicators of soft tissue structures of the face is also a proven fact. In men, higher values of the thickness of the soft tissues of the face were found in representatives of the maxillofacial class I, II and III. The most significant differences were found for the index of the furrow of the upper lip ($t=3.772$; $p<0.001$) [17].

And of course, the ethnic component is important. A group of researchers [9] revealed soft tissue cephalometric indicators that are different ($p<0.05$) for Nigerians, Ghanaians and Senegalese: length of the upper lip, Li-esthetic line, angle of the tip of the nose, N-Pr-Pg, Pg-Ls, B-N pogonion and pogonion-mandibular angle. In addition, such indicators as the nasolabial angle, mentolabial angle, depth of the nose, general convexity of the soft tissues of the face are excellent for the mentioned nationalities and Europeans.

Differences were also found for the Japanese population, which, compared to the European population, has higher average face projection values [22].

Regarding the inhabitants of Northern India, differences were also found in the COGS analysis indicators compared to European data, namely, they have lower values of the base of the skull, height of the face, higher values of the chin protrusion and the inclination of the mandibular incisors [10]. A similar kind of study, however, regarding residents of East India revealed the following features compared to European data: higher values of protrusion of the upper and lower lips, prognathia of the lower jaw [21].

Conclusion

1. Between Ukrainian YW (more pronounced) or YM with different types of faces who have an orthognathic bite, reliable or trends of discrepancies of teleroentgenometric indicators related to the profile of soft tissues of the face according to the COGS method were established.

2. Between YM and YW with the corresponding facial types, the manifestations of sexual dimorphism of teleroentgenometric indicators related to the profile of the soft tissues of the face according to the COGS method are slightly expressed.

References

[1] Amayeri, M., Saleh, F., & Saleh, M. (2014). The position of hyoid bone in different facial patterns: A lateral cephalometric study. *European scientific journal,* 10(15), 19-34.

[2] Asiry, M. A., & AlShahrani, I. (2019). Prevalence of malocclusion among school children of Southern Saudi Arabia. *Journal of orthodontic science,* 8, 2. doi: 10.4103/jos.JOS_83_18

[3] Ata-Ali, F., Ata-Ali, J., Penarrocha-Oltra, D., & Penarrocha-Diago, M. (2014). Prevalence, etiology, diagnosis, treatment and complications of supernumerary teeth. *Journal of clinical and experimental dentistry*, 6(4), e414-e418. doi: 10.4317/jced.51499

[4] Bergman, R. T., Waschak, J., Borzabadi-Farahani, A., & Murphy, N. C. (2014). Longitudinal study of cephalometric soft tissue profile traits between the ages of 6 and 18 years. *The Angle Orthodontist,* 84(1), 48-55. doi: 10.2319/041513-291.1

[5] Bozga, A., Stanciu, R. P., & Manuc, D. (2014). A study of prevalence and distribution of tooth agenesis. *Journal of medicine and life,* 7(4), 551-554. PMID: 25713620

[6] Burstone, C. J., James, R. B., Legan, H., Murphy, G. A., & Norton, L. A. (1979). Cephalometrics for orthognathic surgery. *J. Oral. Surg,* 36, 269-277. PMID: 273073

[7] Durao, A. R., Bolstad, N., Pittayapat, P., Lambrichts, I., Ferreira,

A. P., & Jacobs, R. (2014). Accuracy and reliability of 2D cephalometric analysis in orthodontics. *Revista Portuguesa de Estomatologia, Medicina Dentaria e Cirurgia Maxilofacial,* 55(3), 135-141. doi: 10.1016/j.rpemd.2014.05.003

[8] Ekram, S., Arunkumar, K. V., Mowar, A., & Khera, A. (2021). Evaluation of stability and esthetic outcome following rigid fixation of a new sagittal genioplasty technique-A clinical study. *National Journal of Maxillofacial Surgery,* 12(1), 17-24. doi: 10.4103/njms.NJMS_76_20

[9] Fadeju, A. D., Otuyemi, O. D., Ngom, P. I., & Newman-Nartey, M. (2013). A study of cephalometric soft tissue profile among adolescents from the three West African countries of Nigeria, Ghana and Senegal. *Journal of orthodontics,* 40(1), 53-61. doi: 10.1179/1465313312Y.0000000033

[10] Girhe, V., Borle, R., Datey, P., Shirivastav, S., & Bhola, N. (2022). Cephalometric norms for the north Indian population: A systematic review. *National Journal of Maxillofacial Surgery,* 13(2), 172-179. doi: 10.4103/njms.NJMS_34_20

[11] Harshitha, K. R., Srinath, N., Christopher, S., & Kumar, H. N. (2014). Evaluation of soft and hard tissue changes after anterior segmental osteotomy. *Journal of clinical and diagnostic research: JCDR*, 8(9), ZC07-10. doi: 10.7860/JCDR/2014/9409.4791

[12] Lingeshbabu Pawar, A., Basavapattana Shivasubramanya, J., Kolothu Parambil, S., Shivamoga Raju, A., & Debata, A. (2021). Cephalometric Analysis of Hard and Soft Tissue Changes Following Anterior Maxillary Osteotomy Distraction in Cleft Maxillary Hypoplasia. *Journal of Maxillofacial and Oral Surgery,* 20, 680-688. doi: 10.1007/s12663-020-01404-0

[13] Navarro, R. D. L., Oltramari-Navarro, P. V. P., Fernandes, T. M. F., Oliveira, G. F. D., Conti, A. C. D. C. F., Almeida, M. R. D., & Almeida, R. R. D. (2013). Comparison of manual, digital and lateral CBCT cephalometric analyses. *Journal of Applied Oral Science,* 21, 167-176. doi: 10.1590/1678-7757201302326

[14] Nesterenko, Y. A., Shinkaruk-Dykovytska, M. M., Chugu, T. V., Dudik, O. P., & Gunas, V. I. (2022). Determination of cephalometric parameters according to the COGS method, which characterize the position of individual teeth relative to cranial structures depending on the types of faces in Ukrainian young men and young women with an orthognathic bite. *Reports of Morphology,* 28(3), 32-37. doi: 10.31393/morphology-journal-2022-28(3)-05

[15] Parappallil, C. J., Parameswaran, R., Vijayalakshmi, D., & Mavelil, B. G. T. (2018). A comparative evaluation of changes in soft tissues after single-jaw surgery and bimaxillary surgery in skeletal class III Patients. *Journal of Maxillofacial and Oral Surgery,* 17, 538-546. doi: 10.1007/s12663-017-1079-7

[16] Pedro, F. L., Bandeca, M. C., Volpato, L. E., Marques, A. T., Borba, A. M., Musis, C. R., & Borges, A. H. (2014). Prevalence of impacted teeth in a Brazilian subpopulation. *The journal of contemporary dental practice,* 15(2), 209-213. doi: 10.5005/jp-journals-10024-1516

[17] Perovic, T., & Blazej, Z. (2018). Male and female characteristics of facial soft tissue thickness in different orthodontic *malocclusions evaluated by cephalometric radiography. Medical science monitor,* 24, 3415-3424. doi: 10.12659/MSM.907485

[18] Pietila, I., Pietila, T., Svedstrom-Oristo, A. L., Varrela, J., & Alanen, P. (2013). Comparison of treatment costs and outcome in public orthodontic services in Finland. *The European Journal of Orthodontics,* 35(1), 22-28. doi: 10.1093/ejo/cjr053

[19] Proffit, U. R., Fildz, G. U., & Saver, D. M. (2006). *Современная ортодонтия* (перевод с английского Д. С. Персина) [*Modern orthodontics* (translation from English by D. S. Persina)]. M.: МЕДпресс-информ - M.: MEDpress-inform.

[20] Qamruddin, I., & Alam, M. K. (2015). Cephalometry: is it just an orthodontic record?. *Bangladesh Journal of Medical Science,* 14(4), 313-315. doi: 10.3329/bjms.v14i4.23078

[21] Sahoo, N., Mohanty, R., Mohanty, P., Nayak, T., Nanda, S. B., & Garabadu, A. (2016). Cephalometric norms for east Indian population using Burstone Legan analysis. *Journal of International Oral Health*, 8(12), 1076-1081. doi: 10.2047/jioh-08-12-06

[22] Shindoi, J. M., Matsumoto, Y., Sato, Y., Ono, T., & Harada, K. (2013). Soft tissue cephalometric norms for orthognathic and cosmetic surgery. *Journal of Oral and Maxillofacial Surgery,* 71(1), e24-e30. doi: 10.1016/j.joms.2012.08.015

[23] Tanna, N. K., AlMuzaini, A. A., & Mupparapu, M. (2021). Imaging in orthodontics. *Dental Clinics*, 65(3), 623-641. doi: 10.1016/j.cden.2021.02.008

ВИЗНАЧЕННЯ ЦЕФАЛОМЕТРИЧНИХ ПАРАМЕТРІВ ЗА COGS-МЕТОДОМ, ЩО ВІДНОСЯТЬСЯ ДО ПРОФІЛЮ М'ЯКИХ ТКАНИН ОБЛИЧЯ В ЗАЛЕЖНОСТІ ВІД ТИПІВ ОБЛИЧЧЯ В УКРАЇНСЬКИХ ЮНАКІВ І ДІВЧАТ ІЗ ОРТОГНАТИЧНИМ ПРИКУСОМ

Нестеренко Є. А., Шінкарук-Диковицька М. М., Мунтян В. Л., Прокопенко С. В., Кириченко В. І.

Застосування цефалометричного аналізу бокових телерентгенограм дозволяє ортодонтам, зубо-щелепним хірургам та іншим суміжним спеціалістам спланувати план лікування пацієнта. Проте, для повноцінного застосування цього методу необхідно попередньо визначити, які показники для нього можуть вважатися нормою, а що вже є патологією. Мета дослідження - в українських юнаків і дівчат із ортогнатичним прикусом і з різними типами обличчя встановити особливості цефалометричних параметрів за COGS-методом, що відносяться до профілю м'яких тканин обличя. 46 юнакам і 72 дівчатам, які належали у трьох колінах до мешканців України європеоїдної раси та мали ортогнатичний прикус, проведено цефалометрію за COGS-методом показників, що відносяться до профілю м'яких тканин обличя. Тип обличчя визначено відповідно морфологічного індексу Гарсона. Статистичну обробку отриманих результатів проводили в ліцензійному пакеті "Statistica 6.0" з використанням непараметричних методів оцінки. Між українськими дівчатами з різними типами обличчя встановлені наступні достовірні або тенденції відмінностей телерентгеноментричних показників, що відносяться до профілю м'яких тканин обличчя за COGS-методом: у представниць із дуже широким обличчям - менші значення величини кута Gl'-Sn-Pog' і співвідношення Sn-Gn'/H-Gn' (порівняно з середнім і вузьким обличчями) та кута Cotg-Sn-Ls і відстані Ls-(Sn-Pog') (порівняно з середнім обличчям); у представниць із широким обличчям - більші значення величини відстані Ls-(Sn-Pog') та менші значення величини відстані Stms-I (порівняно з середнім типом обличчя); у представниць із вузьким обличчям - більші значення величини відстані Gl'-Sn і співвідношення Gl'-Sn/Sn-Me' (порівняно з середнім обличчям), співвідношення Sn-Gn'/H-Gn' (порівняно з широким обличчям) та менші значення величини відстані Sm-(Li-Pog') (порівняно з широким обличчям). Між українськими юнаками з різними типами обличчя встановлені наступні достовірні або тенденції відмінностей телерентгеноментричних показників, що відносяться до профілю м'яких тканин обличчя за COGS-методом: у представників

із дуже широким обличчям - більші значення величини відстані Gl'-Pog' (порівняно з середнім обличчям) та менші значення величини співвідношення Sn-Gn'/H-Gn' і відстані Stms-I (порівняно з середнім обличчям); у представників із широким обличчям - більші значення величини співвідношення Sn-Stms/Stmi-Me (порівняно з середнім обличчям) та менші значення величини співвідношення Gl'-Sn/Sn-Me' (порівняно з середнім обличчям); у представників із вузьким обличчям - більші значення величини співвідношення Gl'-Sn/Sn-Me' (порівняно з дуже широким і широким обличчям). Між юнаками та дівчатами з різними типами обличчя також встановлені незначні прояви статевого диморфізму цефалометричних параметрів визначених за COGS-методом, що відносяться до профілю м'яких тканин обличчя.

Ключові слова: *телерентгенографія, цефалометрія за COGS-методом, кефалометрія, показники профілю м'яких тканин обличя, юнаки, дівчата, ортогнатичний прикус, типи обличчя, статеві розбіжності.*

DOI: 10.31393/morphology-journal-2023-29(2)-02 Reports of Morphology, Vol. 29, №2, Pages 12-17

ISSN 1818-1295 eISSN 2616-6194

REPORTS OF MORPHOLOGY

Official Journal of the Scientific Society of Anatomists, Histologists, Embryologists and Topographic Anatomists of Ukraine

journal homepage: https://morphology-journal.com

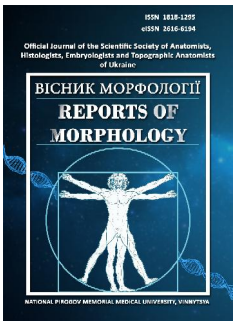

Evaluation of morphological changes of the pancreas in the conditions of experimental action of sodium glutamate

Litvak Yu. V.
Uzhhorod National University, Uzhhorod, Ukraine

ARTICLE INFO
Received: 18 January 2023
Accepted: 21 February 2023

UDC: 611.37.08: 599.23:547.466.64

CORRESPONDING AUTHOR
e-mail: yulia.litvak@uzhnu.edu.ua
Litvak Yu. V.

CONFLICT OF INTEREST
The authors have no conflicts of interest to declare.

FUNDING
Not applicable.

Sodium glutamate, also known as monosodium glutamate (MSG), is frequently used as a flavor enhancer in the food industry. Excessive consumption of sodium glutamate can be harmful to human health. The aim of this study was to investigate the morphological features of the exocrine part of the pancreatic gland under experimental conditions with prolonged exposure to sodium glutamate in the diet. In the experimental study on rats after modeling the action of monosodium glutamate (sodium glutamate) at a dose of 70 mg/kg body weight, the exocrine part of the pancreatic gland was examined using light and electron microscopy after 2, 3, and 5-7 weeks. The experimental study was conducted on white male laboratory rats of reproductive age with an average weight of 168.0±5.0 g. The animals were randomized into two groups: group 1 (n=6) included intact rats and group 2 (n=15) consisted of animals receiving sodium glutamate in their diet. Histological specimens were stained with hematoxylin, eosin, and azan, and electron microscopy samples were stained using the Reynolds method. The results were statistically analyzed using ANOVA analysis with Statistics 20.0.0.2 software. At the early stage of the experiment, changes were observed in the acini with the formation of small clusters comprising 2-3 acinar cells exhibiting increased accumulation of zymogen, which is an early important sign of pancreatitis. Swelling and replacement of the pancreatic gland with connective and adipose tissue progressed over the study period and were accompanied by structural alterations in the pancreatic gland. Round-cell infiltrates appeared in the areas where ducts and vascular bundles were located starting from the 5th week of observation, indicating the development of an inflammatory process. Histopathological changes at the 6th and 7th weeks following prolonged administration of sodium glutamate were similar to the pattern of pancreatitis in humans. Atrophy, degenerative changes, and inflammation were observed in the exocrine part of the pancreatic gland after 6-7 weeks of prolonged oral sodium glutamate intake. Thus, prolonged inclusion of sodium glutamate at a dose of 70 mg/kg body weight in the diet leads to irreversible destructive, degenerative, and inflammatory changes in the pancreatic gland.

Keywords: *histology, experiment, rats, sodium glutamate, pancreas.*

Introduction

Sodium glutamate, monosodium glutamate, is used as a flavor enhancer in the food industry [15, 16, 17]. Glutamate is one of the 20 amino acids involved in nitrogen and energy metabolism and is necessary for supporting many aspects of metabolism. In glutamate metabolism, reactions can have anabolic or catabolic nature depending on the tissue, glutamate dehydrogenase, which is located in mitochondria, and transaminases [3, 4]. The Food and Drug Administration (FDA) has stated that sodium glutamate is safe as a flavor enhancer, but its safety as a food additive remains a subject of debate, considering the significant number of articles discussing its potential negative impact on the body. Despite the widespread use of sodium glutamate in the food industry, some questions regarding its influence on the body remain unanswered.

Currently, over 2500 additives are deliberately added to food products to preserve their properties and extend their shelf life. One of the most widely used additives in Ukraine and worldwide is sodium glutamate [8, 9, 11], which enhances appetite and intensifies the taste of products, leading to increased daily food consumption. Excessive energy in the body can disrupt metabolism, contribute to

overweight, and ultimately lead to obesity and organ system disorders [2, 4, 6, 18]. Therefore, studying the effects of sodium glutamate on various systems and organs of the body, particularly in association with the state of the pancreas, is an important medical and social issue. Consequently, one approach to expanding our understanding of the effects of sodium glutamate is to investigate its pathogenesis using experimental animal models [5, 6, 9, 11]. This approach is an integral part of modern medicine as it allows for the creation of models and provides unlimited possibilities for studying causal factors that contribute to pathogenesis depending on the research objectives. However, in recent years, the use of monosodium glutamate (sodium glutamate) as a food additive to improve taste and prolong shelf life has become widespread worldwide.

The aim of the study is to determine the morphological characteristics of the exocrine part of the pancreas under experimental conditions during prolonged inclusion of sodium glutamate into the diet.

Materials and methods

The article is a fragment of the research work 28A-2019 "Morphological characteristics of internal organs and vascular channel in normal ontogenesis and regularities of their restructuring in obesity and the influence of physical factors on the body" № state registration 0119U102059, 2019-2023.

Animals. The white laboratory rats were randomized into two groups: group 1 (n=6) involved the intact rats; group 2 (n=15) included animals that received MSG. The rats were maintained in the vivarium of Danylo Halytsky Lviv National Medical University. Animals were killed by decapitation under anesthesia 2, 3, 5, 6 and 7 weeks after the start of the experiment, which was necessary for blood collection for biochemical studies. The experiment was carried out according to the provisions of the European Convention for the Protection of Vertebrate Animals Used for Experimental and Other Scientific Purposes (Strasbourg, 1986), Council of Europe Directive 86/609/EEC (1986) and the Law of Ukraine № 3447-IV "On the protection of animals from cruelty".

Monosodium Glutamate Administration. Rats of the experimental group received the food supplement at a dose of 70 mg/kg rat weight daily for 7 weeks [4]. MSG was administered orally through a pipette. The dose of 70 mg chosen by us for a rat corresponds to 700 or 816 mg for a human weighing 60 or 70 kg, respectively [1]. The control group of animals received a standard diet without the addition of sodium glutamate.

Histological study. The pancreatic tissue of rats was fixed in a 10 % neutral formalin solution, dehydrated in ascending concentrations of alcohols (ethanols), cleared in xylene, and embedded in paraffin.

Serial 7-10 microns thick sections were obtained using the Reichert microtome (Austria). The deparaffinised sections were stained with hematoxylin and eosin (combination) and azan. Photomicrographs of the specimens were obtained using a research microscope Olympus BX63 (Germany) with "CellSens Dimension 1.8.1" software.

The focus of the study was the exocrine part of the pancreas. For objectivization, histological slices were analyzed semi-quantitatively (in points) by three parameters: "acini structure", "fat tissue replacement", and "connective tissue replacement".

The following scale was used to estimate pancreatic acini: 0 - normal structure, 1 point - the presence of single small acini, which included 2-4 acinar cells, the main mass made up of large acini (more than 9 cells); 2 points - the presence of 30-50 % small acini, solitary large acini, destructive changes in acinar cells are observed; 3 points - the presence of more than 50 % small acini, blurred cell membrane contour, destruction in acinar cells is observed.

The growth of connective tissue in the pancreas area was evaluated: 1 point - formation around single ducts; 2 points - around 50 % of ducts; 3 points - formation around ducts and between acini.

Replacement of the pancreatic tissue by adipose tissue: 1 point - scattered individual adipocytes; 2 points - approximately 30 % between lobules; 3 points - between lobules and acini.

Electron-microscopic study. Pancreatic fragments were fixed in a buffered 4 % glutaraldehyde solution. Post-fixation was performed in a 1 % solution of osmium tetroxide (OsO_4) followed by dehydration in ethyl alcohol (from 50° to 100°) and acetone. Then, the samples were impregnated with a mixture of epoxy resin and Araldite. Ultrathin sections (50 to 100 nm) were prepared using the LKB 2188 Ultrotom NOVA ultramicrotome (Ukraine), and they were contrasted with uranyl acetate and lead citrate using the Reynolds method. The analysis of the sections was performed using a Tesla BS-500 transmission electron microscope (Sweden).

Statistical analysis. The average values of the obtained digital indicators were presented as $M \pm \sigma$ (M - average value, σ - standard deviation). To determine the differences between the developmental weeks in pancreatic gland disorders, the Kruskal-Wallis test was used. A p-value of less than 0.05 was considered significant.

Results

Study of the effect of sodium glutamate on the pancreatic gland (2 weeks). The exocrine part of the pancreatic gland mainly exhibited normal morphology. In the majority of acinar cells, nuclei were polarly located, uniform in shape and size, and featured 2-4 nucleoli. Electron microscopy revealed increased functional activity of acinar cells, with an elevated content of zymogen granules in the cytoplasm, displacing the nucleus towards the cell membrane. Some mitochondria exhibited elongated shape, with disrupted cristae organization. The Golgi complex showed a reduction

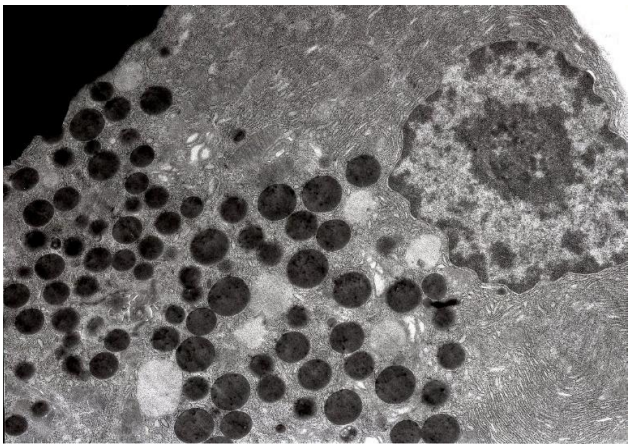

Fig.1. Two weeks after the start of the experiment. Acinar cell. Nucleus with festooned shape and invaginations of the nuclear membrane. Cytoplasm containing zymogen granules of varying sizes. Vacuoles. Contrasted using Reynolds' method. x10000.

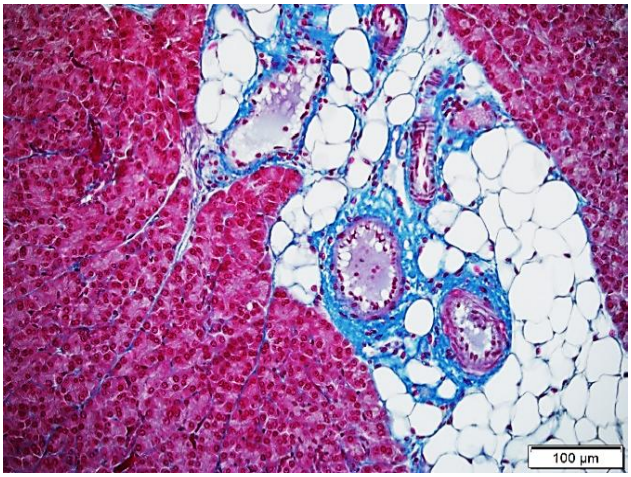

Fig. 2. Fragment of rat pancreas: the proliferation of adipose and connective tissue, acini of different sizes. Five weeks after the start of the experiment. Azan. x100.

with isolated secretory vesicles. The endoplasmic reticulum consisted of tightly arranged narrow tubules, although some regions exhibited dilated and disorganized segments. Autophagic vacuoles were present. In certain acinar cells, nuclei displayed festooned shape with areas of nuclear membrane lysis (Fig. 1).

Due to the functional activity of cells, we observed an overflow of ducts with granular eosinophilic masses. After the azan staining, it was found that the vessels between the slices were dilated and filled with red blood cells. No changes in lymphatic vessels were found.

Study of the effect of sodium glutamate on the pancreas (3 weeks). The pancreatic parenchyma contained acini of various sizes, and the acinar cells had a conical or prismatic shape. As in the previous follow-up period, the cells maintained their polarity but were overflowing with zymogen granules. The intensity of staining of zymogen granules decreased from the periphery of the gland to the center. Additionally, small acini were present in the outer regions of the organ. In certain acini, acinar cells with signs of necrosis were identified.

The intercalated ducts were dilated due to swelling. Ultrastructural analysis of the centroacinar cells revealed isolated cells with pyknotic nuclei, and their mitochondria exhibited a low density of cristae with a disrupted arrangement.

In the interlobular ducts, homogeneous fluid and large peripherally located vacuolar inclusions were observed. Empty intercalated vessels and congested interlobular vessels were also observed.

Study of the effect of sodium glutamate on the pancreas (5 weeks). During this period the increase of destructive changes in the pancreas was revealed. The thickening of its capsule and expansion of connective tissue partitions between lobules and acini, separating them from each other, were revealed. The connective tissue also extended between the acini, separating them from each other.

In addition, the adipose tissue areas were found around the vessels and interlobular ducts (Fig. 2). Structural disorders were also found in acini. Significantly enlarged acini were observed, which consisted of up to 15 acinar cells, as well as small-sized acini with 2-4 cells showing disrupted polarity.

Acini were unevenly distributed throughout the territory of the pancreas. Some acinar cells contained pyknotic nuclei. Swelling of connective tissue between acini was observed throughout the territory, and dilated and congested intercalated blood capillaries were present.

Sometimes, near dilated interlobular ducts, signs of acinar destruction, desquamation, and necrosis of acinar cells were observed, along with foci of fibroblast proliferation. Fragments of acini were located within the loose connective tissue, where round-cell infiltrates (Fig. 3) were identified, indicating the development of an

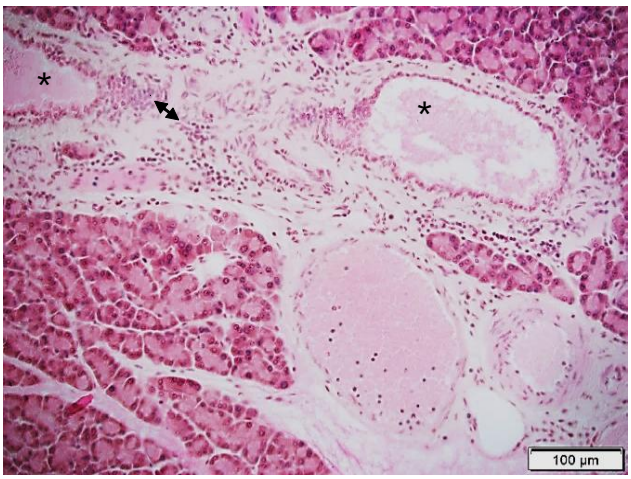

Fig. 3. Fragment of rat pancreas: signs of acinar destruction, desquamation, and necrosis of exocrine pancreatic cells. Foci of round-cell infiltration. ( ). Interlobular ducts with granular pink proteinaceous precipitate (*). Five weeks after the start of the experiment. Hematoxylin-eosin. x100.

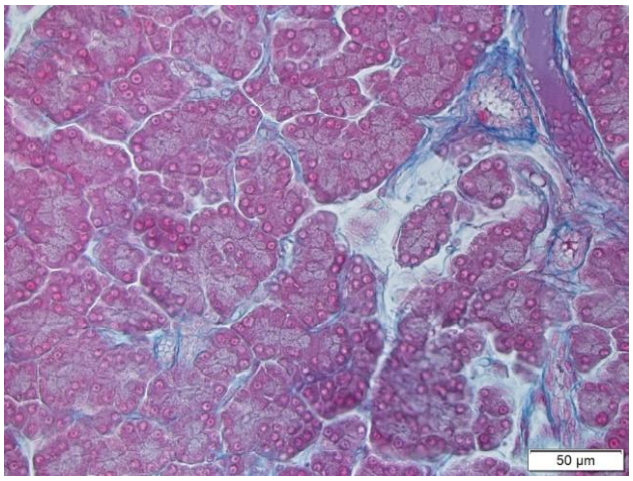

Fig. 4. Fragment of the rat pancreas. Disruption of acinar structure. Connective tissue. Seven weeks after the start of the experiment. Hematoxylin-eosin. x200.

Table 1. The results of the assessment of the structure of the pancreatic gland based on individual histological parameters (M±σ).

Term, week	Histological parameters (points, n=21)		
	Connective tissue	Adipose tissue	Acini
2	1.189±0.091	0.242±0.103	0.380±0.112
3	1.292±0.133	0.331±0.110	0.902±0.139
5	1.948±0.110	0.869±0.162	1.570±0.113
6	2.101±0.102	1.289±0.101	1.673±0.132
7	2.483±0.109	1.813±0.162	2.142±0.130

inflammatory process. Interlobular vessels were dilated, with flattened and elongated endothelium, containing fluid with occasional blood cells. The lumen of interlobular ducts showed a granular pink proteinaceous precipitate.

Study of the effect of sodium glutamate on the pancreas (6 weeks). The histological picture of the pancreatic gland at this stage of the experiment did not differ from that observed after 5 weeks. Its exocrine part consisted of acini of varying sizes and shapes with moderately pronounced signs of acinar cell degeneration. Connective tissue proliferation was detected in interlobular and interacinar areas. Increased areas of adipose tissue were observed around blood vessels and interlobular ducts.

Study of the effect of sodium glutamate on the pancreas (7 weeks). During this period, there was an intensification of degenerative changes in the exocrine portion of the pancreatic gland. Small-sized acini of various shapes were predominantly present, and clear boundaries were not defined between some of them. Acinar cells were disorganized, and pyknotic nuclei were observed in some cells. These cells exhibited mitochondria of varying sizes, with many showing signs of swelling, matrix clarification, and disrupted cristae organization. Some cells exhibited lysed nuclear membranes, reduced components of the Golgi complex, and lysed membranes of the granular endoplasmic reticulum, along with decreased mitochondrial density and cristae disruption. Centroacinar cells also showed signs of degeneration, with a significant portion of their mitochondria being swollen and exhibiting low cristae density.

Connective tissue proliferated between acini, lobules, and in the interstitial spaces. Some acini were separated by layers of connective and adipose tissue (Fig. 4). Marked swelling was observed throughout the organ.

Perivascular edema and signs of hemostasis were observed. Some ducts were dilated.

During the application of the statistical method using the Kruskal-Wallis test (Table 1), a significant difference was found among the study periods of 2, 3, 5-7 weeks in terms of histological indicators: connective tissue (H=30.47, p=0.0001), adipose tissue (H=40.08, p=0.0001), and acini (H=30.92, p=0.0001).

Degenerative changes in the structure of the pancreatic gland increased with the duration of the experiment.

Discussion

The focus of our work was to study the changes in the pancreatic gland of rats after prolonged administration of sodium glutamate. According to the available data [11], in industrially developed countries (Europe and the USA), the average daily consumption of sodium glutamate per person is estimated to be 300-1000 mg/day. In the UK, it ranges from 600-2000 mg/day, and in Nigeria, it is 560-1000 mg/day. However, these values depend on the sodium glutamate content in food products and individual taste preferences. For our study, we chose a dosage of 70 mg/kg of sodium glutamate (equivalent to 600 or 816 mg per day for an average-weight person of 60 or 70 kg) based on preclinical animal studies that demonstrated toxic effects on the heart, liver, kidneys, and other systems at high concentrations of sodium glutamate (0.5-6 g) [6]. To draw accurate conclusions regarding the use of lower concentrations of sodium glutamate, further research is necessary.

Using histological methods in rat experiments, it was found that the administration of sodium glutamate at doses of 40 and 80 mg/kg for 28 days resulted in damage to neurons in the brain, hippocampus, and cerebellum [12], administration for 42 days led to degenerative and atrophic changes in the liver [4], while at a dosage of 15 and 30 mg/kg, the structure of the pancreatic gland in rats was disrupted after 30 days [8]. This may be due to the temporary high concentration of sodium glutamate in the plasma, which exhibits its toxic effects, particularly with chronic use [13]. The localization of lysosomal hydrolases with digestive enzymes also leads to necrosis and apoptosis of acinar cells, which may be a mechanism for zymogen activation and its detrimental effects on cells. Another mechanism could be the damage to acinar cell organelles, accompanied by the activation of redox signaling (reactive oxygen species), which is an important early event in the pathogenesis of pancreatitis [13]. Localization of lysosomal

hydrolases with digestive enzymes also leads to necrosis and apoptosis of acinar cells, which can be a mechanism for the activation of zymogen and its destructive impact on cells. Another mechanism can be the damage to acinar cell organelles accompanied by the activation of redox signaling (reactive oxygen species), which is an important early sign in the pathogenesis of pancreatitis [13]. Additionally, during the early stage of pancreatitis, acinar cells synthesize and release cytokines and chemokines, which attract and activate inflammatory cells [13, 14]. In our study, with increasing duration of the experimental period, we observed progressive edema, replacement of pancreatic parenchyma with connective and adipose tissues, and deviations in the histological structure of the acini in the pancreatic gland. Our findings are consistent with other studies where obesity in animals was induced by high-fat diets, resulting in pancreatic steatosis, inflammation, and fibrosis [1, 7, 9, 10].

Thus, the experimental modeling of sodium glutamate and subsequent investigation of the structure of the pancreatic gland allowed us to identify the main pathomorphological changes. It was established that the damage to acinar cells triggers a complex mechanism that disrupts the exocrine component of the pancreatic gland.

In the future, we plan to study the metabolic changes in the organism and their correlation with histological alterations during the modeling of pancreatic gland obesity in animals using sodium glutamate.

Conclusion

1. Electron microscopy examination after 2 weeks from the beginning of the experiment revealed early disruptions in the organization of acinar cells, increased presence of zymogen granules, and mild changes in their membranous organelles.

2. During the 5-7 week study period, the exocrine part of the pancreatic gland exhibited the appearance of infiltrates, indicating the development of a local inflammatory process, along with the formation of connective and adipose tissue in the interstitial space and parenchyma. These changes can be classified as pancreatitis.

References

[1] Boonnate, P., Waraasawapati, S., Hipkaeo, W., Pethlert, S., Sharma, A., Selmi, C., … & Cha'on, U. (2015). Monosodium Glutamate Dietary Consumption Decreases Pancreatic β-Cell Mass in Adult Wistar Rats. *PloS One*, 10(6), e0131595. doi: 10.1371/journal.pone.0131595

[2] Chuffa, L. G. A., Lupi, L. A., Cucielo, M. S., Silveira, H. S., Reiter, R. J., & Seiva, F. R. F. (2019). Melatonin Promotes Uterine and Placental Health: Potential Molecular Mechanisms. *International Journal of Molecular Sciences,* 21(1), 300. doi: 10.3390/ijms21010300

[3] Cynober, L., Fernstrom, J. D., Koletzko, B., Rietjens, I. M. C. M., Roberts, A., Tennant, D. R., … & Vorhees, C. V. (2018). Introduction and Summary of the 2018 Dietary Glutamate Workshop. *Annals of Nutrition & Metabolism*, 73(5), 1-4. doi: 10.1159/000494775

[4] Eweka, A., Igbigbi, P., & Ucheya, R. (2011). Histochemical studies of the effects of monosodium glutamate on the liver of adult wistar rats. *Ann. Med. Health. Sci. Res.*, 1(1), 21-29.

[5] Hidayati, L., Widodo, A. D. W., & Hidayati, B. (2020). Animal Models with Metabolic Syndrome Markers Induced by High Fat Diet and Fructose. *Medical Laboratory Technology Journal,* 6(1), 13-20. doi: 10.31964/mltj.v6i1.266

[6] Hordiienko L. P. (2017). Effect of monosodium glutamate on body weight and development of obesity (literature review). *Herald of Problems of Biology and Medicine,* 3(4), 33-37. doi: 10.29254/2077-4214-2017-4-3-141-33-37

[7] Katsuda, Y., Ohta, T., Miyajima, K., Kemmochi, Y., Sasase, T., Tong, B., … & Yamada, T. (2014). Diabetic complications in obese type 2 diabetic rat models. *Experimental Animals,* 63(2), 121-132. doi: 10.1538/expanim.63.121

[8] Leschenko, I. V., Shevchuk, V. G., Falalyeyeva, T. M., & Beregova, T. V. (2012). Вплив тривалого введення глутамату натрію на структуру підшлункової залози щурів [The influence of long-term monosodium glutamate feeding on the structure of rats pancreas]. *Фізіологічний журнал - Physiological Journal,* 58(2), 59-65. doi: 10.15407/fz58.02.059

[9] Maluly, H. D. B., Arisseto-Bragotto, A. P., & Reyes, F. G. R. (2017). Monosodium glutamate as a tool to reduce sodium in foodstuffs: Technological and safety aspects. *Food Science & Nutrition*, 5(6), 1039-1048. doi: 10.1002/fsn3.499

[10] Nahok, K., Phetcharaburanin, J., Li, J. V., Silsirivanit, A., Thanan, R., Boonnate, P., … & Cha'on, U. (2021). Monosodium Glutamate Induces Changes in Hepatic and Renal Metabolic Profiles and Gut Microbiome of Wistar Rats. *Nutrients,* 13(6), 1865. doi: 10.3390/nu13061865

[11] Nnadozie, J. O., Chijioke, U. O., Okafor, O. C., Olusina, D. B., Oli, A. N., Nwonu, P. C., ... & Chijioke, C. P. (2019). Chronic toxicity of low dose monosodium glutamate in albino Wistar rats. *BMC Res. Notes.*, 12(1), 593. doi: 10.1186/s13104-019-4611-7

[12] Onaolapo, O. J., Onaolapo, A. Y., Akanmu, M. A, & Gbola, O. (2016). Evidence of alterations in brain structure and antioxidant status following 'low-dose' monosodium glutamate ingestion. *Pathophysiology,* 23(3), 147-156. doi: 10.1016/j.pathophys.2016.05.001

[13] P?rez, S., Pereda, J., Sabater, L., & Sastre, J. (2015). Redox signaling in acute pancreatitis. *Redox Biology,* (5), 1-14. doi: 10.1016/j.redox.2015.01.014

[14] Rebours, V., Garteiser, P., Ribeiro-Parenti, L., Cavin, J. B., Doblas, S., Page, G., … & Couvelard, A. (2018). Obesity-induced pancreatopathy in rats is reversible after bariatric surgery. *Sci. Rep.,* 8(1), 16295. doi: 10.1038/s41598-018-34515-3

[15] Shi, Z., Luscombe-Marsh, N. D., Wittert, G. A., Yuan, B., Dai, Y., Pan, X., & Taylor, A. W. (2010). Monosodium glutamate is not associated with obesity or a greater prevalence of weight gain over 5 years: findings from the Jiangsu Nutrition Study of Chinese adults. *The British Journal of Nutrition*, 104(3), 457-463. doi: 10.1017/S0007114510000760

[16] Thu Hien, V. T., Thi Lam, N., Cong Khan, N., Wakita, A., & Yamamoto, S. (2013). Monosodium glutamate is not associated with overweight in Vietnamese adults. *Public Health Nutrition,* 16(5), 922-927. doi: 10.1017/S1368980012003552

[17] Walker, R., & Lupien, J. R. (2000). The safety evaluation of monosodium glutamate. *The Journal of Nutrition*, 130 (4S Suppl), 1049S-52S. doi: 10.1093/jn/130.4.1049S

[18] Zanfirescu, A., Cristea, A. N., Nitulescu, G. M., Velescu, B. S., & Gradinaru, D. (2017). Chronic Monosodium Glutamate Administration Induced Hyperalgesia in Mice. *Nutrients,* 10(1), 1. doi: 10.3390/nu10010001

ОЦІНКА МОРФОЛОГІЧНИХ ЗМІН ПІДШЛУНКОВОЇ ЗАЛОЗИ В УМОВАХ ЕКСПЕРИМЕНТАЛЬНОЇ ДІЇ ГЛУТАМАТУ НАТРІЮ

Литвак Ю. В.

В якості підсилювачу смаку в харчовій промисловості часто використовують натрієву сіль глутамінової кислоти або глутамат натрію. Надмірне споживання глутамату натрію може завдати шкоди здоров'ю людини. Мета роботи: встановити морфологічні особливості екзокринної частини підшлункової залози в умовах експерименту при тривалому введенні в раціон глутамату натрію. В експериментальному дослідженні на щурах після моделювання дії мононатрієвої солі глутамінової кислоти (глутамату натрію) 70 мг/кг маси тіла досліджували екзокринну частину підшлункової залози через 2, 3, 5-7 тижнів методами світлової та електронної мікроскопії. Експериментальне дослідження проводили на білих лабораторних щурах-самцях репродуктивного віку із середньою масою 168,0±5,0 г. Тварини були рандомізовані на дві групи: група 1 (n=6) включала інтактних щурів; до групи 2 (n=15) увійшли тварини, які отримували глутамат натрію у раціон. Отримані гістологічні препарати зафарбовували гематоксиліном, еозином та азаном, електронно-мікроскопічні - за Рейнольдсом. Результати оброблені статистично програмою Statistics 20.0.0.2 з використанням аналізу ANOVA. На ранній стадії розвитку експерименту були виявлені зміни в ацинусах з утворенням малих форм з 2-3 ацинарними клітинами з підвищеним в них накопиченням зимогену, котрий є ранньою важливою ознакою панкреатиту. Набряк, заміщення підшлункової залози сполучною і жировою тканинами прогресує з термінами дослідження і супроводжується порушенням будови підшлункової залози. Ми спостерігали появу круглоклітинних інфільтратів в ділянках розташування проток і судинних пучків, починаючи з 5-го тижня спостереження, що відображає розвиток запального процесу. Гістопатологічні зміни на 6-7-му тижні після тривалого введення глутамату натрію аналогічні картині панкреатиту у людини. Через 6-7 тижнів після тривалого введення глутамату натрію per os в екзокринній частині підшлункової залози спостерігалися атрофічні, дегенеративні та запальні зміни. Таким чином, тривалий прийом у раціон глутамату натрію у дозі 70 мг/кг маси тіла призводить до незворотніх деструктивних, дегенеративних та запальних змін підшлункової залози.

Ключові слова: *гістологія, експеримент, щури, глутамат натрію, підшлункова залоза.*

DOI: 10.31393/morphology-journal-2023-29(2)-03 Reports of Morphology, Vol. 29, №2, Pages 18-25

ISSN 1818-1295 eISSN 2616-6194

REPORTS OF MORPHOLOGY

Official Journal of the Scientific Society of Anatomists, Histologists, Embryologists and Topographic Anatomists of Ukraine

journal homepage: https://morphology-journal.com

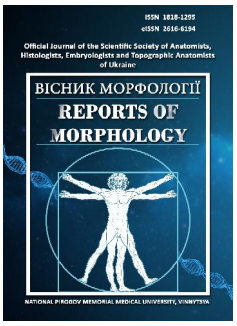

Serum myostatin and irisin as predictive biomarkers of sarcopenia, malnutrition and mortality in patients with decompensated liver cirrhosis

Motsiuk V. M., Pentiuk N. O.
National Pirogov Memorial Medical University, Vinnytsya, Ukraine

ARTICLE INFO
Received: 31 January 2023
Accepted: 24 February 2023

UDC: 616.74:616.36-004:621.3.088.6

CORRESPONDING AUTHOR
e-mail: pentiuk.na@gmail.com
Pentiuk N. O.

CONFLICT OF INTEREST
The authors have no conflicts of interest to declare.

FUNDING
Not applicable.

Malnutrition and sarcopenia are nowadays considered the main complications of liver cirrhosis (LC). Myokines are signal peptides synthesized in muscles that regulate muscle strength and mass and mediate crosstalk between skeletal muscles and other organs. It is unknown whether circulating myokines can be used as biomarkers of malnutrition and sarcopenia and have independent prognostic value in LC. The purpose of the study was to assess the relationship of serum levels of myokines myostatin and irisin with nutritional status, skeletal muscle status, and survival in decompensated LC patients. 74 patients (55.30±11.40 years) were involved in the prospective study. Nutritional status was assessed using the Patient-Generated Subjective Global Assessment, and skeletal muscle mass was assessed using the Skeletal Muscle Index. The concentration of serum myostatin and irisin was determined by enzyme immunoassay. Statistical data processing was performed in SPSS22 (© SPSS Inc.). It was established that the concentration of serum myostatin and irisin is not related to the LC severity according to the Child-Turcotte-Pugh, Model For End-Stage Liver Disease, and the grade of ascites. Patients with overt encephalopathy have higher myostatin levels. Patients with severe hypoalbuminemia have higher serum myostatin and lower serum irisin levels. The development of malnutrition and sarcopenia in decompensated LC patients is associated with increased serum myostatin concentration and decreased serum irisin concentration. Serum myostatin level can predict sarcopenia (AUC 0.834 in males and 0.827 in females, p<0.01). Serum irisin level can predict severe malnutrition (AUC 0.830, p<0.001). The mortality of patients with high myostatin levels (above 5.25 ng/ml in males and 3.55 ng/ml in females) and low irisin levels (less than 1.72 ng/ml) is significantly higher. In conclusion, the circulating myokines levels may be useful in the assessment of nutritional and skeletal muscle status, and prediction of mortality in LC patients.

Keywords: *myostatin, irisin, malnutrition, sarcopenia, survival, liver cirrhosis.*

Introduction

Malnutrition and its clinical consequence, sarcopenia, are today considered the main complications of liver cirrhosis (LC) [34, 35]. Recent data indicate that malnutrition and loss of skeletal muscle mass are independent factors of poor prognosis and are associated with a decreased quality of life, higher risk of decompensation and acute-on-chronic liver failure [5, 18, 20, 28]. Sarcopenic patients face a higher risk of developing hepatic encephalopathy, infectious complications, and sepsis [13, 16, 23]. It has been demonstrated that malnutrition and sarcopenia are associated with an extended stay at the hospital, increased treatment cost and reduced survival [4, 5, 10, 20].

Currently, there are no effective approaches for the treatment of malnutrition and sarcopenia in LC. Liver transplantation ameliorates portal hypertension and liver failure but does not eliminate nutritional and muscle failure in most cases [7, 31, 36, 37]. The identification of potential therapeutic targets is complicated by the insufficient understanding of the pathophysiology, the lack of assessment tools, and sensitive biomarkers.

In recent years, it has grown evident that skeletal muscles have the properties of an endocrine organ. Muscles synthesize and secrete several signal peptides, myokines, which act in an autocrine, paracrine, or endocrine manner.

Myokines regulate many physiological processes, including energy expenditure, carbohydrate and lipid metabolism, liver functions, insulin sensitivity, and inflammation [15, 32]. Myokines synthesized during physical activity regulate muscle strength and mass and mediate crosstalk between skeletal muscles and other organs, including bones, adipose tissue, blood vessels, the liver, brain [33]. It is assumed that abnormal formation and secretion of myokines can negatively affect skeletal muscle status. However, data on the role of myokines in malnutrition and sarcopenia in LC are limited. Recent research shows that age-related sarcopenia is associated with a decreased level of myokines which promote the growth and differentiation of skeletal muscles (apelin, decorin, insulin-like growth factor-1, irisin), and an increased level of myostatin which promotes catabolism and skeletal muscles atrophy [15]. It is unknown whether circulating myokines can be used as biomarkers of malnutrition and sarcopenia and have independent prognostic value in LC patients.

The purpose of the study was to assess the relationship of serum myokines myostatin and irisin with nutritional status, skeletal muscle status, and survival in decompensated LC patients.

Materials and methods

Between 2019 and 2021, 74 patients, including 29 females and 45 males (mean age 55.30±11.40), hospitalized in Vinnytsia City Clinical Hospital No. 1 due to LC decompensation, were involved in the prospective study.

All subjects were informed about the purpose of the study and provided their written consent. The *Committee on Bioethics* of National Pirogov Memorial Medical University, Vinnytsia (*Protocol No 8 from 17.10.2019*) found that the study does not contradict the basic bioethical standards of the Declaration of Helsinki, the Council of Europe Convention on Human Rights and Biomedicine (1977), the relevant WHO regulations and Ukrainian law. Viral (HBV, HCV) etiology of LC was confirmed in 8, alcohol-related - in 49, and viral-alcohol-related - in 17 patients. All patients met the criteria of decompensated LC according to the classification of G. D'Amico et al. (2018) [6]. Stage B according to the Child-Turcotte-Pugh (CTP) score was diagnosed in 24 patients, and Stage C - in 50 patients. The Model For End-Stage Liver Disease (MELD) score was 28.50±7.04 and fluctuated between 15.4 to 38.9 points. Acute LC decompensation was the cause of hospitalization in 39 patients. None of the patients had clinical signs of acute infection, gastrointestinal bleeding, or acute-on-chronic liver failure. The follow-up period lasted until June 2022. During this time, 42 patients died due to LC complications.

The nutritional status of patients was assessed using the Patient-Generated Subjective Global Assessment (PG-SGA) [11, 25]. The PG-SGA evaluates the patient's weight loss, food intake and symptoms that affect food intake, activity and functioning, metabolic needs, and data from the patient's nutrition-oriented examination. The overall PG-SGA score allocates patients to three categories: well-nourished (Stage A), moderate/suspected malnutrition (Stage B), and severely malnourished (Stage C). The study used a translated and cross-culturally adapted Ukrainian version of the PG-SGA [27] based on the original v4.3.20 PG-SGA (available at http://pt-global.org).

Skeletal muscle mass was assessed using computed tomography. The cross-sectional skeletal muscle area at the L3 level was visualized and calculated in the range -29 +150 HU using NIH ImageJ version 1.52a software. The result was normalized to height, and the skeletal muscle index (SMI) was calculated [17, 28]. Reference values of SMI for the Ukrainian population were >52.2 and >39.3 cm^2/m^2, in males and females, respectively [22]. A decrease in SMI was considered sarcopenia.

The content of serum myostatin and irisin was determined by enzyme immunoassay using MyBioSource Inc. commercial test systems (San Diego, USA), Cat. No. MBS9716424, MBS2903725. Blood sampling was performed in the morning after a night's rest in the fasting state. Patients were advised to avoid physical exertion for 12 hours before blood sample collection because physical exertion affects the synthesis of myokines.

Statistical data was processed in the SPSS22 software package (©SPSS Inc). The mean, standard deviation, and standard error of the mean were calculated. The parametric Student's t-test and the non-parametric Mann-Whitney U-test were used to assess the intergroup difference, while Spearman rank and Pearson's correlation analysis were used to determine the relationships between values. The prognostic value of myostatin and irisin was analyzed in ROC analysis. Analysis of patient survival was performed using the Kaplan-Meier method. The comparison of survival curves was performed using the Logrank test. Results are demonstrated as M±SD and Me (P_{25} - P_{75}). The difference was considered significant at $p<0.05$.

Results

The percentile distribution of the serum myostatin and irisin is presented in the Table 1. The level of myostatin in males was higher than in females, 5.25 (3.31 - 7.24) versus 3.55 (1.95 - 6.40) ng/ml, respectively. The level of irisin in males and females was not significantly different, 1.52 (1.10 - 3.63) versus 2.04 (1.11 - 3.63) ng/ml, respectively. Myostatin inversely correlated with irisin ($r = -0.407$, $p = 0.000$).

Serum myokines were weakly associated with the severity of the underlying disease (Table 2). Myostatin was significantly higher and irisin was significantly lower in CTP class C compared to class B patients. However, the levels of myostatin and irisin did not correlate with the numeric CTP ($r = 0.228$, -0.268, respectively, $p>0.05$). Patients with overt encephalopathy had higher myostatin levels. Patients with severe hypoalbuminemia had higher myostatin levels and lower irisin levels. Myostatin and irisin weakly correlated with the serum albumin ($r = -0.307$, 0.397,

Table 1. Serum myostatin and irisin levels in patients with decompensated LC.

Variables	M±m	s	Me	P_5	P_{10}	P_{25}	P_{75}	P_{90}	P_{95}
Myostatin, ng/ml	Total LC patients, n=74								
	4.621±0.302	2.60	4.51	0.88	1.15	2.34	6.39	8.11	9.72
	Males, n=45								
	5.251±0.406	2.72	5.25	0.76	1.42	3.31	7.24	9.23	10.20
	Females, n=29								
	3.653±0.368	1.99	3.55*	0.85	0.98	1.95	5.19	6.40	6.94
Irisin, ng/ml	Total LC patients, n=74								
	2.302±0.192	1.65	1.72	0.39	0.66	1.11	3.22	5.24	6.13
	Males, n=45								
	2.142±0.241	1.61	1.52	0.29	0.68	1.10	2.73	5.27	5.94
	Females, n=29								
	2.518±0.323	1.71	2.04	0.34	0.46	1.11	3.63	5.25	6.34

Note: * - p<0.05 comparatively to male patients.

Table 2. Serum myostatin and irisin levels according to LC severity, Me (P_{25}-P_{75}).

Variables		Myostatin, ng/ml	Irisin, ng/ml
CTP	Class B, n=24	2.96 (1.33-6.29)	2.93 (1.20-4.43)
	Class C, n=50	5.15 (3.31-6.46) p=0.036	1.47 (1.07-2.23) p=0.036
MELD	≥29, n=39	4.13 (1.46-6.52)	2.11 (1.24-4.11)
	<29, n=35	4.99 (3.38-6.30) p=0.200	1.45 (0.98-2.53) p=0.070
Ascites	0-1 degree, n=48	4.55 (2.08-6.36)	2.10 (1.19-4.09)
	2-3 degrees, n=26	4.51 (2.88-6.43) p=0.760	1.37 (1.07-2.15) p=0.083
Hepatic encephalopathy	0-1 stage, n=28	3.22 (1.38-5.79)	2.57 (1.20-4.38)
	2-3 stage, n=46	5.19 (3.36-6.71) p=0.008	1.53 (1.05-2.23) p=0.071
Albumin	≥30 g/l, n=37	3.99 (1.53-6.18)	2.24 (1.27-4.07)
	<30 g/l, n=37	5.22 (3.30-6.95) p=0.031	1.45 (0.97-2.18) p=0.016

respectively, p<0.05), but did not correlate with the MELD (r = 0.152, -0.223, respectively, p>0.05) and the severity of ascites (r = -0.036, -0.088, respectively, p>0.05).

Our data shows that malnutrition and loss of skeletal muscle mass are closely associated with elevated serum myostatin and decreased serum irisin levels (Table 3). The content of myostatin in severely malnourished patients was significantly higher than in patients with moderate/ suspected malnutrition or well-nourished patients. Median myostatin concentrations in sarcopenic males and females were more than three times higher than in patients with normal skeletal muscle mass. Myostatin weakly correlated with the numerical PG-SGA score (r = 0.394, p<0.005) and moderately correlated with the radiological SMI (r = -0.644 for males, -0.608 for females, respectively, p<0.005). Serum irisin was more dependent on nutritional status than on skeletal muscle status. The concentration of this myokine significantly decreased with the progress of malnutrition severity and moderately correlated with the numerical PG-SGA score (r = -0.615, p<0.005). Irisin concentrations in sarcopenic males and females were more than half as low as in nonsarcopenic patients. There was a moderate correlation between irisin and SMI in males and females (r = 0.430, 0.408, respectively, p<0.005).

The ROC analysis (Table 4) established that the level of serum myostatin can predict sarcopenia in patients with decompensated LC (AUC 0.834 and 0.827 for males and females, p<0.01, respectively). The cut-offs of myostatin concentration for predicting low SMI in males and females were 4.20 ng/ml (Se 77.1 %, Sp 80.0 %) and 2.72 ng/ml

Table 3. Serum myostatin and irisin levels according to nutritional status and muscle mass in patients with decompensated LC, Me (P_{25} - P_{75}).

Variables			Myostatin, ng/ml	Irisin, ng/ml
PG-SGA	1	*Stage A*. Well-nourished, n=18	2.18 (1.28-4.52)	3.90 (2.91-5.24)
	2	*Stage B*. Moderate/suspected malnutrition, n=26	3.79 (1.24-5.49) $p_{1,2}$=0.163	2.07 (1.34-2.61) $p_{1,2}$=0.003
	3	*Stage C*. Severely malnourished, n=30	6.10 (4.25-7.08) $p_{1,3}$=0.000 $p_{2,3}$=0.013	1.04 (0.71-1.66) $p_{1,3}$=0.000 $p_{2,3}$=0.000
SMI	4	Nonsarcopenic males, n=10	1.53 (0.96-2.72)	4.78 (3.85-5.66)
	5	Sarcopenic males, n=35	6.22 (4.22-7.75) $p_{4,5}$=0.000	1.32 (1.05-2.05) $p_{4,5}$=0.000
	6	Nonsarcopenic females, n=9	1.34 (0.99-2.18)	4.22 (3.30-5.36)
	7	Sarcopenic females, n=20	4.90 (3.30-6.07) $p_{6,7}$=0.000	1.50 (0.91-2.18) $p_{6,7}$=0.000

Table 4. The area under curves for malnutrition and sarcopenia prediction according to serum myokines levels in patients with decompensated LC.

Variables			AUC	p
Severe malnutrition: *Stage C* PG-SGA	Myostatin (all patients, n=74)	0.652	0.036	0.501-0.802
	Irisin (all patients, n=74)	0.830	0.000	0.712-0.914
Sarcopenia: SMI ≤52,2 cm²/m² for males; SMI ≤39,3 cm²/m² for females	Myostatin (males, n=45)	0.834	0.003	0.674-0.995
	Myostatin (females, n=29)	0.827	0.007	0.667-0.987
	Irisin (all patients, n=74)	0.639	0.074	0.478-0.794

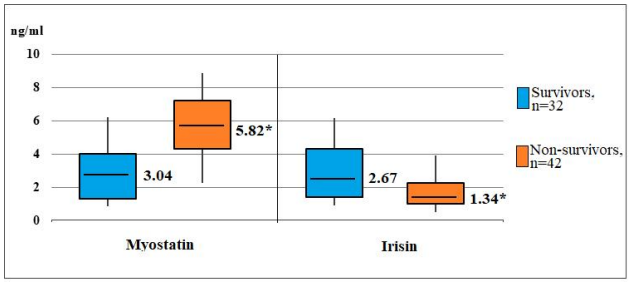

Fig. 1. Serum myostatin and irisin levels according to survival status of patients with decompensated liver cirrhosis. The upper and lower limits of the boxes correspond to P_{25} and P_{75}, the lines outside the boxes - P_{10} and P_{90}, and the line inside the boxes - Me; P_{10}, P_{25}, P_{75}, P_{90}, - percentiles. * - p<0.005.

(Se 85.0 %, Sp 77.8 %), respectively. A low concentration of serum irisin can predict malnutrition (AUC 0.830, p<0.001). The cut-off of irisin concentration for predicting severe malnutrition according to the PG-SGA was 1.78 ng/ml (Se 83.3 %, Sp 72.1 %).

During the follow-up (Me 367 (82-569) days), no patient was lost to analysis, and 42 (56.8%) patients died due to LC complications. Deceased patients had significantly higher myostatin and lower irisin levels at baseline than patients who survived (Fig. 1). We allocated patients into groups with relatively high (higher than Me) and relatively low (lower than Me) myokine levels to determine the relationship between circulating myokine and survival. Kaplan-Meier analysis showed that the overall survival of patients with high (higher than 5.25 ng/ml in males and 3.55 ng/ml in females) myostatin was significantly lower (Fig. 2). The estimated survival time in the high myostatin group was 272.0±42.8 (95% CI: 188-355) versus 654.0±58.1 (95% CI: 541-798) days in the low myostatin group. Patients with low irisin (less than 1.72 ng/ml in males and females) had significantly lower survival than patients with high irisin.

Discussion

To the best of our knowledge, the presented work is one of the few studies of circulating levels of myokines as biomarkers of malnutrition and sarcopenia in patients with LC. We focused on a high-risk cohort of patients. All subjects had MELD scores of more than 15 points. About half of them died during the follow-up. More than 70 % of patients were diagnosed with malnutrition and sarcopenia.

In our study, the serum levels of myostatin and irisin in decompensated LC patients were weakly associated with the severity of the underlying disease. Although CTP class C patients had higher myostatin and lower irisin levels than CTP class B patients, we found no correlation between myokine levels and CTP and MELD. Patients with minimal and pronounced ascites had similar levels of myostatin and irisin. Previously, Nishikawa H. et al. (2017) showed that the concentration of serum myostatin of CTP class B and C patients was higher than that of CTP class A patients [24]. M. Kukla et al. (2020) did not find a difference in the serum irisin between LC patients depending on CTP, MELD, and ascites [14]. M. Pazgan-Simon et al. (2020) demonstrated that the serum irisin in patients with LC and hepatocellular carcinoma (HCC) is lower compared to controls, but not related to the LC severity and the stage of

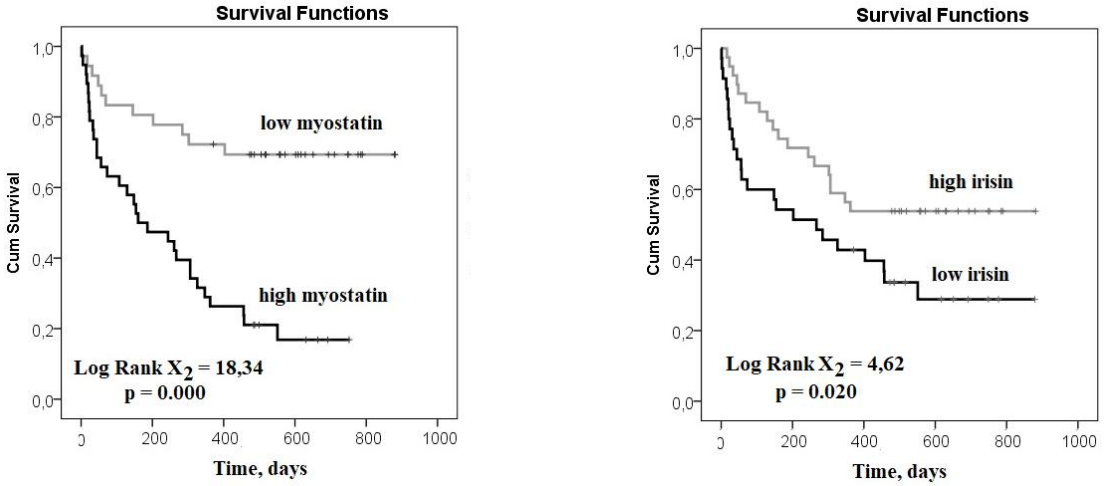

Fig. 2. Kaplan-Meier analysis for survival according to the serum myokines levels.

HCC [26]. The deterioration of liver function and the worsening of portal hypertension are unlikely to have a pivotal effect on the serum myokines in LC patients.

In our study, patients with overt hepatic encephalopathy had higher serum myostatin than patients with minimal encephalopathy. This observation is consistent with previous findings of an association between hepatic encephalopathy and skeletal muscle atrophy. M. Merli et al. (2013) demonstrated that ammonia content in venous blood is higher in patients with sarcopenia [19]. It is assumed that hyperammonemia is associated with the depletion of the branched-chain amino acids pool required for muscle tissue formation, activation of muscle autophagy, and increased expression of myostatin [9]. On the other hand, sarcopenia promotes hyperammonemia and hepatic encephalopathy, as up to 50% of circulating ammonia is detoxified in skeletal muscles [17].

Our data demonstrate that severe malnutrition and sarcopenia in decompensated LC patients are associated with an increase in serum myostatin. Myostatin was the first among the identified myokines and acts as a powerful negative regulator of myogenesis [33]. Experimental studies have shown that animals with a knockout of the myostatin gene have pronounced hypertrophy of skeletal muscles [21, 33]. Existing data suggest that myostatin activates several intracellular signalling pathways to inhibit the proliferation and differentiation of muscle satellite cells, decrease protein synthesis, and stimulate protein degradation in muscle fibres [38]. In clinical studies, high levels of myostatin are associated with muscle wasting, myopathy, and sarcopenia in elderly patients with renal failure and fractures [8, 39, 42].

In our study, myostatin was moderately correlated with the radiological SMI and weakly correlated with the numerical PG-SGA in males and females. We showed that the concentration of serum myostatin (cut-off 4.20/2.72 ng/ml in males/females) can predict sarcopenia in decompensated LC patients (AUC>0.800, p<0.01). A negative relationship between high levels of myostatin and skeletal muscle mass was demonstrated in a retrospective study by H. Nishikawa et al. (2017). The study included 198 Japanese LC patients, 59% of them had a viral aetiology of the disease, 62% - compensated LC, 38% - decompensated LC, and 20% - had HCC. It was established that the concentration of serum myostatin was negatively correlated with the radiological index of the psoas muscle [24]. Later, S. Sato et al. (2021) found a negative correlation between myostatin levels and SMI in patients with viral but not alcohol-related LC [30]. Recently, S. Boga, et al. (2022) using regression analysis demonstrated that a high level of myostatin is an independent predictor of sarcopenia in LC in the Turkish population [2]. The relationship between circulating levels of myostatin and muscle wasting was more pronounced in decompensated patients [2].

Our data suggest that serum irisin was less dependent on muscle condition than myostatin. Sarcopenic LC patients had lower levels of this myokine than patients with normal skeletal muscle mass. Irisin was weakly correlated with SMI and had limited value in predicting sarcopenia in ROC analysis. Previously, M. Kukla et al. (2020) did not find an association between irisin concentration and midarm muscle circumference and transversal psoas muscle index in a similar cohort of patients [14]. However, in another multicenter retrospective study involving 262 LC patients of mainly viral aetiology, it was established that irisin decreases in sarcopenic patients, correlates with SMI, and is an independent predictor of sarcopenia in regression analysis [41].

Our data show that the level of serum irisin was more dependent on the nutritional status of LC patients than on the skeletal muscle status. The concentration of this myokine decreased significantly even in patients with moderate/suspected malnutrition and continued to decrease in severely malnourished patients. Irisin moderately correlated with the numerical PG-SGA score, and the concentration of serum irisin (cut-off 1.78 ng/ml) predicted severe malnutrition according to the PG-SGA (AUC 0.830, p<0.001). The latest data demonstrated that irisin is secreted not only in skeletal muscles but also in adipose tissue, which allows it to be classified as an adipomyokine [3, 29]. The biological effects of irisin are related to energy expenditure, thermoregulation, and the transformation of white adipose tissue into brown adipose tissue [29]. Irisin is an insulin-sensitizing hormone, as it promotes the assimilation of glucose by skeletal muscles, reduces lipogenesis and gluconeogenesis in the liver, and activates lipid oxidation and glycolysis [32]. Anti-inflammatory properties of this regulatory peptide were recently discovered: irisin inhibits the expression of pro-inflammatory cytokines tumor necrosis factor-alpha and interleukin-6 and reduces the migration of macrophages in adipose tissue [1]. Pointing to the important role of irisin in the regulation of metabolism and energy expenditure, we suggest that the loss of adipose and muscle tissue in malnourished LC patients is closely associated with a decline in serum irisin.

We aimed to evaluate the relationship between myokine levels and prognosis in decompensated LC patients. In the Kaplan-Meier analysis, we showed that a high level of myostatin and a low level of irisin have a negative impact on patient survival. Literature data on the prognostic value of myokines in patients with end-stage liver disease are limited and contradictory. A recent retrospective study by J.H. Kim et al. (2020) involving 1077 alcohol-related LC patients is noteworthy. Patients with high serum myostatin levels were shown to have a significantly higher 5-year risk of HCC than patients with low serum myostatin levels (HR 7.53, p<0.001) [12]. S. Yoshio et al., 2021 showed that high-level serum myostatin is an independent predictor of mortality in patients with HCC associated with nonalcoholic fatty liver disease, regardless of muscle status [40]. H. Nishikawa et al. (2017) demonstrated that the 5-year

and 7-year cumulative survival of LC patients with high-level serum myostatin were significantly lower than that of patients with low-level serum myostatin (53% and 39%, versus 78% and 73%, respectively) [24]. However, a recent study by S. Boga et al. (2022) demonstrated that decreased irisin levels were associated with increased cirrhosis-related 4-year mortality in CTP class A patients, while myostatin did not show good prognostic value [2].

In conclusion, the circulating myokines levels may be useful in the assessment of nutritional and skeletal muscle status, and prediction of mortality in LC patients.

Further prospective studies are needed to confirm the prognostic value of myokines in LC patients.

Conclusions

1. The serum myokines myostatin and irisin levels in decompensated LC patients are not related to the LC severity according to the CTP, MELD score, and the degree of ascites. Patients with overt encephalopathy have higher serum myostatin. Patients with severe hypoalbuminemia have higher serum myostatin and lower serum irisin.

2. Malnutrition and sarcopenia are associated with an increase in serum myostatin and a decrease in serum irisin. The myostatin concentration can predict sarcopenia in LC (AUC 0.834 in males, 0.827 in females, $p<0.01$). The irisin concentration can predict severe malnutrition (AUC 0.830, $p<0.001$).

3. An increase in serum myostatin and a decrease in serum irisin are associated with worsening patients' survival. The overall mortality of patients with high levels of serum myostatin (above 5.25 ng/ml in males and 3.55 ng/ml in females) and low levels of serum irisin (less than 1.72 ng/ml) is significantly higher.

References

[1] Askari, H., Rajani, S. F., Poorebrahim, M., Haghi-Aminjan, H., Raeis-Abdollahi, E., & Abdollahi, M. (2018). A glance at the therapeutic potential of irisin against diseases involving inflammation, oxidative stress, and apoptosis: An introductory review. *Pharmacological Research,* 129, 44-55. doi: 10.1016/j.phrs.2018.01.012

[2] Boga, S., Yildirim, A. E., Ucbilek, E., Koksal, A. R., Sisman, S. T., Durak, I., … & Alkim, C. (2022). The effect of sarcopenia and serum myokines on prognosis and survival in cirrhotic patients: a multicenter cross-sectional study. *European Journal of Gastroenterology & Hepatology,* 34(12), 1261-1268. doi: 10.1097/MEG.0000000000002461

[3] Bostrom, P., Wu, J., Jedrychowski, M. P., Korde, A., Ye, L., Lo, J. C., … & Spiegelman, B. M. (2012). A PGC1-alpha-dependent myokine that drives brown-fat-like development of white fat and thermogenesis. *Nature,* 481(7382), 463-468. doi: 10.1038/nature10777

[4] Chapman, B., Goh, S. K., Parker, F., Romero, S., Sinclair, M., Gow, P., … & Testro, A. (2022). Malnutrition and low muscle strength are independent predictors of clinical outcomes and healthcare costs after liver transplant. *Clinical Nutrition ESPEN,* 48, 210-219. doi: 10.1016/j.clnesp.2022.02.013

[5] Dajti, E., Renzulli, M., Ravaioli, F., Marasco, G., Vara, G., Brandi, N., … & Colecchia, A. (2022). The interplay between sarcopenia and portal hypertension predicts ascites and mortality in cirrhosis. Digestive and liver disease : official journal of the Italian Society of Gastroenterology and the Italian Association for the Study of the Liver, S1590-8658(22)00789-7. Advance online publication. doi: 10.1016/j.dld.2022.11.011

[6] D'Amico, G., Morabito, A., D'Amico, M., Pasta, L., Malizia, G., Rebora, P., & Valsecchi, M. G. (2018). Clinical states of cirrhosis and competing risks. *Journal of Hepatology,* 68(3), 563-576. doi: 10.1016/j.jhep.2017.10.020

[7] Dasarathy, S. (2013). Posttransplant sarcopenia: an underrecognized early consequence of liver transplantation. *Digestive Diseases and Sciences,* 58(11), 3103-3111. doi: 10.1007/s10620-013-2791-x

[8] de Sire, A., Baricich, A., Reno, F., Cisari, C., Fusco, N., & Invernizzi, M. (2020). Myostatin as a potential biomarker to monitor sarcopenia in hip fracture patients undergoing a multidisciplinary rehabilitation and nutritional treatment: a preliminary study. *Aging Clinical and Experimental Research,* 32(5), 959-962. doi: 10.1007/s40520-019-01436-8

[9] Di Cola, S., Nardelli, S., Ridola, L., Gioia, S., Riggio, O., & Merli, M. (2022). Ammonia and the Muscle: An Emerging Point of View on Hepatic Encephalopathy. *Journal of Clinical Medicine*, 11(3), 611. doi: 10.3390/jcm11030611

[10] Hassan, E. A., Makhlouf, N. A., Ibrahim, M. E., Dabbous, H. M., Salah, M. A., Aboalam, H. S., … & Salama, M. A. R. (2022). Impact of Sarcopenia on Short-Term Complications and Survival After Liver Transplant. *Experimental and Clinical Transplantation: Official Journal of the Middle East Society for Organ Transplantation,* 20(10), 917-924. doi: 10.6002/ect.2022.0293

[11] Jager-Wittenaar, H., & Ottery, F. D. (2017). Assessing nutritional status in cancer: role of the Patient-Generated Subjective Global Assessment. *Current opinion in Clinical Nutrition and Metabolic Care,* 20(5), 322-329. doi: 10.1097/MCO.0000000000000389

[12] Kim, J. H., Kang, S. H., Lee, M., Youn, G. S., Kim, T. S., Jun, B. G., … & Suk, K. T. (2020). Serum Myostatin Predicts the Risk of Hepatocellular Carcinoma in Patients with Alcoholic Cirrhosis: A Multicenter Study. *Cancers,* 12(11), 3347. doi: 10.3390/cancers12113347

[13] Krell, R. W., Kaul, D. R., Martin, A. R., Englesbe, M. J., Sonnenday, C. J., Cai, S., & Malani, P. N. (2013). Association between sarcopenia and the risk of serious infection among adults undergoing liver transplantation. *Liver transplantation : official publication of the American Association for the Study of Liver Diseases and the International Liver Transplantation Society,* 19(12), 1396-1402. doi: 10.1002/lt.23752

[14] Kukla, M., Skladany, L., Menzyk, T., Derra, A., Stygar, D., Skonieczna, M., … & Koller, T. (2020). Irisin in Liver Cirrhosis. *Journal of clinical medicine,* 9(10), 3158. doi: 10.3390/jcm9103158

[15] Kwon, J. H., Moon, K. M., & Min, K. W. (2020). Exercise-Induced Myokines can Explain the Importance of Physical Activity in the Elderly: An Overview. *Healthcare* (Basel, Switzerland), 8(4), 378. doi: 10.3390/healthcare8040378

[16] Lee, D. U., Fan, G. H., Ahern, R. R., & Karagozian, R. (2021). The effect of malnutrition on the infectious outcomes of hospitalized patients with cirrhosis: analysis of the 2011-2017 hospital data. *European Journal of Gastroenterology & Hepatology,* 32(2), 269-278. doi: 10.1097/

MEG.0000000000001991

[17] Levitt, D. G., & Levitt, M. D. (2018). A model of blood-ammonia homeostasis based on a quantitative analysis of nitrogen metabolism in the multiple organs involved in the production, catabolism, and excretion of ammonia in humans. *Clinical and Experimental Gastroenterology,* 11, 193-215. doi: 10.2147/CEG.S160921

[18] Mauro, E., Crespo, G., Martinez-Garmendia, A., Gutierrez-Acevedo, M. N., Diaz, J. M., Saidman, J., … & Gadano, A. (2020). Cystatin C and Sarcopenia Predict Acute on Chronic Liver Failure Development and Mortality in Patients on the Liver Transplant Waiting List. *Transplantation,* 104(7), e188-e198. doi: 10.1097/TP.0000000000003222

[19] Merli, M., Giusto, M., Lucidi, C., Giannelli, V., Pentassuglio, I., Di Gregorio, V., ... & Riggio, O. (2013). Muscle depletion increases the risk of overt and minimal hepatic encephalopathy: results of a prospective study. *Metabolic Brain Disease*, 28(2), 281-284. doi: 10.1007/s11011-012-9365-z

[20] Montano-Loza, A. J., Duarte-Rojo, A., Meza-Junco, J., Baracos, V. E., Sawyer, M. B., Pang, J. X., ... & Myers, R. P. (2015). Inclusion of Sarcopenia Within MELD (MELD-Sarcopenia) and the Prediction of Mortality in Patients With Cirrhosis. *Clinical and translational gastroenterology,* 6(7), e102. doi: 10.1038/ctg.2015.31

[21] Mosher, D. S., Quignon, P., Bustamante, C. D., Sutter, N. B., Mellersh, C. S., Parker, H. G., & Ostrander, E. A. (2007). A mutation in the myostatin gene increases muscle mass and enhances racing performance in heterozygote dogs. *PLoS genetics,* 3(5), e79. doi: 10.1371/journal.pgen.0030079

[22] Motsiuk, V. M., & Pentiuk, N. O. (2021). Діагностичне та прогностичне значення показників товщини та площі поперекового м'язу у хворих на цироз печінки, ускладений саркопенією [Diagnostic and prognostic value of indicators of the thickness and area of the lumbar muscle in patients with liver cirrhosis complicated by sarcopenia]. *Вісник Вінницького національного медичного університету - Reports of Vinnytsia National Medical University,* 25(4), 551-558. doi: 10.31393/reports-vnmedical-2021-25(4)-06

[23] Nardelli, S., Lattanzi, B., Torrisi, S., Greco, F., Farcomeni, A., Gioia, S., Merli, M., & Riggio, O. (2017). Sarcopenia Is Risk Factor for Development of Hepatic Encephalopathy After Transjugular Intrahepatic Portosystemic Shunt Placement. *Clinical Gastroenterology and Hepatology: the Official Clinical Practice Journal of the American Gastroenterological Association,* 15(6), 934-936. doi: 10.1016/j.cgh.2016.10.028

[24] Nishikawa, H., Enomoto, H., Ishii, A., Iwata, Y., Miyamoto, Y., Ishii, N., … & Nishiguchi, S. (2017). Elevated serum myostatin level is associated with worse survival in patients with liver cirrhosis. *Journal of Cachexia, Sarcopenia and Muscle*, 8(6), 915-925. doi: 10.1002/jcsm.12212

[25] Ottery, F. D. (1996). Definition of standardized nutritional assessment and interventional pathways in oncology. *Nutrition* (Burbank, Los Angeles County, Calif.), 12(1 Suppl), S15-S19. doi: 10.1016/0899-9007(96)90011-8

[26] Pazgan-Simon, M., Zuwala-Jagiello, J., Menzyk, T., Bator, M., Derra, A., Lekstan, A., … & Kukla, M. (2020). Serum betatrophin and irisin levels in hepatocellular carcinoma. *Journal of Physiology and Pharmacology: an Official Journal of the Polish Physiological Society,* 71(1), 1. doi: 10.26402/jpp.2020.1.11

[27] Pentiuk, N. O., Motsiuk, V. M., & Ferree, A.S. (2021). Адаптація та валідизація україномовної версії шкали оцінки нутритивного стану Patient-Generated Subjective Global Assessment (PGSGA) у хворих на цироз печінки [Adaptation and validation of the Ukrainian version of the Patient-Generated Subjective Global Assessment (PGSGA) nutritional status scale in patients with liver cirrhosis]. *Сучасна гастроентерологія - Modern Gastroenterology,* 117(1), 58-66. doi: 10.30978/MG-2021-1-58

[28] Praktiknjo, M., Clees, C., Pigliacelli, A., Fischer, S., Jansen, C., Lehmann, J., … & Trebicka, J. (2019). Sarcopenia Is Associated With Development of Acute-on-Chronic Liver Failure in Decompensated Liver Cirrhosis Receiving Transjugular Intrahepatic Portosystemic Shunt. *Clinical and Translational gastroenterology,* 10(4), e00025. doi: 10.14309/ctg.0000000000000025

[29] Rodriguez, A., Becerril, S., Ezquerro, S., Mendez-Gimenez, L., & Fruhbeck, G. (2017). Crosstalk between adipokines and myokines in fat browning. *Acta Physiologica* (Oxford, England), 219(2), 362-381. doi: 10.1111/apha.12686

[30] Sato, S., Namisaki, T., Murata, K., Fujimoto, Y., Takeda, S., Enomoto, M., … & Yoshiji, H. (2021). The association between sarcopenia and endotoxin in patients with alcoholic cirrhosis. *Medicine,* 100(36), e27212. doi: 10.1097/MD.0000000000027212

[31] Shen, W., Punyanitya, M., Wang, Z., Gallagher, D., St.-Onge, M.-P., Albu, J., Heymsfield, S. B., Heshka, S. (2004) Total body skeletal muscle and adipose tissue volumes: Estimation from a single abdominal cross-sectional image. *J. Appl. Physiol.,* 97, 2333-2338. doi: 10.1152/japplphysiol.00744.2004

[32] Senesi, P., Luzi, L., & Terruzzi, I. (2020). Adipokines, Myokines, and Cardiokines: The Role of Nutritional Interventions. *International Journal of Molecular Sciences,* 21(21), 8372. doi: 10.3390/ijms21218372

[33] Severinsen, M. C. K., & Pedersen, B. K. (2020). Muscle-Organ Crosstalk: The Emerging Roles of Myokines. *Endocrine Reviews,* 41(4), 594-609. doi: 10.1210/endrev/bnaa016

[34] Tandon, P., Montano-Loza, A. J., Lai, J. C., Dasarathy, S., & Merli, M. (2021). Sarcopenia and frailty in decompensated cirrhosis. *Journal of Hepatology*, 75(Suppl 1), S147-S162. doi: 10.1016/j.jhep.2021.01.025

[35] Traub, J., Reiss, L., Aliwa, B., & Stadlbauer, V. (2021). Malnutrition in Patients with Liver Cirrhosis. *Nutrients,* 13(2), 540. doi: 10.3390/nu13020540

[36] Tsien, C., Garber, A., Narayanan, A., Shah, S. N., Barnes, D., Eghtesad, B., … & Dasarathy, S. (2014). Post-liver transplantation sarcopenia in cirrhosis: a prospective evaluation. *Journal of Gastroenterology and Hepatology,* 29(6), 1250-1257. doi: 10.1111/jgh.12524

[37] van Vugt, J. L. A., Buettner, S., Alferink, L. J. M., Bossche, N., de Bruin, R. W. F., Darwish Murad, S., … & Izermans, J. N. M. (2018). Low skeletal muscle mass is associated with increased hospital costs in patients with cirrhosis listed for liver transplantation-a retrospective study. *Transplant International: Official Journal of the European Society for Organ Transplantation,* 31(2), 165-174. doi: 10.1111/tri.13048

[38] Verzola, D., Barisione, C., Picciotto, D., Garibotto, G., & Koppe, L. (2019). Emerging role of myostatin and its inhibition in the setting of chronic kidney disease. *Kidney International,* 95(3), 506-517. doi: 10.1016/j.kint.2018.10.010

[39] Widajanti, N., Soelistijo, S., Hadi, U., Thaha, M., Aditiawardana, Widodo, Firdausi, H., … & Syakdiyah, N. (2022). Association between Sarcopenia and Insulin-Like Growth Factor-1, Myostatin, and Insulin Resistance in Elderly Patients Undergoing Hemodialysis. *Journal of Aging Research,* 2022, 1327332. doi: 10.1155/2022/1327332

[40] Yoshio, S., Shimagaki, T., Hashida, R., Kawaguchi, T., Tsutsui, Y., Sakamoto, Y., … & Kanto, T. (2021). Myostatin as a fibroblast-activating factor impacts on postoperative outcome in patients with hepatocellular carcinoma. *Hepatology research: the Official Journal of the Japan Society of Hepatology,* 51(7), 803-812. doi: 10.1111/hepr.13667

[41] Zhao, M., Zhou, X., Yuan, C., Li, R., Ma, Y., & Tang, X. (2020). Association between serum irisin concentrations and sarcopenia in patients with liver cirrhosis: a cross-sectional study. *Scientific Reports,* 10(1), 16093. doi: 10.1038/s41598-020-73176-z

[42] Zunner, B. E. M., Wachsmuth, N. B., Eckstein, M. L., Scherl, L., Schierbauer, J. R., Haupt, S., … & Moser, O. (2022). Myokines and Resistance Training: A Narrative Review. *International Journal of Molecular Sciences,* 23(7), 3501. doi: 10.3390/ijms23073501

МІОСТАТИН ТА ІРИСИН СИРОВАТКИ КРОВІ ЯК ПРОГНОСТИЧНІ БІОМАРКЕРИ САРКОПЕНІЇ, МАЛЬНУТРИЦІЇ ТА СМЕРТНОСТІ У ХВОРИХ НА ДЕКОМПЕНСОВАНИЙ ЦИРОЗ ПЕЧІНКИ

Моцюк В.М., Пентюк Н.О.

Мальнутриція та саркопенія сьогодні розглядаються як основні ускладнення цирозу печінки (ЦП). Міокіни є сигнальними пептидами, котрі синтезуються у м'язах, здійснюють регуляцію м'язової сили та маси, а також забезпечують зв'язок між скелетними м'язами та іншими органами. Невідомо, чи можуть циркулюючі міокіни слугувати біомаркерами мальнутриції та саркопенії й мати самостійну прогностичну цінність у хворих на ЦП. Метою нашого дослідження стало оцінити зв'язок сироваткових рівнів міокінів міостатину та ірисину з нутритивним станом, станом скелетних м'язів та виживанням хворих на декомпенсований цироз печінки. До проспективного дослідження увійшли 74 хворих (середній показник віку хворих становив 55,30±11,40 роки). Нутритивний стан оцінювали за шкалою сукупного суб'єктивного оцінювання стану пацієнта (Patient-Generated Subjective Global Assessment), масу скелетних м'язів оцінювали за індексом скелетних м'язів (Skeletal Muscle Index). Вміст міостатину та ірисину в сироватці крові визначали методом імуноферментного аналізу. Статистичну обробку даних проводили у SPSS22 (© SPSS Inc.). Встановлено, що вміст міостатину та ірисину у хворих на декомпенсований ЦП не пов'язаний із важкістю ЦП за шкалами Child-Turcotte-Pugh, Model For End-Stage Liver Disease та ступенем асциту. Пацієнти з маніфестною енцефалопатією мають вищий рівень міостатину, а пацієнти з тяжкою гіпоальбумінемією - вищі рівні міостатину та нижчі рівні ірисину в сироватці крові. Розвиток мальнутриції та саркопенії у хворих на декомпенсований ЦП асоціюється з підвищенням концентрації міостатину та зниженням концентрації ірисину в сироватці крові. Сироватковий рівень міостатину може прогнозувати саркопенію (AUC 0,834 у чоловіків та 0,827 у жінок, p<0,01), сироватковий рівень ірисину може прогнозувати тяжку мальнутрицію (AUC 0,830, p<0,001). Загальна смертність пацієнтів з високими рівнями міостатину (вище 5,25 нг/мл у чоловіків та 3,55 нг/мл у жінок) та низькими рівнями ірисину (менше 1,72 нг/мл) є достовірно вищою. Таким чином, оцінка циркулюючих рівнів міокінів може бути корисною для оцінки нутритивного стану, стану скелетних м'язів та прогнозу у хворих на ЦП.

Ключові слова: *міостатин, ірисин, мальнутриція, саркопенія, виживаність, цироз печінки.*

DOI: 10.31393/morphology-journal-2023-29(2)-04 Reports of Morphology, Vol. 29, №2, Pages 26-31

ISSN 1818-1295 eISSN 2616-6194

REPORTS OF MORPHOLOGY

Official Journal of the Scientific Society of Anatomists, Histologists, Embryologists and Topographic Anatomists of Ukraine

journal homepage: https://morphology-journal.com

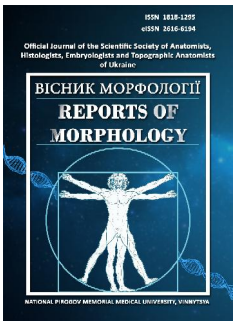

Immunohistochemical characteristics of the gray matter of the human spinal cord in the late prenatal period

Dovgan A. V.[1], Vlasenko O. V.[1], Popadynets O. G.[2], Semenenko A. I.[1], Gunas I. V.[1], Bobruk V. P.[1]

[1]National Pirogov Memorial Medical University, Vinnytsia, Ukraine
[2]Ivano-Frankivsk National Medical University, Ivano-Frankivsk, Ukraine

ARTICLE INFO
Received: 03 February 2023
Accepted: 07 March 2023

UDC: 616:832.2:611.013

CORRESPONDING AUTHOR
e-mail: dovgan@vnmu.edu.ua
Dovgan A. V.

CONFLICT OF INTEREST
The authors have no conflicts of interest to declare.

FUNDING
Not applicable.

The study is dedicated to the relevant problem of studying the patterns of age-related (prenatal) restructuring in the brain and spinal cord and provides opportunities for predicting and correcting the occurrence of congenital defects. The aim of the research was to establish the nature of immunohistochemical marker expression in the gray matter structures of the human spinal cord during the late prenatal period. The material for the study consisted of spinal cord preparations from 27 human fetuses at gestational age 35-40 weeks. The following methods were used during the research: anatomical, general histological, special histological, immunohistochemical, morphometric, and statistical analysis of the obtained data. It was found that at 35-36 weeks of the gestational period, the proliferation of neural stem cells (NSCs) occurs more intensively in the ventral neuroepithelium of spinal cord segments compared to the dorsal neuroepithelium. In the ventral neuroepithelium, there are 5-6 mitotic or post-mitotic NSCs, while in the dorsal part, there are only 2-3 cells. In fetuses at 39-40 weeks, the proliferative activity of neural stem cells in the dorsal neuroepithelium is higher in cervical and lumbar segments, where Ki-67 expression is detected in 6 % of cells (reactive in 7-8 cells), and in thoracic and sacral segments, it is 4 % (reactive in 3-4 cells). In contrast to the dorsal neuroepithelium, in the ventral part of the neuroepithelium of the segments, the proliferative activity of neural stem cells is slightly less intense. In cervical and lumbar segments, Ki-67 expression occurred in 4 % of cells (reactive in 3-4 cells), and in thoracic and sacral segments, it was 2 % (reactive in 1-2 cells). At 35-36 weeks of gestation, high vimentin expression was observed around the neuroepithelium, at the base of the posterior horns, and along the posterior median septum. Vimentin expression in the mantle layer was relatively weak and persisted along blood vessels and in the area of spinal cord root formation. Before birth, relatively weak vimentin expression was detected in the remnants of radial glia surrounding the neuroepithelial layer. Vimentin expression was absent in the neuroepithelium proper, but focal vimentin expression was observed around blood vessels. The absence of vimentin expression in the neuroepithelium indicates the disappearance of radial cells. At 35-40 weeks of the gestational period, relatively strong synaptophysin expression was observed in the mantle layer of spinal cord segments, indicating the intensity of neuronal connectivity establishment and myelination of nerve fibers. These processes continue after birth. Synaptophysin expression was absent in the neuroepithelium proper.

Keywords: *brain, spinal cord, central nervous system, radial glia, neural stem cells, prenatal period, immunohistochemistry, neuron.*

Introduction

The stages of emergence, genetic mechanisms of development, and processes of differentiation of neural stem cells in the gray matter of the brain and spinal cord of human embryos and fetuses have always been a priority in scientific research [6]. Such studies contain a large amount of scientific data and facts, but to this day, the results of such work have conflicting aspects that require further clarification [3].

As a result of the emergence of modern research techniques, such as immunohistochemical or immunofluorescent analysis, as well as computer morphometry etc., new opportunities arise for thorough

studies of the structures of the human central nervous system [1].

It is known that neural stem cells and progenitor cells are the source of neuroblasts and glioblasts, which may exhibit different morphological and cytochemical properties at different stages of ontogenesis and in different structures of the central nervous system [11]. Neural stem cells arise in the neuroepithelium of the spinal cord. The coexistence of neuronal and glial cell precursors in the ventricular zone of the neural tube at very early stages has been confirmed using cell markers such as neuron-specific enolase and glial fibrillary acidic protein [4]. In contrast, the available literature lacks results regarding the application of immunohistochemical markers such as vimentin, S-100, CDX-2, and synaptophysin in the study of structures in the human fetal spinal cord.

The aforementioned techniques have allowed us to establish that neuroblasts, originating from the neuroepithelium, subsequently migrate in a targeted manner through amoeboid movements in various directions towards their sites of further differentiation along the radial glial fibers [5]. There is a viewpoint that these "guiding" glial cells disappear after the maturation of neurons. Cessation of further neuronal migration in the adult brain is attributed to the disappearance of glial radial processes [17]. However, the authors have not described the sequential morphology of radial glia during prenatal human ontogenesis, which requires further investigation and clarification. As the neuronal cytoplasm differentiates, the growth and differentiation of its processes occur, and intercellular connections, including the formation of synaptic structures, are established [7].

The active study of neural stem cells over the past twenty years has been associated with the creation of opportunities for tissue and organ regeneration in damaged or aging organisms, thus improving quality of life and extending lifespan [9, 16].

Thus, the significance of the research results on the morphology of the development of the brain and spinal cord in clinical practice is exempt from any doubt.

The aim of the study is to determine the expression pattern of immunohistochemical markers in the structures of the gray matter of the human spinal cord during the late prenatal period.

Materials and methods

The material for the study consisted of spinal cord specimens from 27 human fetuses at a gestational age of 35-40 weeks. These specimens were obtained during medical abortions or from relatively healthy women due to stillbirths. The fetuses had perished due to causes unrelated to anomalies in the development of the brain or spinal cord.

During the examination, it was found that the materials used in this study comply with the fundamental bioethical norms of the Helsinki Declaration adopted by the General Assembly of the World Medical Association, the Convention on Human Rights and Biomedicine of the Council of Europe (1977), relevant provisions of the WHO, the International Council of Medical Scientific Societies, the International Code of Medical Ethics (1983), the Convention for the Protection of Vertebrate Animals Used for Experimental and Other Scientific Purposes of the Council of Europe of 18.03.1986, Directive 86/609/EEC of 24.11.1986, and Order No. 281 of the Ministry of Health of Ukraine of 01.11.2000. The bioethical examination has determined that this research may be presented for the publication of the obtained results.

This work is a part of the planned scientific research of the Department of Human Anatomy at Vinnytsia National Medical University named after M. I. Pirogov, titled "Establishment of Morphological Changes in the Formations of the Human Central Nervous System during the Prenatal Ontogenesis Period (Macroscopic, Histological, Morphometric, Immunohistochemical Study)", with the state registration number 0118U001043.

The spinal cord histological specimens were stained with silver nitrate (Bilshovsky impregnation), hematoxylin-eosin, and the Nissl staining method was applied.

Immunohistochemical techniques (monoclonal antibodies) were used as follows: Ki 67 as a marker of neural cell proliferation, vimentin as a marker of radial glial fibers and radial cells [10]; S-100 as a marker of glial cells, and synaptophysin as a marker of synaptic vesicles [8]. A semi-quantitative scale was used to assess protein expression intensity, with the following scoring: 0 - an absence of positive cells, weak - 30 % positive cells, moderate - 31-60 % positive cells, strong - 60 % or more stained cells [2].

Morphometry of the spinal cord formations was performed using a light microscope, with the following magnifications: x4, x10, x40, x100, and x200. Cytohistometry was carried out using PhotoM 1.21 software (computer histometry).

Statistical analysis of the quantitative data obtained from the results was performed on a personal computer using the standard software package "Statistica 6.1" by StatSoft (owned by the Scientific and Research Center of National Pirogov Memorial Medical University, Vinnytsia, license number BXXR901E246022FA). The correctness of the feature distribution was assessed for each variation series, including the calculation of mean values and standard deviations for each feature. The differences between independent variables were considered significant at $p<0.05$.

Results

In fetuses at 35-36 weeks of gestation, the proliferation of neural stem cells (NSCs) occurs more prominently in the ventral neuroepithelium of the spinal cord segments compared to the dorsal neuroepithelium. It has been found that the ventral neuroepithelium contains 5-6 mitotic or postmitotic NSCs (Fig. 1). While the dorsal region of the neuroepithelium has only 2-3 such cells.

NSCs migration from the neuroepithelium after mitosis occurs along the remnants of radial glial fibers. The radial direction is maintained only at a certain distance around

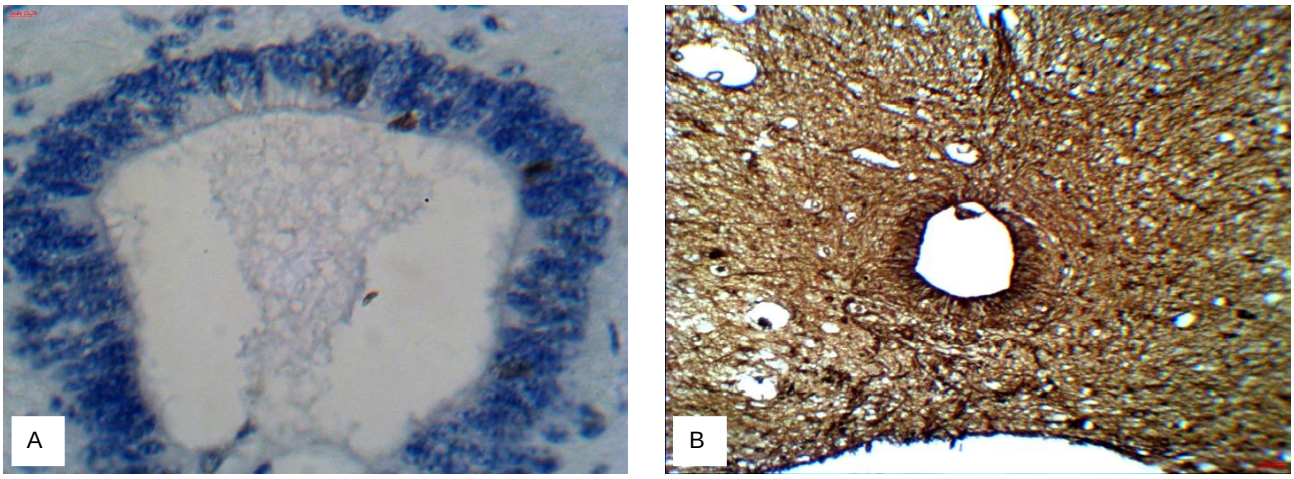

Fig. 1. Horizontal section of the human fetal spinal cord at 35-36 weeks. A - expression of Ki-67 in the neuroepithelium. Ki-67. x400. B - remnants of radial glia. Vimentin; x100.

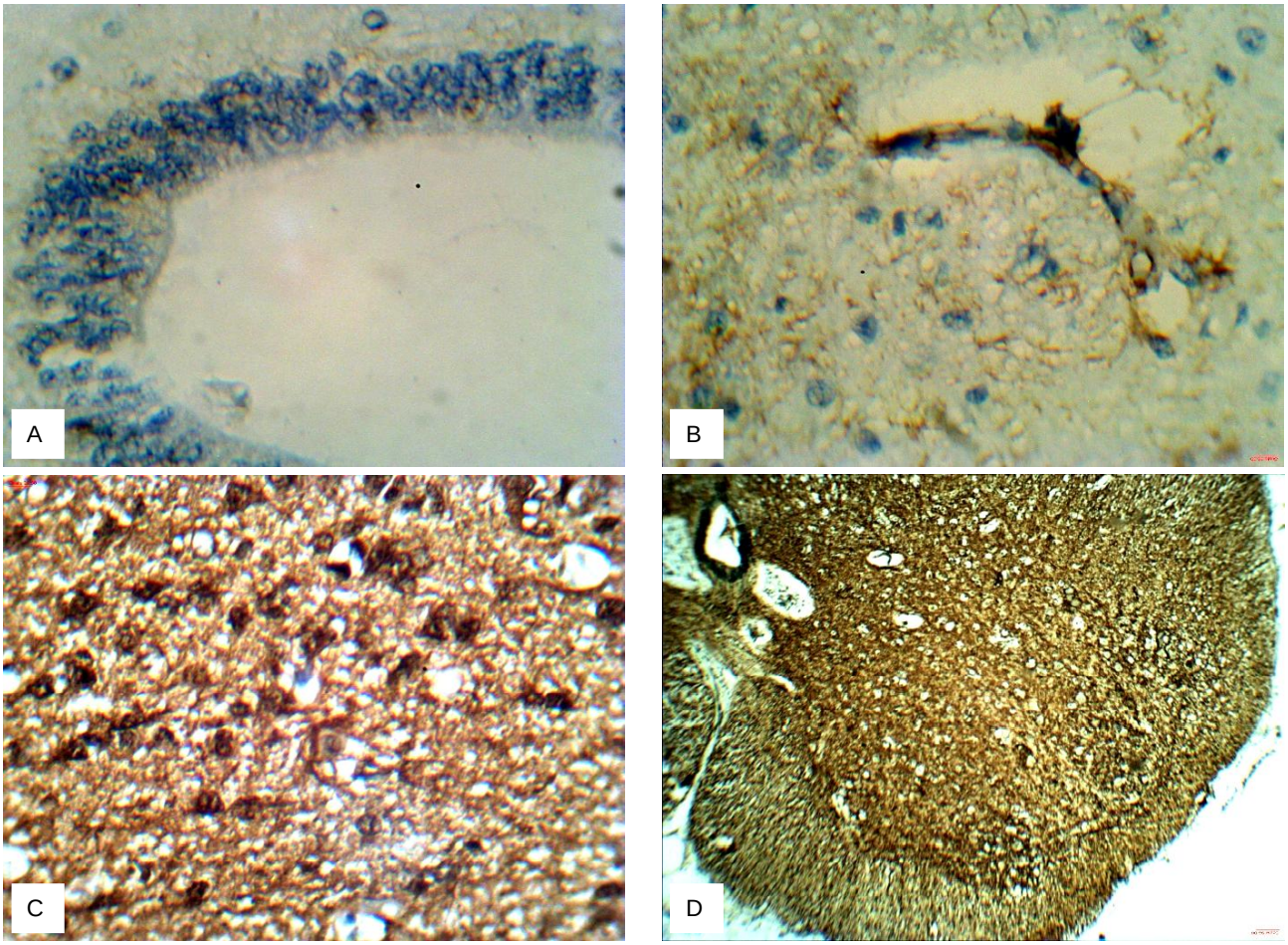

Fig. 2. Horizontal section of the human fetal spinal cord at 39-40 weeks. A - Ki-67 expression in the neuroepithelium. Ki-67. x400. B - remnants of radial glial fibers near blood vessels. Vimentin; x100. C - S-100 expression in the mantle layer glial cells of the segments. S-100. x400. D - a relatively strong expression of synaptophysin in the gray matter of the segments. Synaptophysin. x40.

the neuroepithelium (see Fig. 1). Additionally, the radial glial fibers change direction and extend in a fan-like pattern into the boundaries of the dorsal horns. Short fibers are located within the neuroepithelium, starting from the basal membrane and comprising its thickness. Long radial glial fibers extend from the basal membrane of the dorsal neuroepithelium and run along the posterior median septum. Strong vimentin expression was observed in the

neuroepithelium and along the posterior median septum (see Fig. 1). In the mantle layer, vimentin expression was relatively weak and persisted along the blood vessels and at the site of spinal cord root formation. Within the marginal zone, there was weak vimentin expression, indicating the absence of radial glia.

During the investigation of S-100 expression in glioblasts and gliocytes in spinal cord segments, it was found that strong expression occurred in the neuroepithelial layer (reacted in 100 % of cells). Additionally, strong S-100 expression was observed in the gray matter of the anterior horns (reacted in 90 % of gliocytes). We also observed a similar pattern of strong S-100 expression in glial cells of the gray matter in the posterior horns (reacted in 92 % of cells).

Relatively strong expression of synaptophysin was observed in the segments of the spinal cord, particularly in the mantle layer, indicating the intensity of neuronal connectivity processes. Additionally, synaptophysin expression in the marginal layer was moderate, while no expression of synaptophysin was detected in the neuroepithelium itself.

In fetuses at 39-40 weeks, the proliferative activity of neural stem cells in the dorsal neuroepithelium is relatively highest in the cervical and lumbar segments, where Ki 67 expression was observed in 6 % of cells (7-8 cells reacted), and in the thoracic and sacral segments, where it was 4 % (3-4 cells reacted) (Fig. 2). In contrast to the dorsal neuroepithelium, the ventral neuroepithelium of the segments showed the slightly lower intensity of proliferative activity of neural stem cells. Specifically, in the cervical and lumbar segments, Ki-67 expression occurred in 4 % of cells (3-4 cells reacted), and in the thoracic and sacral segments, it was 2 % (1-2 cells reacted) (see Fig. 2).

During this age period, a slowdown in the migration processes of NSCs is observed, both in the gray matter of the anterior regions and in the gray matter of the posterior horns, where their differentiation into neurons and glial cells occurs. In the mantle layer of the spinal cord segments, mitoses were only observed in glial cells. It should be noted that the intensity of glial cell mitoses was relatively higher in the posterior horns compared to the anterior horns, which may be associated with the relatively higher cell density in this area of the segments. In qualitative terms, Ki-67 expression in the posterior horns was weak, with 8 % of cells reacting, while in the anterior horns, it was 3 %. No mitoses of neuroblasts were detected in the mantle layer.

In fetuses at 39-40 weeks, vimentin expression was relatively weak in the remnants of radial glia surrounding the neuroepithelial layer. No vimentin expression was observed in the neuroepithelium itself, while focal vimentin expression was detected around blood vessels (see Fig. 2). Therefore, the absence of vimentin expression in the neuroepithelial layer indicates the absence of radial cells among the epithelial cells of the neuroepithelium.

S-100 expression in the segments of the spinal cord is relatively strong at the base of the anterior and posterior horns. There is a relatively higher density of glial cells in the posterior horns compared to the anterior horns. Specifically, S-100 expression occurred in 98 % of glial cells in the posterior horns and in 77 % of glial cells in the anterior horns (see Fig. 2).

Discussion

In their study, A. Ruiz-Sauri et al. [12] indicate that during the first half of the prenatal period, the intensity of mitosis in neural stem cells occurs more prominently in the ventral neuroepithelium than in the dorsal neuroepithelium. However, this pattern changes to the opposite before birth.

In our study, overall, evaluating the expression of Ki-67 in the neuroepithelium of the segments during this age period using a semi-quantitative scale, it was weak in both the ventral and dorsal regions. In terms of percentage, the cell expression accounted for 6 % in the ventral region and 3 % in the dorsal region.

It should be noted that further differentiation of neuroblasts takes place in the mantle layer itself. We did not observe neuroblast proliferation. In the gray matter of the anterior horns, the expression of Ki-67 in glial cells was weak, as only 10 % of the cells showed expression. The proliferation of satellite glial cells in the anterior horns was also low, with only 1-2 mitotic cells observed. Relative cell density was maintained in the gray matter of the posterior horns, despite a relatively low intensity of mitosis in glial cells within the posterior horns. The expression of Ki-67 in the mantle layer of the posterior horns was also weak, accounting for 17 % of the cells. The degree of Ki-67 expression in the marginal layer was quantitatively weak, where mitoses were observed in 6 % of the cells.

The results of our study coincide with the findings of V. S. Shkolnikov et al. [14], who state that strong expression in the fibers of the radial glia in the spinal cord segments occurs until the 17-18th week. Subsequently, a gradual involution of the radial glia takes place, and by birth, the expression of vimentin is observed only in its remnants within the neuroglial complexes and along blood vessels.

During the investigation of CDX-2 expression in the fibers of the radial glia in the spinal cord segments, it was found that for this age period, the expression of this protein is absent. The results of the study by V. S. Shkolnikov and S. V. Vernygorodskyi [13] provide data indicating that CDX-2 expression in the fibers of the spinal cord radial glia occurs only during the embryonic period.

Evidence that in the human fetal spinal cord at 39-40 weeks, the neuroepithelium is composed of ependymocytes and the absence of radial glial cells is the relatively strong expression of S-100 in the neuroepithelium. It should be noted that some neurons also exhibited S-100 expression. In their study, S. Skarlatou et al. [15] support the idea that S-100 is not expressed in neurons before birth, which is consistent with our findings at 39-40 weeks. In the neuroepithelial layer, radial glial cells are absent.

The relatively strong expression of synaptophysin in the gray matter of the spinal cord segments at 39-40 weeks, especially within the neuro-glia complexes, indicates the ongoing processes of establishing interneuronal connections and myelination of nerve fibers that continue until birth. However, synaptophysin expression is absent in the neuroepithelium proper.

The prospect of further research lies in studying the peculiarities of immunohistochemical marker expression in the formations of the spinal cord in mature individuals and comparing the obtained results with similar ones in fetuses.

Conclusion

1. At 35-36 weeks, the proliferation of neural stem cells is more intensive in the ventral neuroepithelium compared to the dorsal neuroepithelium. However, at 39-40 weeks, the proliferation of neural stem cells in the dorsal neuroepithelium becomes relatively higher than in the ventral neuroepithelium.

2. The vimentin expression indicates that at 35-36 weeks, radial glia is present around the neuroepithelium and in the posterior horns. However, by the time of birth, radial glia is only retained near the blood vessels of the gray matter segments.

3. Until birth, there is a relatively strong expression of S-100 in the glial cells of both the anterior and posterior horns.

4. The relatively strong expression of synaptophysin in the gray matter of the spinal cord segments, especially within the neuroglial complexes, indicates the ongoing processes of establishing interneuronal connections and myelination of nerve fibers.

References

[1] Cai, W., Liu, H., Zhao, J., Chen, L. Y., Chen, J., Lu, Z., & Hu, X. (2017). Pericytes in brain injury and repair after ischemic stroke. *Translational Stroke Research,* 8, 107-121. doi: 10.1007/s12975-016-0504-4

[2] Cassaro, M., Rugge, M., Tieppo, C., Giacomelli, L., Velo, D., Nitti, D., & Farinati, F. (2007). Indefinite for non-invasive neoplasia lesions in gastric intestinal metaplasia: the immunophenotype. *Journal of Clinical Pathology,* 60(6), 615-621. doi: 10.1136/jcp.2006.040386

[3] Cedeno, D. L., Smith, W. J., Kelley, C. A., & Vallejo, R. (2020). Spinal cord stimulation using differential target multiplexed programming modulates neural cell-specific transcriptomes in an animal model of neuropathic pain. *Molecular Pain,* 16, 1744806920964360. doi: 10.1177/1744806920964360

[4] Haring, M., Zeisel, A., Hochgerner, H., Rinwa, P., Jakobsson, J. E., Lonnerberg, P., ... & Ernfors, P. (2018). Neuronal atlas of the dorsal horn defines its architecture and links sensory input to transcriptional cell types. *Nature Neuroscience,* 21(6), 869-880. doi: 10.1038/s41593-018-0141-1

[5] Hawthorne, A. L. (2014). Repurposing Reelin: The new role of radial glia, Reelin and Notch in motor neuron migration. *Experimental Neurology,* 256, 17-20. doi: 10.1016/j.expneurol.2014.02.024

[6] Hori, K., & Hoshino, M. (2012). GABA-ergic neuron specification in the spinal cord, the cerebellum, and the cochlear nucleus. Neural Plasticity, 2012. doi: 10.1155/2012/921732

[7] Ma, J. J., Zhang, T. Y., Diao, X. T., Yao, L., Li, Y. X., Suo, Z. W., ... & Liu, Y. N. (2021). BDNF modulated KCC2 ubiquitylation in spinal cord dorsal horn of mice. European Journal of Pharmacology, 906, 174205. doi: 10.1016/j.ejphar.2021.174205

[8] Mauti, O., Sadhu, R., Gemayel, J., Gesemann, M., & Stoeckli, E. T. (2006). Expression patterns of plexins and neuropilins are consistent with cooperative and separate functions during neural development. *BMC Developmental Biology,* 6(1), 1-13. doi: 10.1186/1471-213X-6-32

[9] Peirs, C., Williams, S. P. G., Zhao, X., Arokiaraj, C. M., Ferreira, D. W., Noh, M. C., ... & Seal, R. P. (2021). Mechanical allodynia circuitry in the dorsal horn is defined by the nature of the injury. *Neuron,* 109(1), 73-90. doi: 10.1016/j.neuron.2020.10.027

[10] Petit, A., Sanders, A. D., Kennedy, T. E., Tetzlaff, W., Glattfelder, K. J., Dalley, R. A., ... & Roskams, A. J. (2011). Adult spinal cord radial glia display a unique progenitor phenotype. *PloS One,* 6(9), e24538. doi: 10.1371/journal.pone.0024538

[11] Prajerova, I., Honsa, P., Chvatal, A., & Anderova, M. (2010). Neural stem/progenitor cells derived from the embryonic dorsal telencephalon of D6/GFP mice differentiate primarily into neurons after transplantation into a cortical lesion. *Cellular and Molecular Neurobiology,* 30, 199-218. doi: 10.1007/s10571-009-9443-x

[12] Ruiz-Sauri, A., Orduna-Valls, J. M., Blasco-Serra, A., Tornero-Tornero, C., Cedeno, D. L., Bejarano-Quisoboni, D., ... & Vallejo, R. (2019). Glia to neuron ratio in the posterior aspect of the human spinal cord at thoracic segments relevant to spinal cord stimulation. *Journal of Anatomy*, 235(5), 997-1006. doi: 10.1111/joa.13061

[13] Shkolnikov, V. S., & Vernygorodskyi, S. V. (2017). Особливості структурної організації сегментів спинного мозку плодів людини з аненцефалією 17-18 тижнів внутрішньоутробного розвитку [Peculiarities of spinal cord segments structural organization in human fetuses with anencephaly of 17-18 weeks of intrauterine development]. *Патологія - Pathologia,* 1(39), 100-106. doi: 10.14739/2310-1237.2017.1.97226

[14] Shkolnikov, V. S., Prykhodko, S. O., Polishchuk, S. S., Kryvoviaz, O. V., & Galunko, G. M. (2020). Морфологія радіальної глії спинного мозку ембріонів та плодів людини [The morphology of radial glial spinal cord of embryos and human fetuses]. *Світ біології та медицини - World of Medicine and Biology,* 2(72), 229-334. doi: 10.26724/2079-8334-2020-2-72-229-234

[15] Skarlatou, S., Herent, C., Toscano, E., Mendes, C. S., Bouvier, J., & Zampieri, N. (2020). Afadin signaling at the spinal neuroepithelium regulates central canal formation and gait selection. *Cell Reports,* 31(10), 107741. doi: 10.1016/j.celrep.2020.107741

[16] Znamenskaya, T. K., Martyniuk, V. Yu., & Shveikina, V. B. (2019). Морфофункціональні особливості розвитку головного мозку та системи кровообігу в онтогенезі [Morphofunctional peculiarities of brain development and circulatory system in ontogenesis]. *Міжнародний неврологічний журнал - International Neurological Journal,* 6(108), 17-29. doi: 10.22141/2224-0713.6.108.2019.180531

[17] Zozulya, Yu. A., Malysheva, T. A., Rozumenko, V. D., Orlov, Yu. A., & Shamayev, M. I. (2012). Ембріологічні та молекулярно-генетичні механізми патогенезу пухлин головного мозку [The embryology and molecular-genetic mechanisms of brain tumor pathogenesis]. *Український нейрохірургічний журнал - Ukrainian Neurosurgical Journal,* (1), 23-31.

ІМУНОГІСТОХІМІЧНА ХАРАКТЕРИСТИКА СІРОЇ РЕЧОВИНИ СПИННОГО МОЗКУ ЛЮДИНИ У ПІЗНЬОМУ ПРЕНАТАЛЬНОМУ ПЕРІОДІ

Довгань О. В., Власенко О. В., Попадинець О. Г., Семененко А. І., Гунас І. В., Бобрук В. П.

Дослідження присвячене актуальній проблемі вивчення закономірностей вікової (пренатальної) перебудови утворів головного та спинного мозку та надає можливості щодо прогнозування та корекції виникнення вроджених вад. Метою дослідження було встановлення характеру експресії імуногістохімічних маркерів у структурах сірої речовини спинного мозку людини у пізньому пренатальному періоді. Матеріалом для дослідження слугували препарати спинного мозку 27 плодів людини гестаційним терміном 35-40 тижнів. Під час проведення дослідження використані наступні методи: анатомічні, загальні гістологічні, спеціальні гістологічні, імуногістохімічні, морфометричні та статистичний аналіз отриманих даних. Встановлено, що у 35-36 тижнів гестаційного періоду проліферація нейральних стовбурових клітин (НСК) більш інтенсивно відбувається у вентральному нейроепітелії сегментів спинного мозку, ніж у дорзальному. У вентральному нейроепітелії налічується 5-6 мітотичних, або постмітотичних НСК, в той же час у дорзальній частині - 2-3 клітини. У плодів 39-40 тижнів проліферативна активність нейральних стовбурових клітин у дорзальному нейроепітелії є вищою у шийних і поперекових сегментах, де експресія Кі-67 відмічена в 6 % клітин (прореагувало 7-8 клітин), у грудних та крижових сегментах - 4 % (прореагувало 3-4 клітин). На відміну від дорзального нейроепітелію у вентральній частині нейроепітелію сегментів проліферативна активність нейральних стовбурових клітин дещо меншої інтенсивності. Так, у шийних та поперекових сегментах експресія Кі-67 відбулась у 4 % клітин (прореагувало 3-4 клітини) та у грудних і крижових - 2 % (прореагувало 1-2 клітини). У 35-36 тижнів гестації висока експресія віментину встановлена навколо нейроепітелію, в основі задніх рогів та вздовж задньої серединної перегородки. У мантійному шарі експресія віментину була відносно слабкою та зберігалась уздовж судин та у місці формування корінців спинного мозку. До народження у залишках радіальної глії навколо нейроепітеліального шару встановлена відносно слабка експресія віментину. У самому нейроепітелії експресія віментину була відсутньою, але навколо судин спостерігалась вогнищева експресія віментину. Відсутність експресії віментину у нейроепітелії свідчить про зникнення радіальних клітин. У 35-40 тижнів гестаційного періоду у сегментах спинного мозку встановлена відносно сильна експресія синаптофізину у мантійному шарі, що свідчить про інтенсивність процесів встановлення нейрональних зв'язків та мієлінізації нервових волокон. До народження дані процеси не закінчуються. Безпосередньо в нейроепітелії експресія синаптофізину відсутня.

Ключові слова: *головний мозок, спинний мозок, центральна нервова система, радіальна глія, нейральні стовбурові клітини, пренатальний період, імуногістохімія, нейрон.*

DOI: 10.31393/morphology-journal-2023-29(2)-05 Reports of Morphology, Vol. 29, №2, Pages 32-37

ISSN 1818-1295 eISSN 2616-6194

REPORTS OF MORPHOLOGY

Official Journal of the Scientific Society of Anatomists, Histologists, Embryologists and Topographic Anatomists of Ukraine

journal homepage: https://morphology-journal.com

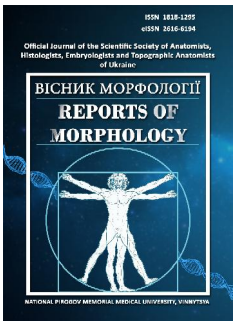

Morphological features of stab-cut wounds of the skin of the trunk and limbs inflicted by kitchen knives

Boymanov F. Kh.[1], Kushbakov A. M.[1], Rashidov F. F.[2]

[1]Samarkand State Medical University, Samarkand, Republic of Uzbekistan
[2]Republican Scientific and Practical Center of Forensic Medical Examination Samarkand Branch, Samarkand, Republic of Uzbekistan

ARTICLE INFO
Received: 09 February 2023
Accepted: 14 March 2023

UDC: 340.6:576.31:616-001.4.77

CORRESPONDING AUTHOR
e-mail: boymanovf@mail.ru
Boymanov F. Kh.

CONFLICT OF INTEREST
The authors have no conflicts of interest to declare.

FUNDING
Not applicable.

Examination of injuries caused by sharp objects is a complex process that requires the application of a whole range of knowledge not only in the field of forensic medicine, but also in human anatomy. Among all sharp objects, stab-cut objects are the most common, namely the kitchen knife. Researching the peculiarities of the morphology of injuries to various anatomical parts of the human body with this subject would improve the quality of forensic research. The purpose of the study is to analyze the morphological features of stab-cut wounds to the skin of the trunk and limbs caused by kitchen knives. A forensic examination of 93 stab wounds of corpses, which were inflicted by kitchen knives with one-sided sharpening and a straight butt, was carried out. Wounds in the chest ranged in size from 1.7x0.2 cm to 4.3x0.6 cm; wounds in the abdomen ranged in size from 1.8x0.4 cm to 3.3x0.7 cm; wounds in the lumbar region had sizes from 1.7x0.2 cm to 4.0x0.6 cm; wounds on the upper extremities - from 1.5x0.9 cm to 3.0x0.6 cm and wounds on the lower extremities from 1.5x0.2 cm to 3.2x0.6 cm. In all cases, the wounds had even edges and a smooth surface of the walls. Wounds located along Langer's line have a linear shape, and those located across Langer's lines have an oval shape. In addition, a different shape of the butt section was found, depending on the localization and the force of immersion. In this way, characteristic differences in the shape of the butt cut were revealed and the existence of differences in its morphology in different anatomical parts of the body was proved. Taking into account the location of the injury according to the location of Langer's lines should be standard procedure in forensic investigations of injuries caused by sharp objects.

Keywords: *stab-cut wound, skin, torso, limbs, kitchen knives.*

Introduction

The classification of tools and the types of wounds they cause is one of the key issues of forensic medicine, because it is critical for the correct interpretation of the phenomenon and its further evaluation from a legal point of view. Classically, such types of wounds as incised, stab, slash and chop are distinguished in forensic medicine [17].

Stab wounds are one of the most common types of wounds, which are formed as a result of the action of the most common sharp object in everyday life - a knife [9]. Indeed, an analysis of homicides in Scotland between 2006 and 2011 found that a kitchen knife was used in 94 % of all homicides involving sharp objects [15]. In 29 % of cases, the use of stab items can end fatally. In most cases (79 %), this category of items is used against the background of alcohol consumption [16].

Stab wounds occupy a leading place in the structure of injuries caused by sharp objects. According to static data, in the vast majority of cases (97.8 %), when inflicting stab damage, knives with one-sided blade sharpening (knives with a butt and a blade) are used [10, 14]. Data from emergency services in the United States from 1990 to 2008 indicate that more than 8 million knife wounds were treated, which is equivalent to 119 wounds per day. The most frequent injuries were localized on the fingers (66 %) and were caused by pocket knives (47 %) or kitchen knives (36 %) [21].

M. U. H. Chowdury with co-authors [8], analyzing the data of fatal cases with the use of stab objects, indicate that 90 % of the victims are men, and the most common localization of damage is the chest with damage to the lungs or heart. Abdominal injuries with damage to the stomach or liver are less common. The third most common

type is multiple wounds on the front and back of the body. The least common type of injury is localization of the lower extremities with damage to a large blood vessel. Similar data on the localization of injuries were also obtained by Norwegian researchers [16].

For the tasks of forensic medical examination, a detailed study of the morphological and morphometric features of stab wounds of clothing, skin, cartilage, bones and internal organs continues. It is emphasized that a thorough study of the macro- and microscopic signs of the wound facilitates the diagnosis of the main properties of the stab object. There is also evidence that the nature, morphology and metric properties of stab wounds of the skin depend on their localization on the human body [2, 11].

One of the parameters that is important in the formation of wounds on the human body is Langer's lines. Their concept was first derived in 1861 by Professor Karl Langer, who in turn performed an analysis of the data of Dupuytren and Malgaigne, who described the shape of injuries on the body of people who survived a suicide attempt, which did not match the shape of the object that caused them and in later confirmed this experimentally on human corpses. Langer, on the other hand, carried out a systematic study on the entire surface of corpses of people (of different ages - from embryos to elderly people; of different physiques, in particular, children with obesity), documenting not only macroscopic changes, but also microscopic ones, in particular, type I collagen fibers, which form a specific diamond-shaped grid, which is the cause of this phenomenon [1, 7].

Another factor that should be taken into account when working with pieces of skin with wounds removed for forensic examination is the change in the shape and size of the damage under the influence of fixing substances. Thus, in one of the studies, damage to the skin of the abdomen decreased by 11 % [23].

Such prevalence of injuries caused by stab objects and the mass of factors that change the pattern of injury require comprehensive research on various anatomical parts of the human body, taking into account Langer's lines.

The purpose of the study is to analyze the morphological features of stab wounds to the skin of the body and limbs caused by kitchen knives.

Materials and methods

The stab wounds of the skin taken from 93 corpses of persons, inflicted by common kitchen knives with one-sided sharpening and a straight butt, were studied. It was revealed that in 79 cases the wounds were multiple, in 14 - single.

The conducted research does not contradict the basic bioethical norms of the Declaration of Helsinki, the Convention of the Council of Europe on Human Rights and Biomedicine (1977), the relevant provisions of the WHO and the laws of the Republic of Uzbekistan.

The study of skin wounds was carried out in stages, using forensic research methods. The following signs of wounds were studied: the length, width of the wound, the shape of the ends (the shape of the blade and butt ends), the nature of the edges, the surface of the walls and the bottom of the wound, the length of the wound channel, the location of the wounds relative to the Langer lines.

Results

Most of the injuries were localized in the chest area (44), and more often they were oriented obliquely. In 27 cases, the wounds were located in the abdomen with a predominance of oblique orientation. 16 wounds were found in the limbs, most of them were oriented obliquely, 6 - in the lumbar region, more often oblique.

Wounds in the chest area, located along the Langer lines, had a linear shape, and those located across the Langer lines had an oval shape. The edges of the wounds are even, the surface of the walls is smooth, the blade end is sharp, and the butt end is U-shaped (Fig. 1). The size of the wounds varied from 1.7x0.2 cm to 4.3x0.6 cm. The length of the wound channels in chest injuries largely depended on the anatomical and physiological characteristics of the damaged organs. In some cases, the wound channel ended blindly in the lung, which caused a decrease in the volume of this organ due to developed hemo-, pneumo- or hemopneumothorax. In most cases, it was impossible to trace the wound channel to the end.

The wounds located in the abdomen, due to the elasticity of the skin, had a more pronounced oval shape with smooth edges, and when comparing the edges, they had a linear-

Fig. 1. Stab wound of the chest.

Fig. 2. Stab wound of the left iliac region.

slit shape. The wounds had smooth edges, a smooth surface of the walls, the ends were acute-angled on the side of the blade, M-shaped on the side of the butt. The wound sizes ranged from 1.8x0.4 cm to 3.3x0.7 cm (Fig. 2). With abdominal injuries, the length of the wound channel may be underestimated due to the fact that the measurement of its length was carried out in a horizontal position of the body. Since the wounds were received in a vertical position of the body, there is a displacement of the abdominal organs downward. When determining the length of the wound channel on a corpse, an error may occur due to some retraction of the anterior abdominal wall.

Stab wounds of the lumbar region have a more pronounced oval shape, smooth edges, a smooth surface of the wall, the ends are acute-angled on the blade side, T-shaped - on the butt side. The size of the wounds varied from 1.7x0.2 cm to 4.0x0.6 cm. Wounds of this localization may have an additional incision (Fig. 3).

Stab wounds of the limbs were more often located on the upper limb, mainly on the outer surface of the shoulders. They often had a linear, less often linear-oval shape and a gaping appearance due to the contraction of well-developed muscles. In addition, there was a dependence of the form of wounds on the degree of development of subcutaneous fat, the position and depth of immersion of the blade. The wounds had even edges and a smooth wall surface. The size of the wounds ranged from 1.5x0.9 cm to 3.0x0.6 cm. The ends of the wounds were acute-angled on the blade side, T-shaped on the butt side. The overhanging nature of the upper edge of the wound was often noted in the direction from bottom to top and somewhat from left to right. The shape of the butt end can also be L- and U-shaped.

Stab wounds of the lower extremities were located more often on the posterior-outer surface, less often on the inner-lateral surface of the thigh. They had an arcuate-linear, angular, elongated shape, a gaping appearance due to muscle contraction. The shape of the wounds was

Fig. 3. Skin flap of the left lumbar region containing a stab wound with an additional incision.

Fig. 4. Skin flap with a stab wound of the inner surface in the lower third of the right thigh.

influenced by the position and depth of the blade. The dimensions of the wounds were from 1.5x0.2 cm to 3.2x0.6 cm, the edges were even, the surface of the walls was smooth, the ends on the blade side were sharp, on the other side of the butt side L-, U-shaped. With these types of wounds, the directions of the wound channels were easily determined. They were directed from top to bottom, from front to back, somewhat from left to right (Fig. 4).

The stab wounds of the upper and lower extremities, located along the lines of Langer, had the same semi-open shape; and the wounds located across the lines of Langer had an oval shape, their edges were open. Along with this, their relationship with the location and direction of the muscles located in this area was observed.

Discussion

Our study confirms the known data that stab wounds are most often localized on the trunk [13, 18]. In a previous study, we established that the most common location for all sharp objects is the chest area (46.6 %). Wounds in the abdomen (28.2 %), limbs (17.5 %) and lower back (7.7 %) were less common. In all cases, the oblique-longitudinal orientation of the wounds prevailed [5].

Also, the data of our previous studies confirm the data of other researchers regarding the predominant number of stab injuries in men. When injuries are caused by national Uzbek knives, the wounds usually have an angular, oval or linear shape. The blade end is classically sharp, while the obtuse end has a different morphological characteristic U-, L-, and T-shaped shapes are noted [6].

Data from literary sources indicate a rare localization of stab injuries in the head or neck region. While injuries to the left half of the chest are quite common and the most dangerous location for stab injuries. It has been noted that this predominant localization of injuries is associated with the deep conviction of the killers that the heart is completely located only in the left part of the chest and that its damage will lead to quick death [20].

In our study, chest area stab wounds amounted to 74.7 %. We agree with the opinion of the authors that the dynamics of the traumatic effect of piercing-cutting objects forms certain morphological features in the wound, which make it possible to identify the traumatic object [22]. The analysis of our data on the study of stab wounds indicates that in all cases there was no complete immersion of the blade, since we did not find additional signs at the ends of the wounds formed by the heel or beard of the blade.

It is known that the trace-perceiving surface of various parts of the body is not uniform. From one knife, damages can be formed that have different metric and morphological features, imitating the actions of various trace-forming objects. It has been established that the most complete morphology of the trace-perceiving elements, which make it possible to identify the damaging object, is reflected in preparations from the back and thigh [3]. This statement does not exclude, but rather suggests further comparative study of wounds of different localizations formed by the same type of knives.

At the same time, important attention should be paid to various types of sharp objects that can cause stab wounds. Thus, in the study of Bolliger S. A. and co-authors [4], the force required to damage the entire thickness of the skin with a pocket knife and paring knife was analyzed on biological imitators of human skin. For the former, the minimum penetration force was 1900 g and for the latter 700 g, which is an unexpected result, given the seemingly identical nature of the knives from the point of view of forensic medicine.

C. Humphrey and colleagues [12] performed an experimental study by stabbing the limbs of pigs with different types of knives. The authors noted a correlation between the strength and the number (r=0.69), width (r=0.63) and depth (r=0.57) of injuries that occurred on the bones of the limbs. In addition, the authors draw attention to the difference in the appearance of wounds caused by knives with and without serrations.

Another group of researchers analyzed injuries caused by stab objects when thrown into an object. In general, the authors indicate that the nature of the injury is largely influenced by the weight of the object, the way it was thrown, and the distance to the object. So, heavy objects such as a chef's knife or a skin pick can penetrate deeply into the body even at a distance of 4 meters. Heavy objects of this type cause damage more than 6 cm deep [19].

In this way, it is possible to point to the existence of a whole array of different research methods for studying the effect of stab objects, which confirms the relevance of studying the effect of sharp objects on the human body. The features of stab wounds that we have identified can contribute to their differentiation depending on the localization on the body.

Conclusion

1. The study of stab-cut injuries caused by the most common kitchen knives showed that all the wounds we examined had smooth edges and walls with a smooth surface. However, there is a difference in the shape of the wound depending on their localization.

2. Wounds in the chest area, located along the Langer line, have a linear shape, and located across the Langer lines - an oval shape. Stab-cut injuries of the abdomen had a more pronounced oval shape, as well as wounds located in the lumbar region. The wounds of the limbs have an arcuate-linear, semi-open shape.

3. A different shape of the butt section was found. For chest wounds in the region of the butt, a U-shaped incision is characteristic, the abdomen is M-shaped, and the lower back is T-shaped. For wounds of the upper extremities, the butt incision can be T-shaped, L- and U-shaped, for the lower extremities - L-shaped and U-shaped. The blade edge of stab-cut injuries is sharp in all cases.

References

[1] Abyaneh, M. A. Y., Griffith, R., Falto-Aizpurua, L., & Nouri, K. (2014). Famous lines in history: Langer lines. *JAMA Dermatology,* 150(10), 1087-1087. doi: 10.1001/jamadermatol.2014.659

[2] Andreyko, L. L. (2008). Исторические аспекты изучения колото-резаных повреждений (по данным литературы) [Historical aspects of the study of stab injuries (according to the literature)]. *Избранные вопросы судебно-медицинской экспертизы - Selected Issues of Forensic Medical Examination*, 9, 46-51.

[3] Avdeev, A. I., & Chernyshov, K. A. (2007). Dependence of the morphological and metric properties of stab wounds on the localization of injuries on the human body. *Far Eastern Medical Journal*, (3), 94-96.

[4] Bolliger, S. A., Wallace, E., Dobay, A., Froehlich Knaute, D., Thali, M. J., & Barrera, V. (2020). The cutting edge - an investigation into the pressure necessary for cutting skin with different knife blade types. *International Journal of Legal Medicine,* 134, 1133-1140. doi: 10.1007/s00414-020-02270-8

[5] Boymanov, F. H., Indiaminov, S. I., & Mardonov, T. M. (2018). Differences between morphology and morphometric indices of incised-stab wounds depending on their localization on the body. *Bukovinian Medical Herald,* 22(2(86)), 10-14. doi: 10.24061/2413-0737.XXII.2.86.2018.26

[6] Boymanov, F. K., & Kushbakov, A. M. (2023). Morphological features of heart damages caused by national Uzbek knives. *Reports of Morphology,* 29(1), 46-49. doi: 10.31393/morphology-journal-2023-29(1)-07

[7] Carmichael, S. W. (2014). The tangled web of Langer's lines. *Clinical Anatomy,* 27(2), 162-168. doi: 10.1002/ca.22278

[8] Chowdury, M. U. H., Rubel, A. M. S. A., Uddin, M. S., Deb, K., & Jahan, C. R. (2019). Injury Pattern in Fatal Cases of Stab Wound. *Medicine Today,* 31(2), 76-79. doi: 10.3329/medtoday.v31i2.41955

[9] Dettmeyer, R. B., Verhoff, M. A., & Schutz, H. F. (2014). Pointed, sharp, and semi-sharp force trauma. *Forensic Medicine: Fundamentals and Perspectives*, 135-153. doi: 10.1007/978-3-642-38818-7_9

[10] Gedygushev, I. A. (1999). *Судебно-медицинская экспертиза при реконструкции обстоятельств и условий причинения повреждений (методология и практика) [Forensic medical examination in the reconstruction of the circumstances and conditions of damage (methodology and practice)].* Москва, 2 - Moscow, 2.

[11] Green, M. A. (1978). Stab wound dynamics - a recording technique for use in medico-legal investigations. *Journal of the Forensic Science Society,* 18(3-4), 161-163. doi: 10.1016/s0015-7368(78)71196-5

[12] Humphrey, C., Kumaratilake, J., & Henneberg, M. (2017). Characteristics of bone injuries resulting from knife wounds incised with different forces. *Journal of Forensic Sciences,* 62(6), 1445-1451. doi: 10.1111/1556-4029.13467

[13] Ivanov, I. N. (2001). Современное состояние и перспективные направления научных исследований судебно-медицинской экспертизы колото-резаных повреждений [Current state and promising areas of scientific research in forensic medical examination of stab injuries]. *Альманах судебной медицины - Almanac of Forensic Medicine,* 4(2), 35-37.

[14] Jacques, R., Kogon, S., & Shkrum, M. (2014). An experimental model of tool mark striations by a serrated blade in human soft tissues. *The American Journal of Forensic Medicine and Pathology,* 35(1), 59-61. doi: 10.1097/PAF.0000000000000078

[15] Kidd, S. H., Hughes, N. S., & Crichton, J. H. (2014). Kitchen knives and homicide: A systematic study of people charged with murder in the Lothian and Borders region of Scotland. *Medicine, Science and the Law,* 54(3), 167-173. doi: 10.1177/0025802413496409

[16] Kristoffersen, S., Normann, S. A., Morild, I., Lilleng, P. K., & Heltne, J. K. (2016). The hazard of sharp force injuries: Factors influencing outcome. *Journal of Forensic and Legal Medicine,* 37, 71-77. doi: 10.1016/j.jflm.2015.10.005

[17] Payne-James, J. J. (2016). *Injury, fatal and nonfatal: Sharp and cutting-edge wounds. Encyclopedia of Forensic and Legal Medicine*. Philadelphia, USA: Elsevier, 244-256. doi: 10.1016/B978-0-12-800034-2.00223-8

[18] Sarkisyan, B. A., & Fedorov, S. Yu. (2014). Morphological features of stab-cut skin lesions inflicted by blades with different shapes of the end part through a multilayer barrier. *Forensic Medicine,* 57(2), 28-31.

[19] Schaerli, S., Schulz, R., Gascho, D., Enders, M., Baumann, S., Thali, M. J., & Bolliger, S. A. (2018). Injury potential of thrown sharp kitchen and household utensils. *Forensic Science, Medicine and Pathology,* 14, 31-41. doi: 10.1007/s12024-017-9937-7

[20] Sitepu, A. (2022). Stab Wound on Chest. Interdisciplinary Social Studies, 1(12), 1438-1445. doi: 10.55324/iss.v1i12.288

[21] Smith, G. A. (2013). Knife-related injuries treated in United States emergency departments, 1990-2008. *The Journal of Emergency Medicine,* 45(3), 315-323. doi: 10.1016/j.jemermed.2012.11.092

[22] Zakirov, T. R., & Viter, V. I. (2008). Анализ признаков колото-резаных ран по данным медико-криминалистических исследований [Analysis of the signs of stab wounds according to the data of medical and forensic studies]. *Проблемы экспертизы в медицине - Problems of Expertise in Medicine,* 8(29-1), 10-11.

[23] Zohn, A., & Melinek, J. (2017). Which knife was used? : using a porcine model to assess stab wound size. The American *Journal of Forensic Medicine and Pathology,* 38(3), 180-183. doi: 10.1097/PAF.0000000000000318

МОРФОЛОГІЧНІ ОСОБЛИВОСТІ КОЛОТО-РІЗАНИХ РАН ШКІРИ ТУЛУБА ТА КІНЦІВОК ЗАВДАНИХ КУХОННИМИ НОЖАМИ

Бойманов Ф. Х., Кушбаков А. М., Рашидов Ф. Ф.

Експертиза травм, заподіяних гострими предметами, є складним і комплексним процесом, що вимагає застосування цілого роду знань не тільки з області судової медицини, але й з анатомії людини. Серед усіх гострих предметів найбільшу розповсюдженість мають колючо-ріжучі предмети, а саме такий предмет побуду, що їх заподіює - кухонний ніж. Дослідження особливостей морфології ушкоджень різних анатомічних ділянок тіла людини даним предметом дозволив би поліпшити якість криміналістичних досліджень. Мета дослідження - провести аналіз особливостей морфології колото-різаних ран шкіри тулуба та кінцівок, завданих кухонними ножами. Проведено криміналістичне дослідження 93 колото-різаних ран трупів, котрі були завдані кухонними ножами з односторонньою заточкою і прямим обухом. Рани в ділянці грудей мали розміри від 1.7x0.2 см до 4.3x0.6 см; рани в ділянці живота мали розміри від 1.8x0.4 см до 3.3x0.7 см; рани в поперековій

ділянці мали розміри від 1.7x0.2 см до 4.0x0.6 см; рани на верхніх кінцівках - від 1.5x0.9 см до 3.0x0.6 см і рани на нижніх кінцівках - від 1.5x0.2 см до 3.2x0.6 см. В усіх випадках рани мали рівні краї та гладеньку поверхню стінок. Рани, котрі розташовані по ходу лінії Лангера мали лінійну форму, а ті, котрі розташовані поперек ліній Лангера - овальну. Крім того, виявлено різну форму обушкового розрізу в залежності від локалізації та сили занурення. Таким чином, виявлено характерні відмінності у формі обушкового розрізу і доведено існування відмінностей у його морфології в різних анатомічних ділянках тіла. Прийняття до уваги локалізацію ушкодження відповідно до розташування ліній Лангера має бути стандартною процедурою при проведенні криміналістичних досліджень ушкоджень, заподіяних гострими предметами.
Ключові слова: *колото-різана рана, шкіра, тулуб, кінцівки, кухонні ножі.*

DOI: 10.31393/morphology-journal-2023-29(2)-06 Reports of Morphology, Vol. 29, №2, Pages 38-44

ISSN 1818-1295 eISSN 2616-6194

REPORTS OF MORPHOLOGY

Official Journal of the Scientific Society of Anatomists, Histologists, Embryologists and Topographic Anatomists of Ukraine

journal homepage: https://morphology-journal.com

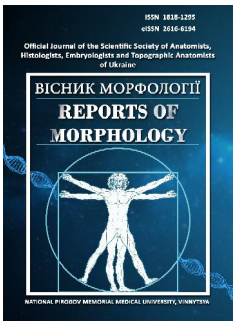

Simulation of peritoneal sepsis and its treatment with serum in an experiment: peculiarities of morphological disorders of liver, spleen and kidney tissues

Hnativ V. V., Plytka O. V.

I. Horbachevsky Ternopil National Medical University, Ternopil, Ukraine

ARTICLE INFO

Received: 15 February 2023

Accepted: 17 March 2023

UDC: 616.36/.411/.61-091.8:616.94:616.831-002]-085.383-092.9

CORRESPONDING AUTHOR

e-mail: plytka@tdmu.edu.ua

Plytka O. V.

CONFLICT OF INTEREST

The authors have no conflicts of interest to declare.

FUNDING

Not applicable.

Sepsis develops as a normal inflammatory response to various infections. It proceeds with the picture of a complex heterogeneous syndrome, which often leads to the development of multiple organ failure. The number of affected organs correlates with mortality. Organ failure is characterized by a sequence - initially pulmonary, then renal, cardiovascular, and in the terminal stage, there is a failure of the central nervous system function. The aim of the study was to model peritoneal sepsis in an experiment, develop a therapeutic serum as an analog of anti-reticular cytotoxic serum by O. O. Bogomolets (ACS), and investigate the therapeutic properties and specific morphological changes in the liver, spleen, and kidneys of septic and treated animals. To simulate peritoneal sepsis, laboratory mice were injected intraperitoneally with a solution of 10 % of filtered fecal suspension of guinea pig (from 0.05 to 3.0 ml), the level of the toxic dose at which all mice died was determined (0.35 ml of fecal suspension) after that lethal bloodletting was administered under thiopental anesthesia. Their spleens were removed, from which therapeutic serum was made. Guinea pigs of the experimental group were injected with a suspension of the spleen of mice with an increasing dose from 0.02 to 0.2 ml after the simulation of fecal peritonitis. The optimal therapeutic dose at which the ants continued to live for 14 days was determined: 0.08 ml. Under thiopental anesthesia (50 mg/kg), their liver, kidneys, and spleen were taken for histological studies. The processing of the obtained histological specimens was carried out according to generally accepted methods. Histological preparations were studied using an SEO SCAN light microscope. It was found that under conditions of peritoneal sepsis in the liver, the lobular organization of hepatocytes was dramatically disturbed. The central veins and vessels of the portal tracts were moderately dilated and filled with blood, but the lumens of the sinusoids were practically not visualized. The sizes of hepatocytes increased sharply, contours were erased, and intercellular connections were disrupted. Histological examination of the kidney revealed a drastic decrease in the blood volume in the vessels of the arterial bed, which is visualized by the structural manifestations in the cortical layer. Collaptoid shrinkage of glomerular vessels was observed, which manifested in their sharp reduction in size. A significant part of the endotheliocytes was damaged. Examination of the spleen revealed a significant increase in the area of the red pulp due to the pronounced expansion of the sinusoids and an increase in their blood supply. The white pulp exhibited small, moderately diffuse foci of lymphocyte clusters. Follicle structures were practically not visualized. Histological examination of the liver in animals with simulated peritoneal sepsis on the background of correction with an extract from the spleen of mice revealed a moderate expansion and full blood vessels of the portal tracts and central veins. The contours of the vast majority of hepatocytes grew clear, intercellular contacts were restored. Histological examination of the kidney revealed a moderate increase in the blood volume in the vessels of the arterial bed, mainly in the cortical layer. A mild expansion and fullness of blood vessels of the glomeruli was observed, which was manifested by their increase in size. An increase in macrophage-type cells was observed in the perivascular areas. Histological examination of the spleen revealed a pretty large area of red pulp, moderate

expansion and fullness of the sinusoids, and pronounced perisinusoidal edema. However, a rapid expansion of the white pulp was observed, which manifested in the formation of follicles.

Keywords: *peritoneal sepsis, morphological changes, liver, spleen, kidneys, therapeutic immune serum.*

Introduction

Sepsis is a potentially life-threatening pathology caused by infection and characterized by a poorly controlled systemic inflammatory response [7]. Sepsis, severe sepsis, and septic shock pose significant problem for the global healthcare system [15]. In the United States alone, over 600,000 cases of sepsis are registered annually, with more than 200,000 people dying from severe sepsis and its complications each year [17]. It is evident that there is a need for the development of improved treatment methods to reduce the mortality rate among patients with severe sepsis.

Peritoneal sepsis is complicated by the development of multiple organ dysfunction in 25 % of cases [7], characterized by structural damage to organs and tissues, which can result in death [5, 12]. Despite the wide range of intensive therapy and antibiotic treatments available, the mortality rate for severe forms of sepsis remains at 50.8 % [5]. In 1925, our distinguished compatriot, O. O. Bogomolets, developed a serum (an extract from organs responsible for the immune response) and named it antireticular cytotoxic serum (ACS) [10, 13, 18]. Both in experiments and clinical applications, this serum has demonstrated significant therapeutic effects in sepsis. Over time, the use of Bogomolets' serum has lost its relevance for various reasons [10, 13, 18].

The aim of the study was to model peritoneal sepsis in an experiment, develop a therapeutic serum (analog of ACS), and investigate the therapeutic properties and specific morphological changes in the liver, spleen, and kidneys of septic and treated animals.

Materials and methods

22 white mice weighing 30.51±3.02 g and 26 guinea pigs weighing 950.4±5.0 g were used in the experimental part of the study, they were kept in the vivarium of I. Ya. Horbachevsky Ternopil National Medical University and received a standard diet [11].

During the work with laboratory animals, the rules of humane treatment of experimental animals and the requirements approved by the Bioethics Committee of Ternopil National Medical University and the International requirements for the humane handling of animals according to the "European Convention for the Protection of Vertebrate Animals Used for Experimental and Other Scientific Purposes" were followed.

In the first stage of the experiment, we modeled fecal peritonitis in mice [16, 19]. For this purpose, we injected 0.05 ml to 1.0 ml of a 10 % filtered fecal suspension of guinea pigs into the abdominal cavity of the mice. The suspension was obtained by mixing the feces of the animals with an isotonic solution of sodium chloride and double-filtering it through a double layer of gauze. It was administered to the mice in the abdominal cavity using a puncture method. The control group consisted of 6 white mice. At the 6th hour after the introduction of the fecal suspension, the mice became apathetic, less mobile, and sought sources of water. The body temperature increased to 43.82±2.40°C (normal range: 30-40°C) [1, 9]; the respiratory rate decreased to 170.0±10.0/min (normal range: 200-283/min) [1, 9]; the heart rate also decreased to 470.0±20.0/min (normal range: 600-730/min) [3, 9]. The reaction to external stimuli was inhibited, and the animals assumed a lateral position. Starting from the 6th hour, the animals that received the highest doses of toxins were began to die. By titration, we determined the volume of the extract at which half of the mice died (LD50) - 0.2 ml of fecal suspension.

A double dose (2 LD50) of the suspension was administered into the abdominal cavity of the mice, and just before the animals' death, under thiopental anesthesia, lethal bloodletting was performed. We collected the spleen, minced it by grinding in a porcelain mortar, added 5.0 ml of distilled water, centrifuged it, and extracted the liquid portion.

In the second stage of the experiment, we induced fecal peritonitis in guinea pigs. For this purpose, we injected 3.0 ml of a 10 % filtered fecal suspension into their abdominal cavity, obtained by mixing feces from 2-3 intact animals with an isotonic solution of sodium chloride and filtering it twice through a double layer of gauze [2].

The control group consisted of 6 guinea pigs. Within 24 hours, the guinea pigs exhibited hypokinesia, coordination disturbances, slowed reaction to external stimuli, and an elevated body temperature of 39.53±0.22°C (normal range: 37.20±0.03°C) [21]. The respiratory rate, initially increased, gradually decreased to 65.01±7.03 breaths per minute (normal range: 89-120 breaths per minute) [1, 21]. The heart rate increased to 430.0±15.0 beats per minute (normal range: 250-355 beats per minute), corresponding to the clinical picture of the terminal stage of peritoneal sepsis [8]. The mucous membranes became gray with a bluish tinge, and their lifespan constituted 50.20±4.50 hours. In the pre-agonistic period of the control group animals, we decapitated them under thiopental anesthesia and collected the liver, spleen, and kidneys for histological examination [14, 18].

After inducing fecal peritonitis in the experimental group of guinea pigs (20 animals), a suspension of mouse spleen was administered to them with an increasing dosage ranging from 0.02 to 0.2 ml. We identified the optimal therapeutic dose of the suspension, which resulted in a

lifespan of over 14 days for guinea pigs with peritonitis, and it was determined to be 0.08 ml. After 72 hours, these guinea pigs were subjected to lethal bloodletting under thiopental anesthesia, and the liver, kidneys, and spleen were collected for histological research.

The tissues were immersed in a 10 % buffered neutral formalin solution, processed using the LogosOne histoprocessor, and embedded in paraffin blocks. Sections of 4-5 μm thickness were obtained using an AMR-400 rotary microtome and stained with hematoxylin and eosin. Histological specimens were examined under a light microscope SEO SCAN and documented using the Vision CCD Camera video camera, which has an image output system for histological slides.

The initial processing of the obtained data was conducted using descriptive statistical methods, presenting the results for quantitative variables as follows: the number of observations (n), the mean (M), and the standard error of the mean (m) [6].

Results

Histological examination of the liver in guinea pigs three days after inducing peritoneal sepsis revealed significant cellular degenerative changes. The lobular organization of hepatocytes was severely disrupted (Fig. 1, 2). Central veins and portal tract vessels moderately dilated and reached a full blood volume capacity, but the sinusoidal lumens were practically not visualized (see Fig. 2). The size of hepatocytes drastically increased, and their contours became blurred, while intercellular connections were disrupted. In a significant portion of cells, the cytoplasm became homogeneous (see Fig. 1), indicating pronounced eosinophilia, although large-droplet fatty dystrophy remained the dominant manifestation (see Fig. 2).

Nuclei were visualized in the majority of cells showing signs of karyopyknosis. Due to the significant presence of intracellular lipid inclusions, their localization was shifted towards the periphery (see Fig. 2). Occasional hepatocyte necrosis was observed. A small number of lymphocytes and histiocytes were visualized in the perivascular spaces of the portal tracts (see Fig. 2).

Histological examination of the kidney revealed a significant decrease in the vascular blood supply of the arterial bed, which was visualized by structural changes in the cortical layer. Collapsoid wrinkling of the glomerular vessels was observed (Fig. 3), resulting in a pronounced reduction in their size. A substantial portion of the endothelial cells was damaged. The inner leaflet of the capsule showed compression, and signs of protein dystrophy were observed. The capsule lumens were practically not visualized.

The lumens of the excretory tubules were significantly narrowed, with some of them containing inclusions in the form of hemoglobin pigment. The basal membranes remained partially intact, with some of them showing increased vascular perfusion. The epithelium of the excretory tubules exhibited various stages of protein dystrophy. The nuclei of the tubular epithelium (intensely stained) were well visualized in practically all cells, mainly located in a peri-basal position (see Fig. 3). The basal membranes partially thickened due to collagenous stromal edema.

The examination of the spleen revealed a significant increase in the area of the red pulp due to pronounced sinusoidal dilation and increased vascular perfusion (Fig. 4). The white pulp was characterized by small, moderately diffuse foci of lymphocyte clusters. Follicular structures were hardly visualized. The number of reticular cells in the germinal centers of periarteriolar areas was virtually non-visualized, while hyperplasia of T-lymphocytes

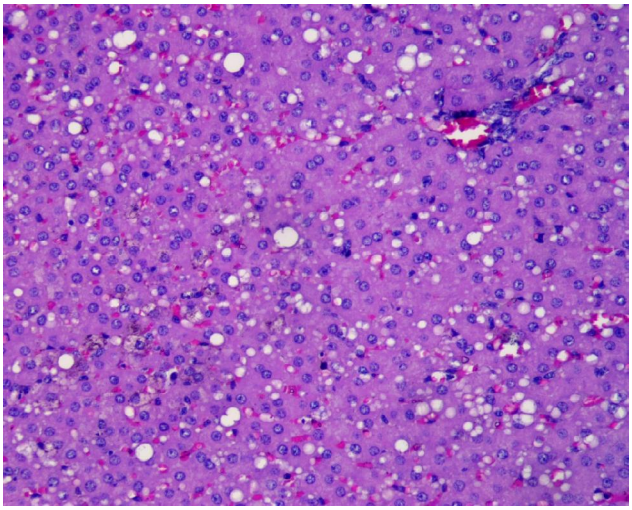

Fig. 1. Liver of an animal with peritoneal sepsis. Severe disruption of lobular structure, absence of lobular organization, and pronounced intracellular fatty dystrophy. Stained with hematoxylin and eosin. x200.

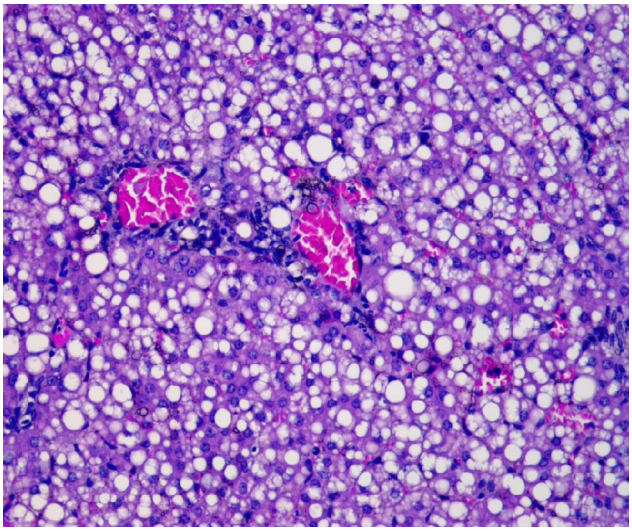

Fig. 2. Liver of an animal with peritoneal sepsis. Disruption of lobular structure, pronounced macrovesicular fatty dystrophy, absence of sinusoidal lumens. Congestion of portal tract vessels. Stained with hematoxylin and eosin. x200.

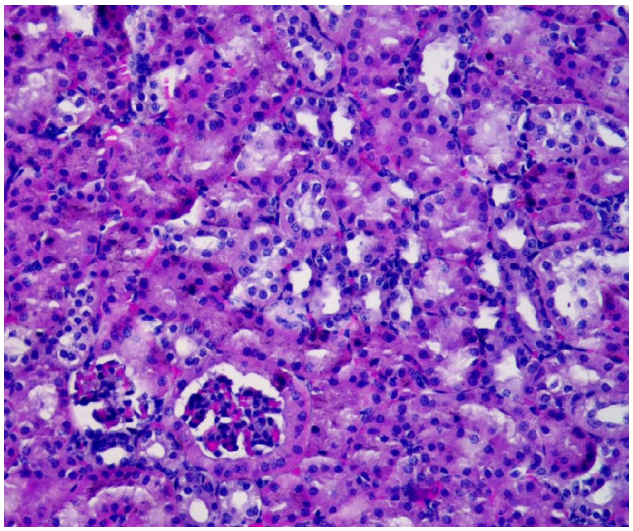

Fig. 3. Kidney of an animal during peritoneal sepsis. Decreased size of glomeruli, markedly reduced vascular perfusion of the arterial layer. Tubular lumens are not visualized. Moderate swelling of the basal membranes. Stained with hematoxylin and eosin. x200.

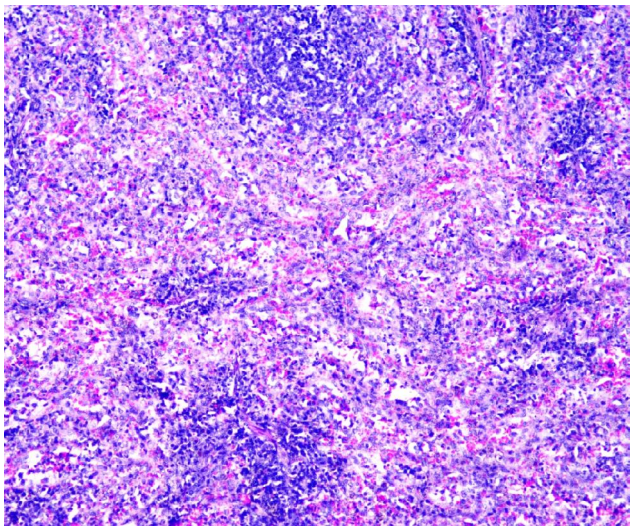

Fig. 4. Spleen of an animal in peritoneal sepsis. Expansion and congestion of marginal zone sinuses, a significant reduction in the area of white pulp, and swelling of intertrabecular areas. Stained with hematoxylin and eosin. x200.

was observed. Throughout the parenchyma of the spleen, a significant number of macrophages with phagocytosed lymphocytes or their fragments were visualized in the sinusoidal lumens, appearing as chromophilic bodies and debris cells, predominantly found in the mantle zones. Sinusoids in the marginal zones showed significant dilation, accompanied by an increased number of erythrocytes within their lumens.

Manifestations of spleen hyperplasia also occurred due to an increase in the number of sideroblasts and siderophages. The congestion and expansion of sinuses were accompanied by an increased presence of freely dispersed granules of hemosiderin. Swelling in the intertrabecular areas of the stroma was observed to progressively intensify.

During the study of structural changes in the liver, kidney, and spleen of guinea pigs suffering from peritonitis and treated with serum (obtained from mouse spleen), the following changes were observed.

Histological examination of the liver revealed moderate dilation and congestion of the portal tracts and central veins. Concurrently, there was expansion and congestion of the sinusoids (Fig. 5). Increased numbers of macrophages were also observed within their lumens (see Fig. 5). The lobular structure showed moderate restoration. Particularly in the periportal tract areas, partial restoration of the trabecular organization was visualized. The contours of the majority of hepatocytes became distinct, and intercellular connections were restored. In the majority of cells, the cytoplasm became finely granular, moderately translucent, and the number of lipid inclusions sharply decreased. Moderate manifestations of protein hyaline droplet dystrophy were observed (see Fig. 5). The number of binucleated hepatocytes increased.

The nuclei were visualized in the vast majority of cells, with a significant portion exhibiting signs of karyopyknosis. Necrosis of hepatocytes remained sporadic. Isolated lymphocytes and histiocytes were visualized in the perivascular spaces of the periportal tracts.

Histological examination of the kidney revealed a moderate increase in the vascular congestion of the arterial vasculature, predominantly in the cortical layer. There was slight dilation and engorgement of the glomerular vessels, accompanied by an increase in their size. The majority of endothelial cells remained damaged. The nephrothelium of the inner layer of the capsule appeared flattened, with

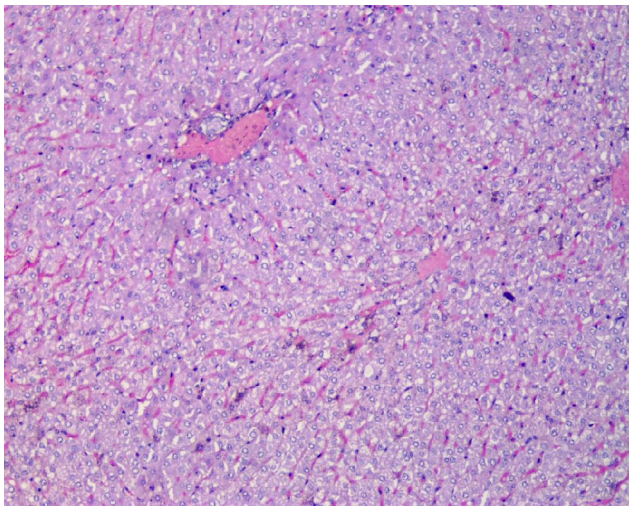

Fig. 5. Liver structure of animals with peritoneal sepsis on the background of correction with suspension from mouse spleen. Dilation and congestion of the portal vein system, a significant presence of macrophages within the sinusoidal lumens, and a marked reduction in manifestations of hepatocellular fatty dystrophy. Stained with hematoxylin and eosin. x100.

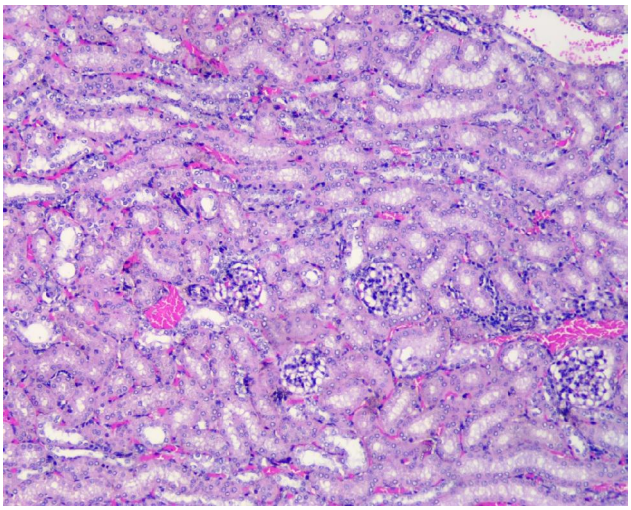

Fig. 6. Structure of the kidney in animals with peritoneal sepsis on the background of correction with mouse spleen suspension. Increased vascularity of the vessels in the areas of basal membranes of the collecting ducts, increased number of macrophages in the stroma. Stained with hematoxylin and eosin. x200.

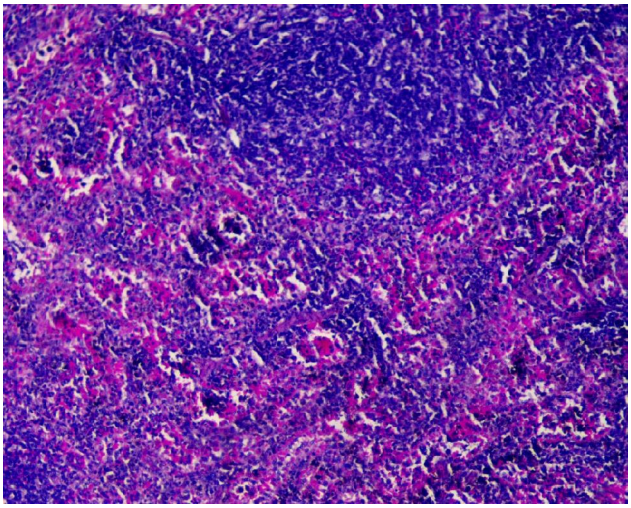

Fig. 7. Structure of the spleen in animals with peritoneal sepsis on the background of correction with mouse spleen suspension. Marked congestion of sinuses, peri-sinusoidal swelling of collagenous stroma, a significant presence of siderophages, and formation of follicles. Stained with hematoxylin and eosin. x200.

signs of protein dystrophy in the cytoplasm, and the capsule lumens were hardly visualized. Perivascular areas showed an increase in macrophage-like cells.

The lumens of certain collecting ducts were moderately dilated, with some of them containing proteinaceous masses. The basal membranes of the ducts remained largely intact, with a moderate increase in their vascularity (Fig. 6), and a slight reduction in perivascular edema. An increase in the number of macrophages was observed. The epithelium of the collecting ducts was at different stages of proteinaceous dystrophy. The nuclei of the epithelial cells appeared slightly brighter, well visualized in almost all cells, and predominantly located basally (see Fig. 6).

The majority of epithelial cells were in different stages of protein dystrophy, with increased cell size, resulting in significantly narrowed lumens of the tubules. However, epithelial cell necrosis was sporadic (see Fig. 6).

Histological examination of the spleen revealed a relatively large area of red pulp, moderate expansion and congestion of sinuses, and pronounced peri-sinusoidal swelling (Fig. 7). However, there was a significant increase in the area of white pulp, characterized by the formation of follicles (see Fig. 7). The white pulp exhibited marked hyperplasia, with a significant increase in the number of reticular cells in the germinal centers of peri-arteriolar regions. Additionally, throughout the parenchyma of the spleen, a considerable number of macrophages containing phagocytosed lymphocytes or their fragments in the form of chromophilic bodies and cellular debris were observed mainly in the marginal zones within the sinusoidal lumens. The sinusoids in the marginal zones remained dilated with a moderate number of erythrocytes within their lumens. The presence of sideroblasts and siderophages remained significant.

Discussion

Thus, our experimental work confirms to an extent the results obtained by our distinguished compatriot O. O. Bogomolets in his use of the developed antireticular cytotoxic serum [10, 13]. However, unlike the original source where O. O. Bogomolets used extracts from the immune organs of large cattle or horses [4, 18, 20], we used white mice as the biological material, whose metabolism occurs much faster than in the guinea pigs, on which peritonitis was modeled.

We found that modeling peritoneal sepsis in guinea pig livers led to a significant disruption of the lobular structure, with acute disturbances in the portal vein system circulation combined with pronounced fatty degeneration. In the kidneys, there was an increase in vascular spasms mainly in the cortical layer, and moderate expansion of the stromal vessel blood supply, resulting in decreased blood supply to the nephrothelium and a significant reduction in organ function. In the spleen, there was hyperplasia of the red pulp with increased sinusoidal blood flow and the development of perisinusoidal stromal edema, accompanied by an increase in the number of siderophages and excessive immune system activity (reduced area of the white pulp).

The use of therapeutic extract contributed to the involution of sepsis and a significant extension of animal life (by 6.7 times). Histological examination of the liver showed a reduction in dystrophic changes (protein and fatty degeneration), decreased venous congestion in the portal vein system, and enhanced hepatocyte regeneration. In the kidney, there was a moderate enlargement of the arterial vessel blood flow, mainly in the cortical layer, significant improvement in the condition of the basal

membranes of the collecting ducts, and a decrease in dystrophic manifestations in the epithelial structures. In the spleen, there was an increase in the area of the white pulp, indicating an enhanced immune status.

Conclusion

1. In the experiment, a therapeutic serum was developed for modeling peritoneal sepsis in white mice by extracting tissue from their spleen.

2. The application of the therapeutic serum in guinea pigs during the modeling of peritoneal sepsis yielded positive results in the histological picture of detoxification organs (liver), the immune system (spleen), and overall blood circulation (kidneys).

3. The extension of the lifespan in guinea pigs suffering from peritonitis and treated with the serum encourages further scientific research in this direction.

References

[1] Bosoi, C. R., Oliveira, M. M., Ochoa-Sanchez, R., Tremblay, M., Ten Have, G. A., Deutz, N. E., ... & Bemeur, C. (2017). The bile duct ligated rat: A relevant model to study muscle mass loss in cirrhosis. *Metabolic Brain Disease*, 32, 513-518. doi: 10.1007/s11011-016-9937-4

[2] Dejager, L., Pinheiro, I., Dejonckheere, E., & Libert, C. (2011). Cecal ligation and puncture: the gold standard model for polymicrobial sepsis? *Trends in Microbiology,* 19(4), 198-208. doi: 10.1016/j.tim.2011.01.001

[3] Ding, J. W., Andersson, R., Norgren, L., Stenram, U., & Bengmark, S. (1992). The influence of biliary obstruction and sepsis on reticuloendothelial function in rats. *The European Journal of Surgery - Acta Chirurgica,* 158(3), 157-164.

[4] Garrido, M., Escobar, C., Zamora, C., Rejas, C., Varas, J., Parraga, M., ... & Montedonico, S. (2017). Bile duct ligature in young rats: A revisited animal model for biliary atresia. *European Journal of Histochemistry: EJH,* 61(3), 2803. doi: 10.4081/ejh.2017.2803

[5] Gibelli, N. E. M., Tannuri, U., De Mello, E. S., & Rodrigues, C. J. (2009). Bile duct ligation in neonatal rats: is it a valid experimental model for biliary atresia studies? *Pediatric Transplantation,* 13(1), 81-87. doi: 10.1111/j.1399-3046.2008.00947.x

[6] Korda, M. M., & Kachuba, O. M. (2021). *Основи медичної статистики та проведення комп'ютерного статистичного аналізу даних статистичними програмами [Basics of medical statistics and computer statistical analysis of data using statistical programs].* Тернопіль. ТНМУ "Укрмедкнига" - Ternopil. TNMU "Ukrmedknyga".

[7] Levy, M. M., Fink, M. P., Marshall, J. C., Abraham, E., Angus, D., Cook, D., ... & International Sepsis Definitions Conference. (2003). 2001 sccm/esicm/accp/ats/sis international sepsis definitions conference. *Intensive care medicine*, 29, 530-538. doi: 10.1097/01.CCM.0000050454.01978.3B

[8] Lewis, A. J., Seymour, C. W., & Rosengart, M. R. (2016). Current murine models of sepsis. *Surgical Infections,* 17(4), 385-393. doi: 10.1089/sur.2016.021

[9] Mortell, A., Montedonico, S., & Puri, P. (2006). Animal models in pediatric surgery. *Pediatric Surgery International,* 22, 111-128. doi: 10.1007/s00383-005-1593-4

[10] Neiman, Is. (1947). Antireticular cytotoxic serum (ACS of Bogomolets). *Chic. Med. Sch. Q.,* 8(3), 11. PMID: 20252180

[11] Parker, S. J., & Watkins, P. E. (2001). Experimental models of gram-negative sepsis. *British Journal of Surgery,* 88(1), 22-30. doi: 10.1046/j.1365-2168.2001.01632.x

[12] Pierrakos, C., & Vincent, J. L. (2010). Sepsis biomarkers: a review. *Critical Care,* 14, 1-18. doi: 10.1186/cc8872

[13] Pomerat, C. M., & Anigstein, L. (1944). Anti-reticular immune serum: its action demonstrated by tissue culture technique. *Science,* 100(2603), 456-456. doi: 10.1126/science.100.2603.456

[14] Saito, H., Sherwood, E. R., Varma, T. K., & Evers, B. M. (2003). Effects of aging on mortality, hypothermia, and cytokine induction in mice with endotoxemia or sepsis. *Mechanisms of Ageing and Development,* 124(10-12), 1047-1058. doi: 10.1016/j.mad.2003.08.002

[15] Sheen, J. M., Huang, L. T., Hsieh, C. S., Chen, C. C., Wang, J. Y., & Tain, Y. L. (2010). Bile duct ligation in developing rats: temporal progression of liver, kidney, and brain damage. *Journal of Pediatric Surgery,* 45(8), 1650-1658. doi: 10.1016/j.jpedsurg.2009.12.019

[16] Shrum, B., Anantha, R. V., Xu, S. X., Donnelly, M., Haeryfar, S. M., McCormick, J. K., & Mele, T. (2014). A robust scoring system to evaluate sepsis severity in an animal model. *BMC Research Notes,* 7(1), 1-11. doi: 10.1186/1756-0500-7-233

[17] Sipeki, N., Antal-Szalmas, P., Lakatos, P. L., & Papp, M. (2014). Immune dysfunction in cirrhosis. *World Journal of Gastroenterology: WJG,* 20(10), 2564. doi: 10.3748/wjg.v20.i10.2564

[18] Spivak, M. Ia., Karpov, O. V., Antonenko, S. V., Barbasheva, O. V., Kvielienkova, K. I., & Voloshchenko, Iu. V. (1997). The depression of the reproduction of the human immunodeficiency virus by the use of Bogomolets antireticular cytotoxic serum. *Microbiological Journal* (Kiev, Ukraine: 1993), 59(5), 57-61. PMID: 9480019

[19] Starr, M. E., Steele, A. M., Saito, M., Hacker, B. J., Evers, B. M., & Saito, H. (2014). A new cecal slurry preparation protocol with improved long-term reproducibility for animal models of sepsis. *PloS One*, 9(12), e115705. doi: 10.1371/journal.pone.0115705

[20] Suttinger, H. (1953). Extent of indication and method of application of the so-called Bogomolets' serum (antireticular cytotoxic serum). *Hippokrates*, 24(4), 120-124. PMID: 13068838

[21] Tannuri, A. C. A., Coelho, M. C. M., de Oliveira Goncalves, J., Santos, M. M., da Silva, L. F. F., Bendit, I., & Tannuri, U. (2012). Effects of selective bile duct ligation on liver parenchyma in young animals: histologic and molecular evaluations. *Journal of Pediatric Surgery,* 47(3), 513-522. doi: 10.1016/j.jpedsurg.2011.10.009

МОДЕЛЮВАННЯ ПЕРИТОНЕАЛЬНОГО СЕПСИСУ ТА ЙОГО ЛІКУВАННЯ СИРОВАТКОЮ В ЕКСПЕРИМЕНТІ: ОСОБЛИВОСТІ МОРФОЛОГІЧНИХ ПОРУШЕНЬ ТКАНИН ПЕЧІНКИ, СЕЛЕЗІНКИ ТА НИРОК

Гнатів В. В., Плитка О. В.

Сепсис розвивається як звичайна запальна відповідь на різні інфекції. Перебіг його, зазвичай, характеризується картиною складного гетерогенного синдрому, котрий часто призводить до розвитку поліорганної недостатності. Кількість органів, що уражуються, корелює зі смертністю. Органна недостатність характеризується послідовністю - спочатку легенева,

потім ниркова, серцево-судинна і у термінальну стадію виникає недостатність функції центральної нервової системи. Метою дослідження було змоделювати в експерименті перитонеальний сепсис; розробити лікувальну сироватку - аналог антиретикулярної цитотоксичної сироватки О. О. Богомольця (АЦС) і дослідити лікувальні властивості та особливості морфологічних змін тканин печінки, селезінки, нирок у септичних і пролікованих тварин. Для моделювання перитонеального сепсису лабораторним мишам внутрішньоочеревинно вводили розчин 10 % профільтрованої калової суспензії мурчаків (від 0,05 до 1,0 мл), встановлювали рівень токсичної дози, при якій усі миші гинули (0,35 мл калової суспензії), після чого під тіопенталовим наркозом проводили летальне кровопускання. У мишей вилучали селезінку, з якої виготовляли лікувальну сироватку. Мурчакам дослідної групи після моделювання калового перитоніту вводили суспензію селезінки мишей з наростаючою дозою від 0,02 до 0,2 мл. Виявили оптимальну лікувальну дозу, при якій мурчаки продовжували жити протягом 14 днів: 0,08 мл. Під тіопенталовим наркозом (50 мг/кг) у них вилучали печінку, нирки та селезінку для гістологічних досліджень. Отримані гістологічні препарати у подальшому обробляли за загальноприйнятою методикою. Гістологічні препарати вивчали за допомогою світлового мікроскопа SEO SCAN. Встановлено, що при перитонеальному сепсисі в печінці часточкова організація гепатоцитів різко порушувалась. Центральні вени та судини портальних трактів помірно розширювались, ставали повнокровними, проте просвіти синусоїдів практично не візуалізувались. Розміри гепатоцитів різко збільшувались, контури стирались, міжклітинні зв'язки порушувались. Гістологічне дослідження нирки виявило різке зниження кровонаповнення судин артеріального русла, що візуалізувалося структурними проявами кіркового шару. Спостерігалось колаптоїдне зморщення судин клубочків, що проявлялось їх різким зменшенням у розмірах. Значна частина ендотеліоцитів пошкоджувалась. Дослідження селезінки виявило значне збільшення площі червоної пульпи через виражене розширення синусоїдів та збільшення їх кровонаповнення. Біла пульпа була представлена дрібними помірнодифузними фокусами скупчень лімфоцитів. Структури фолікулів практично не візуалізувались. Гістологічне дослідження печінки тварин із модельованим перитонеальним сепсисом на фоні корекції екстрактом селезінки мишей виявило помірне розширення й повнокрів'я судин портальних трактів та центральних вен. Контури переважної більшості гепатоцитів ставали більш чіткими, відновлювались міжклітинні контакти. Гістологічне дослідження нирки виявило помірне збільшення кровонаповнення судин артеріального русла, переважно коркового шару. Встановлено незначне розширення та повнокрів'я судин клубочків, що проявлялось збільшенням їх розмірів. У перивaскулярних ділянках спостерігалось збільшення клітин макрофагального типу. Гістологічне дослідження селезінки виявило достатньо велику площу червоної пульпи, помірне розширення та повнокров'я синусоїдів, виражений перисинусоїдальний набряк. Проте, різко збільшувалася площа білої пульпи, котре проявлялось формуванням фолікулів.

Ключові слова: *перитонеальний сепсис, морфологічні зміни, печінка, селезінка, нирки, лікувальна імунна сироватка.*

DOI: 10.31393/morphology-journal-2023-29(2)-07 Reports of Morphology, Vol. 29, №2, Pages 45-50

ISSN 1818-1295 eISSN 2616-6194

REPORTS OF MORPHOLOGY

Official Journal of the Scientific Society of Anatomists, Histologists, Embryologists and Topographic Anatomists of Ukraine

journal homepage: https://morphology-journal.com

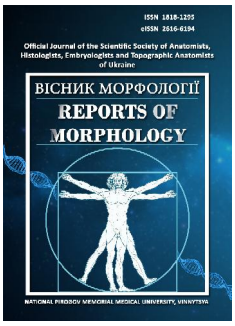

The effect of quercetin on the morphogenesis of the interstitial space in the testes of rats after 90 days with central blockade of luteinizing hormone

Stetsuk Ye. V., Shepytko V. I., Boruta N. V., Vilkhova O. V., Skotarenko T. A., Rud M. V.
Poltava State Medical University, Poltava, Ukraine

ARTICLE INFO
Received: 23 February 2023
Accepted: 21 March 2023

UDC: 616.681:615.35:599.367.4

CORRESPONDING AUTHOR
e-mail: stetsuk78@gmail.com
Stetsuk Ye. V.

CONFLICT OF INTEREST
The authors have no conflicts of interest to declare.

FUNDING
Not applicable.

Leydig cells are responsible for the production of testosterone in the male testicles when stimulated by luteinizing hormone (LH). Dysfunction of Leydig cells, which occurs during inflammation or oxidative stress, is one of the main causes of male infertility. The purpose of the study is to determine the effect of quercetin on the microscopic organization of rat testes, nitric oxide production and the intensity of oxidative stress in rat testes on the 90th day of the experiment, during the experimental central deprivation of LH synthesis caused by the administration of triptorelin acetate solution. The experiment was conducted on 20 sexually mature male white rats. Rats were divided into 2 groups of 10 animals in each group: control group (I), group with central deprivation of LH + quercetin synthesis (II). Animals from the group with central blockade of LH synthesis were injected subcutaneously with triptorelin acetate at a dose of 0.3 mg of the active substance per kg and quercetin at 100 mg per kg of body weight 3 times a week, while the control group was injected with saline. Our study of the interstitial space in the testes of white rats showed heterogeneity of macrophage populations and variability of structural and functional parameters. Central blockade of LH synthesis by the administration of treptorelin with the parallel administration of quercitin to the studied animals on the 90th day of the experiment causes changes in the structure of the interstitial space of rat testes, which is characterized by high variability both in the populations of interstitial endocrinocytes and macrophages. Biochemical indicators on the 90th day of the experiment indicate an increase in NO production in conditions of central blocking of the synthesis of luteinizing hormone by more than three times, which is ensured by the activity of the inducible isoform of NOS (iNOS). At the same time, the increase in the activity of iNOS with a decrease in the activity of the arginase pathway leads to the polarization of macrophages according to the pro-inflammatory type. The introduction of quercetin protects the testicular tissue of rats from oxidative damage caused by the administration of triptorelin on the 90th day of the experiment by increasing antioxidant protection and reducing reactive oxygen species in the tissue.
Keywords: *testes, interstitial endocrinocytes, macrophages, quercetin, triptorelin, oxidative stress, rats.*

Introduction

Male infertility accounts for 50 % of all infertility cases. The main reason is low quality and quantity of sperm. Leydig cells are responsible for the production of testosterone in male testes when stimulated by luteinizing hormone (LH) [2, 16]. Leydig cell dysfunction associated with inflammation and oxidative stress is one of the main causes of male infertility. Men with complete congenital hypogonadotropic hypogonadism usually have azoospermia. Treatment with only exogenous injection of testosterone and follicle-stimulating hormone (FSH) fails to produce sperm. However, the combined treatment of FSH and human chorionic gonadotropin (hCG) is effective [3, 11]. This example shows that intratesticular testosterone plays an important role in spermatogenesis. In addition, testicular histology of men with LH receptor mutations shows hypoplasia, agenesis, dysplasia of Leydig cells with a preserved number of Sertoli cells; the number of sperm is reduced, as in men with a partial inactivating mutation of the androgen receptor.

Certain male hormonal contraceptive protocols or

exogenous androgen abuse cause a negative feedback loop in the hypothalamic-pituitary axis, reducing FSH, LH, and testosterone levels, causing sperm defects and testicular atrophy, leading to abnormal androgen production and impaired spermatogenesis. The minimum level of intratesticular testosterone for normal sperm production is a matter of debate. Interestingly, some animal models have shown that completely testosterone-independent spermatogenesis is possible, potentially due to strong FSH activation. Recent data indicate an important role of macrophages in adult spermatogenesis. Testicular macrophages regulate immune function during inflammation and steroidogenesis of Leydig cells [13, 17, 21]. Thus, inhibition of induced cytoglobin (CYGB) and neuroglobin (NGB), release of nitric oxide (NO) blocked the progression of the cell cycle, reduced testosterone production, and enhanced the expression of inflammatory and apoptotic pathway genes. On the other hand, overexpression of CYGB and NGB decreased the protein expression of the inflammatory cytokine tumor necrosis factor (TNFα) and the inducible enzyme COX-2 and increased the expression of testosterone biogenesis pathway genes under lipopolysaccharide stimulation. In addition, overexpression of CYGB and NGB enhances testosterone production. Inhibition of CYGB and NGB in Leydig cells changed the morphology of macrophages, increased the number of macrophage cells and NO release in lipopolysaccharide co-culture experiments.

One of the strategies developed to attenuate doxorubicin (DOX) toxicity is combination therapy with bioactive compounds such as flavonoids. The protective properties of some flavonoids against DOX toxicity have been investigated and observed mainly in the heart, but also in the liver, kidney, brain, testes or bone marrow [9, 22]. Protective mechanisms include reducing oxidative stress by reducing ROS levels and/or increasing antioxidant defenses and inhibiting autophagy, apoptosis, and inflammation [18, 23]. Cancer cell studies showed that the antitumor activity of DOX was not affected by flavonoids. Moreover, some of them enhanced the efficacy of DOX as an antitumor drug even in multidrug-resistant cells [26].

Quercetin has several pharmacologic actions that may help combat cell-related insults such as altered sperm function, reproductive hormone dysfunction, as well as dysregulated testicular apoptosis, oxidative stress, and inflammation. Studies have shown that quercetin reduces testicular toxicity, mainly by inhibiting the formation of reactive oxygen species with the help of two antioxidant pharmacophores present in its ring structure [12, 21]. Quercetin's free radical scavenging property can alter the signal transduction of oxidative stress-induced apoptosis, prevent inflammation, and improve sperm quality in a hormone-dependent manner. The protective effect of the bioflavonoid quercetin revealed on the experimental model makes it possible to use it to correct testicular dysfunction of various genesis [25]. These facts indicate the need to take measures to identify the causes of reproductive abnormalities, study the mechanisms and find preventive means of correction.

The purpose of the study was to establish the influence of quercetin on the microscopic organization of rat testes, production of nitric oxide and the intensity of oxidative stress in the rat testes on the 90th day of the experiment, during experimental central deprivation of LH synthesis, caused by the introduction of triptorelin acetate solution.

Materials and methods

The study is a fragment of the research project "Experimental morphological study of cryopreserved placenta transplants action diphereline, ethanol and 1 % methacrylic acid on the morphofunctional status in a number of internal organs", state registration No. 0119U102925.

The experiments were carried out on 15 sexually mature male white rats. Rats were divided into 2 groups with 10 animals in each group: the control group (I), the group with central deprivation of LH synthesis + quercetin (II). Animals from the group with central deprivation of testosterone synthesis were injected subcutaneously with triptorelin acetate at a dose of 0.3 mg of the active substance per kg [5, 19] and quercetin 100 mg per kg body weight 3 times a week [20], while the control group was administered saline. Experiment conducted for 90 days. Animals were kept in standard vivarium conditions of the Poltava State Medical University.

Experimental animals were sacrificed in strict compliance with the provisions of the "European Convention for the Protection of Vertebrate Animals Used for Experimental and Other Scientific Purposes"; (Strasbourg, 1986), as well as with the "General Ethical Principles of Animal Experiments" adopted by the First National Congress on Bioethics (Kyiv, 2001). Bioethics protocol № 195 - 06.24.2021.

Using standard methods, the material was imbedded in paraffin blocks, of which sections 4 μm thick were made and stained with hematoxylin and eosin [4]. Histological preparations were examined using Biorex 3 light microscope with digital microfilter with software adapted for these studies (Serial No. 5604).

We carried out all biochemical studies in 10 % homogenate of testis tissue using Ulab 101 spectrophotometer. General activity of NO-synthase (gNOS), activity of constitutive isoforms (cNOS), activity of inducible isoform (iNOS) was determined by increase of nitrite concentration after incubation in buffer solution (pH=7.4) containing 0.3 ml of 320 mM L-arginine solution and 0.1 ml of 1 mM NADPH+H solution [1, 24]. Nitrite concentration was measured with help of Griess reagent [1, 24]. Arginase activity was evaluated by increase of L-ornithine content after incubation in buffer solution (pH=7.0) containing 0.2 ml of 24 mM L-arginine solution [1, 24].

Basic production of superoxide anion radical (SAR), its production by the mitochondrial electron transport chain

(ETC) and microsomal ETC was determined by the growth of diformazan concentration, formed in the reaction of SAR with nitro blue tetrazolium [10]. Superoxide dismutase (SOD) activity was determined by inhibition of adrenaline autooxidation, while catalase activity was determined by the amount of hydrogen peroxide, remained after its catalase-dependent reduction [6]. The concentration of free malondialdehyde (MDA) was determined by reaction with 1-methyl-2-phenylindole resulting in formation of specific colored substance [24].

Statistical processing of the study results was carried out using the Microsoft Office Excel software and the Real Statistics 2019 extension to it. The nonparametric Mann-Whitney test was used to determine the statistical significance of differences between the groups. The difference was considered statistically significant at $p<0.05$.

Results

Studying the histological preparations on the 90th day of the experiment, we established changes in the structure of both the parenchyma and the stroma of the testes. Thus, when we studied the convoluted tubules, testes, the cells were at different stages of spermatogenesis. The basement membrane was tortuous, enlarged, swollen. Disorganization of the cells of both the adluminal and basal layers of the spermatogenic epithelium was found in some places. The cells of the spermatogonia, A and B, are mostly connected to the basement membrane, but the spermatocytes of the first order are detached from them. Second-order spermatocytes and spermatids increased in size, but their number was constant compared to the control group of animals. Spermatozoa were inside the tubules, but morphologically a large number of changed cells were distinguished. Supporting cells are enlarged, swollen. The nucleus and cytoplasm of these cells are mostly illuminated (Fig. 1).

In the experimental group of animals, it was established that the tissue of the actual interstitial space of the testicles was swollen due to all components. When studying the microcirculatory bed of the tissue, it was established that the vessels were enlarged in size both due to the swollen wall of the vessels and due to an increase in their diameter. The number of vessels increased sharply, stasis was noted in them. Intravascular leukocytes inside the vessels form an areole of cells that are active before migration into the interstitial space (Fig. 2). The number of cells in the interstitial space is increased due to the migratory activity of the cells of the leukocyte pool, among which cells of the macrophage series are most often found.

Studying the cell composition of the interstitial space we found that the majority of cells are interstitial endocrinocytes. The number of cells, compared to the control group, was constant. They were clearly detected on sections where cells were located in groups from 2 to 5. These are cells with light basophilic nuclei and heterochromatin, which was clearly visualized. The cytoplasm is light, with an increased content of lipid granules. Outside of the cells, interstitial tissue was

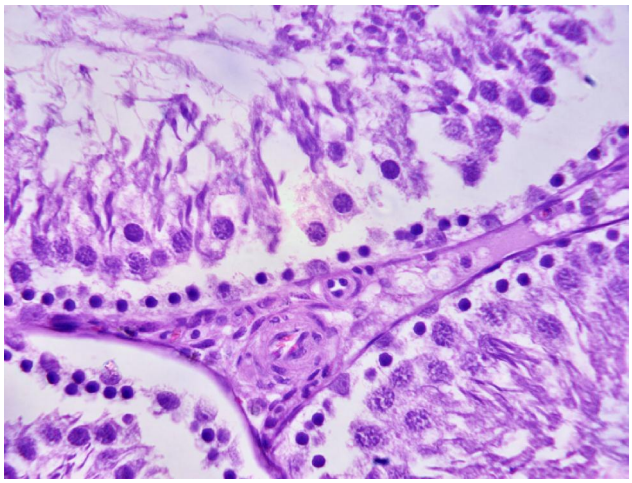

Fig. 1. Seminiferous tubules of experimental rat on the 90th day. Microimage. Stain: hematoxiline and eosine. Lens: 10: Ocular lens: 10.

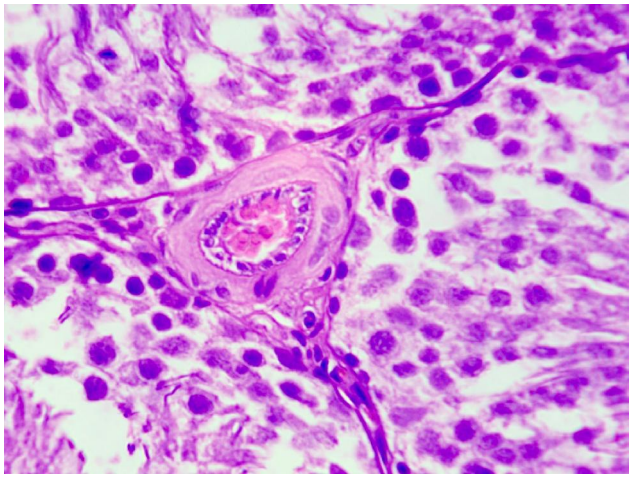

Fig. 2. Seminiferous tubules of experimental rat on the 90th day. Microimage. Interstitial space whith stasis. Stain: hematoxiline and eosine. Lens: 10: Ocular lens: 10.

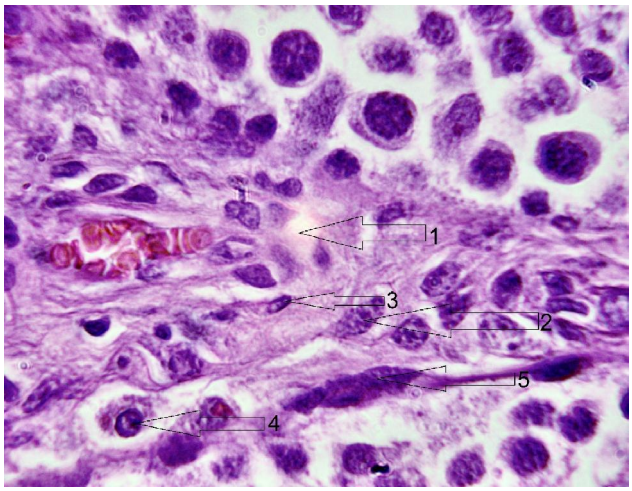

Fig. 3. Interstitial space of experimental rat on the 90th day. Microimage. 1 - interstitial space; 2 - interstitial endocrinocytes large; 3 - interstitial endocrinocytes small; 4 - interstitial macrophages; 5 - parietal macrophages. Stain: hematoxiline and eosine. Lens: 40: Ocular lens: 15.

Table 1. Markers of the NO cycle during the 90-day central blockade of LH + quercetin synthesis (M±m).

Groups	Parameters				
	gNOS activity, mol/min per g of protein	iNOS activity, mol/min per g of protein	cNOS activity, mol/min per g of protein	Arginase activity, mol/min per g of protein	NO2-concentration, nmol/L
Control	0.542±0.041	0.130±0.022	0.411±0.032	2.480±0.052	3.834±0.252
Experimental	0,784±0,060*	0.639±0,061*	0,145±0.021*	0,767±0,020*	13.55±0.37*

Note: * - indicates that the difference is statistically significant when compared with control group (p<0.05).

Table 2. Markers of oxidative stress during the 90-day central blockade of synthesis of LH + quercetin (M±m).

Groups	Parameters					
	SOD activity, c.u.	Catalase activity, nkat/g of tissue	Basic O_2 - production, nmol/s per g of tissue	Production of O_2 - from mithochondrial ETC, nmol/s per g of tissue	Production of O_2 - from microsonal ETC, nmol/s per g of tissue	Free MDA, mmol/g of tissue
Control	1.870±0.111	0.182±0.173	0.261±0.010	7.840±0.132	9.552±0.191	6.643±1.440
Experimental	3.812±0.181*	0.312±0.020*	2.244±0.133*	26.24±0.88*	22.38±0.29*	12.92±0.65*

Note: * - indicates that the difference is statistically significant when compared with control group (p<0.05).

lightened due to the presence of synthesis products in them. The cells usually had a polygonal shape. The established changes in cell sizes made it possible to divide the population of these cells into small and large ones by size and functional activity (Fig. 3).

Macrophages are other, and, in our opinion, the most important cells of the interstitial space of the testes, which affect the hemostasis of the connective tissue. During our study of the macrophage system of testes, several populations of these cells were found. Thus, depending on the localization in the connective tissue and the vascular bed of the testes, the following was established: parietal macrophages had an elongated flattened oval nucleus, they were located near the basal membrane of convoluted tubules, their number was increased, compared to the control group; interstitial macrophages were single and inactive (see Fig. 3), and intravascular macrophages were active before migration (see Fig. 2). Interstitial macrophages were large compared to other cell populations, their nuclei were oval or round in shape, electron dense with a predominance of heterochromatin. The cytoplasm of the cells was small in size with all subcellular elements. Intervascular macrophages morphologically resembled interstitial macrophages (see Fig. 3).

The following results were obtained as a result of the study of biochemical indicators of testicular tissues. Total NOS activity on the 90th day of central blockade of luteinizing hormone synthesis was 0.784±0.060 ?mol/min, which differed from the values of the control group of animals (0.542±0.041 μmol/min) (Table 1), but not reliably. During the study of cNOS activity, indicators decreased by 2.8 times, and iNOS activity increased by 4.9 times, compared to the control group of animals. The concentration of nitrite in the testes of rats increases by 3.5 times, and the indicator of arginase activity decreases by 3.2 times.

The activity of SOD decreased by 2.0 times. The concentration of MDA in the testes of rats was reduced by 1.95 times. Basic production of O_2 - on the 90th day of the experiment increased 8.6 times compared to the control group (Table 2). O_2 production of mitochondrial ETC decreased by 3.3 times, and microsomal ETC - by 2.3 times.

Discussion

The testicle is an immunoprivileged organ that is sensitive to oxidative stress and inflammation, two major factors that affect male infertility. It has been shown that a decrease in the concentration and activity of biomarkers of testicular function is correlated with a disturbance of the hypothalamic-pituitary-testicular axis and oxidative stress. However, the use of natural products to alleviate these changes caused by oxidative stress may be important for improving male reproductive function [8, 15].

Our study aimed to examine the effect of quercetin on triptorelin-induced oxidative stress and inflammation in the testicular interstitial space. The increase in intracellular levels of the oxidative stress system (ROS) was reduced after quercetin treatment, which was confirmed in materials with the induction of oxidative stress by lipopolysaccharide, which almost completely abolished the mRNA and protein expression of nicotinamide adenine dinucleotide phosphate oxidase 2 induced by Salmonella lipopolysaccharide (LPS) stimulation. In addition, it was confirmed in the literature that quercetin inhibited the nuclear translocation of nuclear factor kappa B (NF-kB) and reduced the levels of TNF-α, interleukin 1 (IL-1) and IL-6, which were significantly increased after exposure to LPS [13].

The indicators of our study indicate an increase in NO production in conditions of central blocking of the synthesis of luteinizing hormone, with a direct effect on interstitial endocrinocytes, to testosterone production, which is ensured by the activity of inducible iNOS. At the same time, an increase in iNOS activity with a decrease in the activity of the arginase pathway of L-arginine cleavage may indicate a change in the polarization of testicular macrophages with a preference for the pro-inflammatory phenotype (M1), which we have in the detected active parietal forms. Oxidative stress

caused by the production of reactive oxygen species plays a major role in the inflammatory processes of testes [14]. We hypothesize that modulation of oxidative stress by quercetin may protect against oxidative stress and inflammation in testicular tissue. Our data showed that quercetin reduced triptorelin-induced oxidative stress and inflammation in the testis structure as a result of inhibiting LH production. The obtained results are consistent with the literature, which describes the main points and regularities of the organization of the population of cells in the interstitial space of the testis [8].

The obtained results are a theoretical justification for the development of methods for correcting violations of the generative and endocrine function of the testes in case of extreme effects on the body, with damage to endo- and paracrine regulations. Data on the functional morphology of the testes at the stages of adaptation to changes in the endocrine and immune function of the testes expand the existing understanding of the causes of spermatogenesis disorders and its regulation. The data can be used in research work and teaching issues at departments of medical schools and biological faculties of universities.

Conclusions

1. Central blockade of LH synthesis by the administration of treptorelin with the parallel administration of quercitin to the studied animals on the 90th day of the experiment causes changes in the structure of the interstitial space of rat testes, which is characterized by high variability in the populations of interstitial endocrinocytes and macrophages.

2. Biochemical indicators on the 90th day of the experiment indicate an increase in NO production in conditions of central blocking of the synthesis of luteinizing hormone by more than three times, which is ensured by the activity of inducible iNOS. At the same time, an increase in iNOS activity with a decrease in the activity of the arginase pathway leads to the polarization of macrophages according to the pro-inflammatory type.

3. Administration of quercetin protects testicular tissue of rats from oxidative damage caused by administration of triptorelin on the 90th day of the experiment due to increased antioxidant protection and reduction of reactive oxygen species in the tissue.

References

[1] Akimov, O. Y., & Kostenko, V. O. (2016). Functioning of nitric oxide cycle in gastric mucosa of rats under excessive combined intake of sodium nitrate and fluoride. *The Ukrainian Biochemical Journal,* 88(6), 70-75.

[2] Almeida, S., Rato, L., Sousa, M., Alves, M. G., & Oliveira, P. F. (2017). Fertility and sperm quality in the aging male. *Current pharmaceutical design,* 23(30), 4429-4437. doi: 10.2174/1381612823666170503150313

[3] Atallah, A., Mhaouty-Kodja, S., & Grange-Messent, V. (2017). Chronic depletion of gonadal testosterone leads to blood-brain barrier dysfunction and inflammation in male mice. *Journal of Cerebral Blood Flow & Metabolism,* 37(9), 3161-3175. doi: 10.1177/0271678 X16683961

[4] Bahriy, M. M., Dibrova, V. A., Popadynets, O. H., & Hryshchuk, M. I. (2016). *Методики морфологічних досліджень: монографія [Methods of morphological research: monograph].* Вінниця: Нова книга - Vinnytsya: Nova knyha.

[5] Botte, M. C., Lerrant, Y., Lozach, A., Berault, A., Counis, R., & Kottler, M. L. (1999). LH down-regulates gonadotropin-releasing hormone (GnRH) receptor, but not GnRH, mRNA levels in the rat testis. *Journal of Endocrinology,* 162(3), 409-415. doi: 10.1677/joe.0.1620409

[6] Gosalvez, J., Coppola, L., Fernandez, J. L., Lopez-Fernandez, C., Gongora, A., Faundez, R., ... & Esteves, S. C. (2017). Multi-centre assessment of nitroblue tetrazolium reactivity in human semen as a potential marker of oxidative stress. *Reproductive Biomedicine Online,* 34(5), 513-521. doi: 10.1016/j.rbmo.2017.01.014

[7] Hotta, Y., Kataoka, T., & Kimura, K. (2019). Testosterone deficiency and endothelial dysfunction: nitric oxide, asymmetric dimethylarginine, and endothelial progenitor cells. *Sexual medicine reviews,* 7(4), 661-668. doi: 10.1016/j.sxmr.2019.02.005.

[8] Jovicic, M., Pintus, E., Fenclova, T., Simonik, O., Chmelikova, E., Ros-Santaella, J. L., & Sedmikova, M. (2018). Effect of nitric oxide on boar sperm motility, membrane integrity, and acrosomal status during semen storage. *Polish Journal of Veterinary Sciences*, 21(1), 73-82. doi: 10.24425/119024

[9] Ji, C., Xu, Y., Han, F., Sun, D., Zhang, H., Li, X., ... & Wang, H. (2017). Quercetin alleviates thermal and cold hyperalgesia in a rat neuropathic pain model by inhibiting Toll-like receptor signaling. *Biomedicine & Pharmacotherapy,* 94, 652-658. doi:10.1016/j.biopha.2017.07.145

[10] Kozaeva, R., Klymenko, M. O., Katrushov, O. V., & Kostenko, V. O. (2022). Bioflavonoids as agents for correcting nitro-oxidative stress and salivary gland functions in rats exposed to alcohol during modeled lipopolysaccharide-induced systemic inflammatory response. *Wiad Lek*, 75(3), 685-690. doi: 10.36740/WLek202203121

[11] Liu, F. H., Yang, D. Z., Wang, Y. F., Liang, X. P., Peng, W. M., Cao, C. A., ... & Guo, Z. M. (2007). Making of the animal model with sterilized testes. *Zhonghua nan ke xue= National Journal of Andrology,* 13(2), 125-129. PMID: 17345767

[12] Merseburger, A. S., & Hupe, M. C. (2016). An update on triptorelin: current thinking on androgen deprivation therapy for prostate cancer. *Advances in therapy,* 33, 1072-1093. doi: 10.1007/s12325-016-0351-4

[13] Mossadegh-Keller, N., & Sieweke, M. H. (2018). Testicular macrophages: Guardians of fertility. *Cellular Immunology,* 330, 120-125. doi: 10.1016/j.cellimm.2018.03.009

[14] Morris Jr, S. M. (2016). Arginine metabolism revisited. *The Journal of Nutrition,* 146(12), 2579S-2586S. doi: 10.3945/jn.115.226621

[15] Rawla, P. (2019). Epidemiology of prostate cancer. *World Journal of Oncology,* 10(2), 63. doi: 10.14740/wjon1191

[16] Rice, M. A., Malhotra, S. V., & Stoyanova, T. (2019). Second-generation antiandrogens: from discovery to standard of care in castration resistant prostate cancer. *Frontiers in oncology,* 9, 801. doi: 10.3389/fonc.2019.00801

[17] Scovell, J. M., & Khera, M. (2018). Testosterone replacement therapy versus clomiphene citrate in the young hypogonadal male. *European Urology Focus,* 4(3), 321-323. doi: 10.1016/j.euf.2018.07.033

[18] Skrypnyk, I., Maslova, G., Lymanets, T., & Gusachenko, I.

(2017). L-arginine is an effective medication for prevention of endothelial dysfunction, a predictor of anthracycline cardiotoxicity in patients with acute leukemia. *Experimental Oncology,* 39(4), 308-311. PMID: 29284775

[19] Stetsuk, Ye. V., Kostenko, V. O., Shepitko, V. I., & Goltsev, A. N. (2019). Influence of the 30-days central deprivation of testosterone synthesis on the morphological and functional features of rat testicular interstitial endocrinocytes and sustentocytes. *World of Medicine and Biology,* 4(70), 228-233. doi: 10.26724/2079-8334-2019-4-70-228-233

[20] Stetsuk, Ye. V., Shepitko, V. I., Akimov, O. Y., Yakushko, O. S., & Solovyova, N. V. (2021). Influence of quercetin on biochemical and morphological changes in rat testes after 30 days long central deprivation of luteinizing hormone, *World of Medicine and Biology,* 3(77), 243-248. doi: 10.26724/2079-8334-2021-3-77-243-248

[21] Swelum, A. A. A., Saadeldin, I. M., Zaher, H. A., Alsharifi, S. A., & Alowaimer, A. N. (2017). Effect of sexual excitation on testosterone and nitric oxide levels of water buffalo bulls (Bubalus bubalis) with different categories of sexual behavior and their correlation with each other. *Animal Reproduction Science,* 181, 151-158. doi: 10.1016/j.anireprosci.2017.04.003

[22] Yavtushenko, I. V., Nazarenko, S. M., Katrushov, O. V., & Kostenko, V. O. (2020). Quercetin limits the progression of oxidative and nitrosative stress in the rats' tissues after experimental traumatic brain injury. *Wiadomosci Lekarskie,* 73(10), 2127-2132. PMID: 33310934

[23] Yang, W., Li, L., Huang, X., Kan, G., Lin, L., Cheng, J., ... & Cui, S. (2017). Levels of Leydig cell autophagy regulate the fertility of male naked mole-rats. *Oncotarget,* 8(58), 98677. doi: 10.18632/oncotarget.22088

[24] Yelins'ka, A. M., Liashenko, L. I., & Kostenko, V. O. (2019). Quercetin potentiates antiradical properties of epigallocatechin-3-gallate in periodontium of rats under systemic and local administration of lipopolisaccharide of Salmonella typhi. *Wiadomosci Lekarskie* (Warsaw, Poland: 1960), 72(8), 1499-1503. PMID: 32012499

[25] Xu, D., Hu, M. J., Wang, Y. Q., & Cui, Y. L. (2019). Antioxidant activities of quercetin and its complexes for medicinal application. *Molecules,* 24(6), 1123. doi: 10.3390/molecules24061123

[26] Zhao, Y., Liu, X., Qu, Y., Wang, L., Geng, D., Chen, W., ... & Lv, P. (2019). The roles of p38 MAPK® COX2 and NF-kB® COX2 signal pathways in age-related testosterone reduction. *Scientific Reports,* 9(1), 1-11. doi: 10.1038/s41598-019-46794-5

ВПЛИВ КВЕРЦЕТИНУ НА МОРФОГЕНЕЗ ІНТЕРСТИЦІЙНОГО ПРОСТОРУ В СІМ'ЯНИКАХ ЩУРІВ ЧЕРЕЗ 90 ДНІВ ПРИ ЦЕНТРАЛЬНОМУ БЛОКУВАННІ ЛЮТЕЇНІЗУЮЧОГО ГОРМОНУ

Стецук Є. В., Шепитько В. І., Борута Н. В., Вільхова О. В., Скотаренко Т. А., Рудь М. В.

Клітини Лейдіга відповідають за вироблення тестостерону в чоловічих яєчках при стимуляції лютеїнізуючим гормоном (ЛГ). Дисфункція клітин Лейдіга, що виникає при запаленнях або окисних стресах, є однією з основних причин чоловічого безпліддя. Мета дослідження - встановити вплив кверцетину на мікроскопічну організацію сім'яників щурів, продукцію оксиду азоту та інтенсивність оксидативного стресу в сім'яниках щурів на 90-ту добу експерименту під час експериментальної центральної деприваці синтезу ЛГ, викликаного введенням розчину трипторелін ацетату. Експеримент проводили на 20 статевозрілих самцях білих щурів. Щури були розподілені на 2 групи по 10 тварин у кожній групі: контрольна група (I), група з центральною депривацією синтезу ЛГ + кверцетин (II). Тваринам із групи з центральною блокадою синтезу ЛГ підшкірно вводили трипторелін ацетат у дозі 0,3 мг діючої речовини на кг та кверцетин 100 мг на кг маси тіла 3 рази на тиждень, при цьому контрольній групі вводили фізіологічний розчин. Проведене нами дослідження інтерстиційного простору в сім'яниках білих щурів показало неоднорідність популяцій макрофагів та мінливість структурно-функціональних параметрів. Центральна блокада синтезу ЛГ шляхом введення трипторелін з паралельним введенням кверцитину досліджуваним тваринам на 90-й день експерименту викликає зміни в структурі інтерстиціального простору сім'яників щурів, що характеризується високою варіабельністю як у популяціях інтерстиціальних ендокриноцитів, так і в макрофагів. Біохімічні показники на 90-й день експерименту вказують на підвищення продукції NO в умовах центрального блокування синтезу лютеїнізуючого гормону понад три рази, що забезпечується активністю індуцибельної ізоформи NOS (iNOS). У той же час підвищення активності iNOS при зниженні активності аргіназного шляху призводить до полярізації макрофагів за прозапальним типом. Введення кверцетину захищає тканину яєчок щурів від окисного пошкодження, викликаного введенням трипторелін, на 90-й день експерименту за рахунок підвищення антиоксидантного захисту та зниження активних форм кисню в тканині.

Ключові слова: *сім'яники, інтерстиційні ендокриноцити, макрофаги, кверцетин, трипторелін, оксидативний стрес, щури.*

DOI: 10.31393/morphology-journal-2023-29(2)-08 Reports of Morphology, Vol. 29, №2, Pages 51-56

ISSN 1818-1295 eISSN 2616-6194

REPORTS OF MORPHOLOGY

Official Journal of the Scientific Society of Anatomists, Histologists, Embryologists and Topographic Anatomists of Ukraine

journal homepage: https://morphology-journal.com

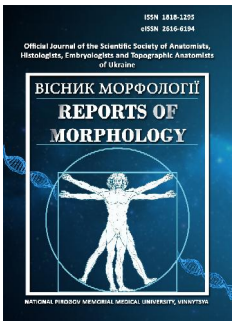

Quantitative characteristics of structural changes in the myocardium of white rats during the modeling of adrenaline myocardiodystrophy and its pharmacological correction

Herasymyuk K. O.

I. Horbachevsky Ternopil National Medical University, Ternopil, Ukraine

ARTICLE INFO

Received: 01 March 2023

Accepted: 03 April 2023

UDC: 616.127-007.17:577.175.522]-085.22-092.9

CORRESPONDING AUTHOR

e-mail: herasymyuk@ukr.net

Herasymyuk K. O.

CONFLICT OF INTEREST

The authors have no conflicts of interest to declare.

FUNDING

Not applicable.

Pathology of the cardiovascular system is one of the leading causes of mortality and disability. In anesthesiology practice, it is the most common comorbid condition that leads to perioperative complications and fatal outcomes. The aim of the study was to substantiate the cardioprotective properties of succinic acid, sodium oxybutyrate, and quercetin based on the study of the myocardial morphological structure in the correction of experimental cardiac pathology. The experiments were conducted on white rats, in which adrenaline-induced myocardial dystrophy was modeled. The correction was performed using succinic acid, sodium oxybutyrate, and quercetin. Morphological studies were conducted at 2 and 24 hours after correction. At 2 hours after adrenaline administration, pronounced venous and arterial congestion was observed in the myocardium. The lumen of vessels appeared dilated, and their walls appeared thinner. In animals that received corrective agents after adrenaline, a positive effect of their application was noted. Vascular congestion was significantly reduced. The arterial walls had normal thickness, and the internal elastic membranes were moderately tortuous. No significant changes were observed in cardiomyocytes. At 24 hours from the start of pathology modeling and its pharmacological correction, the changes in the myocardium of the animals were much more pronounced compared to those with a 2-hour exposure, although in animals treated with corrective agents, the changes were less pronounced than in untreated animals. Rats exposed only to adrenaline showed significant trophic disturbances in cardiomyocytes, which developed against the background of coronary circulation disorders, manifested as wall thickening and narrowing of arterial lumens. The veins were congested, and blood extravasation was observed in the interstitium. Perivascular spaces expanded due to edema. Cardiomyocytes exhibited dystrophic changes, including areas with clarified cytoplasm, often with its homogenization and karyolysis. Histological data were morphometrically confirmed by changes in the Wogenworth index and nuclear-cytoplasmic ratios. The obtained results indicate the positive effect of the used corrective agents. Quercetin demonstrated slightly higher efficacy in this regard.

Keywords: *myocardial dystrophy, correction, cardiomyocytes, arteries, veins.*

Introduction

Pathology of the cardiovascular system today is one of the leading causes of mortality and disability in most countries around the world. It is estimated that by 2030, the mortality rate from these diseases will increase to 23 million or more, surpassing oncological diseases and injuries as the leading cause of death. In Ukraine, approximately 500,000 citizens die each year due to cardiovascular diseases. At the same time, these diseases are among the most common comorbid conditions encountered in anesthesiology practice, leading to the occurrence of perioperative complications and mortality. Therefore, such patients require detailed preoperative examination, identification of risk groups to improve diagnosis, and justification of the choice of anesthesia method with optimal cardioprotective support [7, 12, 19].

Scientific research in recent years is precisely aimed at finding effective means of preventing the development of irreversible necrobiotic processes in the myocardium, including improving the effectiveness of anesthesiological support in cardiothoracic surgeries [7, 13].

However, the majority of modern scientific studies focusing on the impact of correction methods on the heart in its pathological state have a functional nature. At the same time, the number of studies with morphological investigations of their effectiveness, particularly in terms of quantitative characteristics that provide objective confirmation of structural changes occurring in the myocardium, remains insufficient [15].

The aim of the study is to substantiate the cardioprotective properties of succinic acid, sodium oxybutyrate, and quercetin based on the investigation of the morphological structure of the myocardium during the correction of experimental cardiac pathology.

Materials and methods

The experiments were conducted on 54 white laboratory non-pedigreed rats weighing 180-250 g.

The modeling of myocardial damage with the development of signs of cardiovascular insufficiency was carried out using the well-known technique by O.O. Markova [14]. The correction of the disorders was performed by administering succinic acid (at a dosage of 15 mg/kg), sodium oxybutyrate (at a dosage of 100 mg/kg), and quercetin (at a dosage of 1.33 ml/kg) through the enteral route. The drugs were administered 15 minutes after the start of the pathological process simulation. Morphological studies were conducted at 2 and 24 hours after the administration of the corrective agents, corresponding to the onset and peak of myocardial dystrophic lesions [5].

All experimental studies were conducted in accordance with the basic principles of the Resolution of the First National Congress on Bioethics "General Ethical Principles of Experiments on Animals", the Council of Europe Convention for the Protection of Vertebrate Animals Used for Experimental and Other Scientific Purposes, and the Helsinki Declaration.

Histological sections were stained with hematoxylin and eosin, as well as Van Gieson-Weigert stain. The quantitative assessment of vascular reactions was performed by calculating the Wogenwort index (WI), which represents the ratio of the arterial wall area to its lumen area [16]. The functional state of cardiomyocytes was evaluated based on the nuclear-cytoplasmic ratios (NCR) in the left ventricular myocardium [15].

The statistical analysis of the obtained digital data was performed using the Statsoft STATISTICA software package. The difference between the comparative values was determined using the Student's t-test.

Results

Two hours after the administration of a toxic dose of adrenaline, histological sections of the myocardium from experimental animals showed pronounced venous and arterial congestion. The lumen of the blood vessels appeared dilated, while their walls appeared thinner. The internal elastic membranes of the arteries were smoothed. Perivascular spaces were hardly discernible (Fig. 1). This indicated an increased blood flow to the myocardium.

As for the animals to which corrective agents were administered after adrenaline, in all cases, a positive effect of their application could be observed. The vascular congestion was significantly reduced. The arterial walls had normal thickness, and the internal elastic membranes were moderately tortuous. Small aggregates of erythrocytes were observed in the lumens.

At the same time, there were no significant morpho-functional changes observed in cardiomyocytes. Their cytoplasm exhibited normal staining, and the nuclei were well-defined.

During the morphometric studies, it was found that after 2 hours of isolated administration of adrenaline, the expansion of the arterial lumen was significantly confirmed by a 23.9 % decrease in the Wogenwort index ($p<0.05$) compared to the control group (Table 1). Similar reactions were observed in animals that received pharmacological correction after adrenaline administration. However, in these animals, the Wogenwort index showed only a tendency to decrease. Specifically, when quercetin was applied, the degree of decrease in the Vogenwort index was 7.5 %, for sodium oxybutyrate - 10.8 %, and for succinic acid - 11.4 % ($p>0.05$ in all cases). At the same time, in all cases of correction, the Wogenwort index remained significantly higher than the level observed in animals that received adrenaline alone: by 21.6 % with quercetin correction, by 17.2 % with sodium oxybutyrate correction, and by 16.4 % with succinic acid correction ($p<0.05$ in all cases).

Such vascular reactions with corresponding arterial and venous congestion had a certain influence on the morphofunctional state of cardiomyocytes. Despite practically unchanged nuclear area of cardiomyocytes, the area of surrounding cytoplasm significantly increased (Table 2), which could indicate enhanced cellular activity, particularly

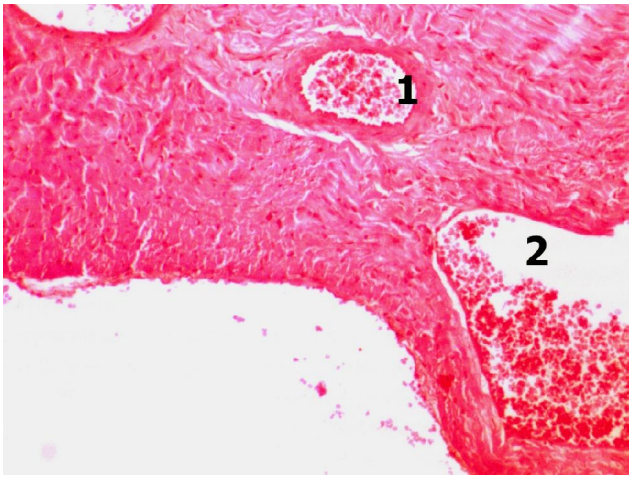

Fig. 1. Histological section of the rat heart wall two hours after the initiation of adrenaline-induced myocardial dystrophy modeling. Lumen of an intramural branch of the coronary artery - 1, erythrocytes in the lumen of a branch of the coronary vein - 2. Hematoxylin and eosin staining. x140.

Table 1. Level of Wogenwort Index (WI) in intramural arteries of the left ventricle of white rats during adrenaline-induced myocardiodystrophy modeling and its correction (M±m).

Values		Study group				
		Control	Adrenaline	Adrenaline + Succinic acid	Adrenaline + Sodium oxybutyrate	Adrenaline + Quercetin
2 hours	WI	170.5±6.9	129.8±5.7*	151.1±4.7#	152.0±4.8#	157.8±3.7#
24 hours	WI	170.5±6.9	218,3±4.5**	197.9±4.4*#	193.4±4.1*#	185.3±6.0#

Notes: * - p<0.05; ** - p<0.01 compared to the control; # - p<0.05 compared to adrenaline.

Table 2. Morphometric characteristics of left ventricular cardiomyocytes in the hearts of white rats during the modeling of adrenaline-induced myocardial dystrophy and its correction (M±m).

Values		Study group				
		Control	Adrenaline	Adrenaline + Succinic acid	Adrenaline + Sodium oxybutyrate	Adrenaline + Quercetin
2 hours	LVCMD	10.70±0.06	11.40±0.03**	11.21±0.06**	11.17±0.03**	11.13±0.03**
	NCD	3.972±0.074	4.012±0.023	4.040±0.033	4.042±0.021	4,041±0.030
	NCR	0.159±0.005	0.141±0.002*	0.149±0.002#	0.150±0.002#	0.152±0.003#
24 hours	LVCMD	10.70±0.06	11.61±0.04**	11.32±0.02**	11.42±0.02**	11.32±0.03**
	NCD	3.970±0.072	4.011±0.030	4.010±0,031	4.083±0.042	4.000±0.030
	NCR	0.159±0.005	0.136±0.003*	0.144±0.002*	0.146±0.003	0.143±0.002*

Notes: * - p<0.05 compared to the control; ** - p<0.01 compared to the control; # - p<0.05 compared to adrenaline; LVCMD - left ventricular cardiomyocyte diameter; NCD - nucleus cardiomyocyte diameter; NCR - nucleus-to-cytoplasm ratio.

in the isolated administration of adrenaline, and could also be an early sign of their hydropic degeneration. The cytoplasmic area of cardiomyocytes, when corrected with succinic acid, sodium oxybutyrate, and especially quercetin, increased to a lesser extent. As a result, the nuclear-cytoplasmic ratio significantly decreased with isolated administration of adrenaline (by 11.3 % compared to the control, with p<0.05), while in combination with corrective agents, there was only a tendency towards reduction: by 6.3 % with succinic acid, 5.7 % with sodium oxybutyrate, and 4.6 % with quercetin (with p>0.05 in all cases). Meanwhile, compared to isolated administration of adrenaline, they significantly exceeded its level by 5.7 %, 6.4 %, and 7.8 %, respectively (with p<0.05 in all cases).

After 24 hours from the onset of modeling the studied pathology and its pharmacological correction, the changes in the myocardium of all experimental animals were significantly greater than in animals with a 2-hour exposure. Although in animals treated with corrective agents, these changes were less pronounced compared to animals without correction.

In rats exposed only to a toxic dose of adrenaline, pronounced disturbances in the trophism of cardiomyocytes were observed, which developed against the backdrop of severe disorders of coronary blood flow characterized by increased wall tone and narrowing of arterial lumen, confirmed by the tortuosity of their internal elastic membranes. Veins were congested, and blood extravasation was observed in the interstitium. Perivascular spaces expanded due to edema.

As a result of the disturbances in blood supply, cardiomyocytes exhibited changes of a dystrophic nature. Foci with clarified cytoplasm were frequently observed, and in some cases, even cytoplasmic homogenization and karyolysis occurred (Fig. 2).

These changes were supported by morphometric evidence. After 24 hours of isolated adrenaline administration, there was a significant increase in LV (left ventricle) on 28.2 % (p<0.05) compared to the control group, rather than a decrease, due to arterial constriction (see Table 1). Similar processes were observed in animals where medicinal correction was applied after adrenaline administration: LV increase with quercetin - by 8.8 % (p>0.05), sodium oxybutyrate - by 13.5 % (p<0.05), and succinic acid - by 15.9 % (p<0.05). However, in all correction cases, LV remained significantly lower than the level registered in

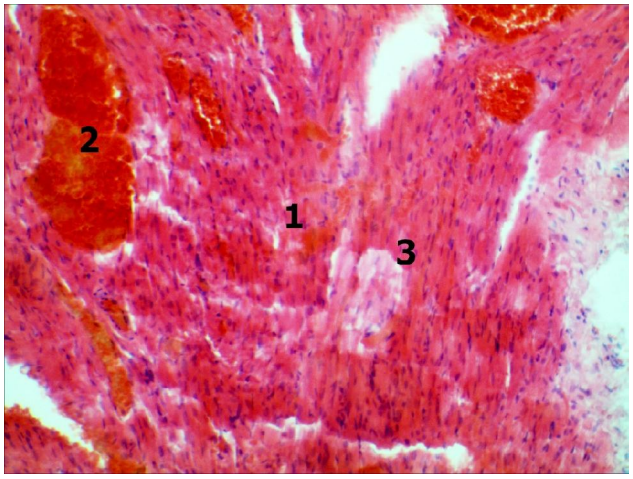

Fig. 2. Histological section of the rat heart wall after 24 hours from the beginning of modeling of adrenaline myocardiodystrophy. Irregular staining and fragmentation of cardiomyocytes - 1, interstitial hemorrhage - 2, focus of cytoplasmic homogenization in cardiomyocytes - 3. Stained with hematoxylin and eosin. x120.

animals receiving only adrenaline: by 21.6 % with quercetin correction, by 17.2 % with sodium oxybutyrate correction, and by 16.4 % with succinic acid correction ($p<0.05$ in all cases), which confirms the effectiveness of their corrective influence.

Against the backdrop of vascular reactions, corresponding changes were also observed in cardiomyocytes, which were quantitatively supported by morphometric research data. Despite almost unchanged nuclear area, the surrounding cytoplasm area significantly increased, particularly more intensely than during the 2-hour observation period (see Table 2), which may be a consequence of intracellular edema development. Moreover, the cytoplasm area increased more intensively specifically during isolated adrenaline administration. The cytoplasm area of cardiomyocytes increased to a lesser extent during succinic acid, sodium oxybutyrate, and especially quercetin correction, but at the same time, more intensively than during the 2-hour observation. As a result, the nuclear-cytoplasmic ratio noticeably decreased in all cases: by 14.5 % ($p<0.05$) during isolated adrenaline administration, by 9.4 % ($p<0.05$) during succinic acid administration, by 8.2 % ($p>0.05$) during sodium oxybutyrate administration, and by 9.1 % ($p<0.05$) during quercetin administration compared to the control.

It should be noted that the difference in indicators between the corrected animals and animals with isolated adrenaline administration was no longer significant and exceeded its level by only 5.1-7.3 % (with $p>0.05$).

Discussion

As it is known, the development of most pathological processes is directly or indirectly associated with the disturbance of oxygen homeostasis in the body. In this regard, both general and local hypoxia are considered as additional factors of damage, initiating mechanisms of necrobiosis and oxidative stress [4].

Hypoxia itself induces a variety of pathological disorders. The main regulator of the body's response to hypoxia is a specific protein found in cell nuclei called hypoxia-inducible factor (HIF-alpha). Under normal oxygen levels, the amount of HIF-alpha is low. However, when cellular oxygen levels sharply decrease, the level of HIF-alpha increases and can lead to cellular apoptosis. Succinate, or in other words, succinic acid, is capable of inhibiting HIF-alpha and stabilizing its level [18].

Pharmaceutical preparations containing succinic acid have been used for a long time as antioxidants that normalize intracellular metabolism and promote the restoration of organ functions impaired by diseases or natural cell aging. The antihypoxic effects of succinic acid salts are enhanced by their antioxidant properties, their ability to modify phospholipids and facilitate their resynthesis, as well as reduce ion permeability of membranes and the efflux of K^+ from mitochondria against the concentration gradient [2, 17].

Due to their broad pharmacodynamic spectrum and low toxicity, quercetin preparations have long attracted the attention of researchers and clinicians. The most important properties of these preparations are their pronounced antioxidant, immunomodulatory, and anti-inflammatory effects. Quercetin primarily acts as a scavenger of free radicals and has the ability to activate enzymes involved in the body's own antioxidant defense. It exerts anti-inflammatory effects by blocking the lipoxygenase pathway of arachidonic acid metabolism, reducing the synthesis of leukotrienes, serotonin, and other inflammatory mediators. Quercetin enhances the activity of phagocytes, T- and B-lymphocytes, and the production of antibodies, thereby reducing the manifestations of secondary immunodeficiency [1, 10, 11].

Moreover, quercetin is one of the most common and readily available flavonoids, which accumulates in the form of glycosides in many medicinal plants [3, 8].

Sodium oxybutyrate belongs to the category of classical antihypoxants. It also exhibits elements of nootropic activity and exerts sedative, hypnotic, narcotic, and muscle-relaxing effects. Importantly, it enhances the body's resistance, including that of the brain, heart, and retinal tissue, to hypoxia by activating oxidative processes [6].

Potentially, all antihypoxants, regardless of their chemical structure, can have secondary antioxidant effects due to their energy-stabilizing and antacid properties, which prevent excessive formation of free radicals and suppress endogenous ones [17].

Thus, the obtained results indicate a positive effect of the administered medications. In their selection, we focused on the fact that they share common antihypoxic properties. It is worth noting that quercetin showed slightly higher effectiveness compared to others due to its combination of cardioprotective and angioprotective properties [6, 9, 13].

The obtained results indicate the need for further study of cardioprotective agents with morphological justification of their effectiveness.

Conclusion

1. A cardiotoxic dose of adrenaline induces dystrophic changes in the cardiomyocytes of rats, which progressively increase from 2 to 24 hours of observation after administration of the drug.

2. Succinic acid, sodium oxybutyrate, and quercetin have a cardioprotective effect by exerting a positive regulatory influence on coronary blood flow and reducing myocardial hypoxia.

3. Quercetin is slightly more effective as a cardioprotective and angioprotective agent compared to succinic acid and sodium oxybutyrate.

References

[1] Alrawaiq, N. S., & Abdullah, A. (2014). A review of flavonoid quercetin: metabolism, bioactivity and antioxidant properties. *International Journal of PharmTech Research,* 6(3), 933-941.

[2] Arason, K. M., & Bergmeier, S. C. (2002). The synthesis of succinic acids and derivatives. A review. *Organic Preparations and Procedures International,* 34(4), 337-366.

doi: 10.1080/00304940209458074
[3] Bischoff, S. C. (2008). Quercetin: potentials in the prevention and therapy of disease. *Current Opinion in Clinical Nutrition & Metabolic Care,* 11(6), 733-740. doi: 10.1097/MCO.0b013e32831394b8
[4] Bonazzi, A., Mastyugin, V., Mieyal, P. A., Dunn, M. W., & Laniado-Schwartzman, M. (2000). Regulation of cyclooxygenase-2 by hypoxia and peroxisome proliferators in the corneal epithelium. *Journal of Biological Chemistry,* 275(4), 2837-2844. doi: 10.1074/jbc.275.4.2837
[5] Chebotar, L. D. (2011). Функціональний стан серця щурів в умовах гіпофункції епіфізу на тлі розвитку адреналінової міокардіодистрофії [Functional state of rat hearts under conditions of pineal gland hypofunction against the development of adrenaline myocardiodystrophy]. *Актуальні проблеми сучасної медицини: Вісник української медичної стоматологічної академії - Current issues in modern medicine: Bulletin of the Ukrainian Medical Dental Academy,* 11(2 (34)), 103-106.
[6] Dzuba, D. O., & Nedashkivskyi, S. M. (2013). Оксибутират натрію: знайомий незнайомець [Sodium oxybutyrate: a familiar stranger]. *Гострі та невідкладні стани у практиці лікаря - Acute and Emergency Conditions in Medical Practice* 4-5(36). https://urgent.com.ua/ua/archive/2013/4-5 %2836%29/article-469/oksibutirat-natriyu-znayomiy-neznayomec
[7] Dzuba, D. O., Zhurovska, Y. M., & Loskutov, O. A. (2017). Питання анестезіологічного забезпечення в інтервенційній кардіології [Issues of anesthetic support in interventional cardiology]. *Медицина невідкладних станів - Emergency Medicine,* 1(80), 125-128.
[8] Fortunato, L. R., Alves, C. D. F., Teixeira, M. M., & Rogerio, A. P. (2012). Quercetin: a flavonoid with the potential to treat asthma. *Brazilian Journal of Pharmaceutical Sciences*, 48, 589-599. doi: 10.1590/S1984-82502012000400002
[9] Koval', N. I., & Klishch, I. M. (2013). Вплив поєднаного застосування пірацетаму і Кислоти бурштинової на показники прооксидантно-оксидантного гомеостазу та активність мітохондріальних ферментів у щурів за умов експериментальної тканинної гіпоксії [The impact of combined use of piracetam and succinic acid on indicators of prooxidant-antioxidant homeostasis and mitochondrial enzyme activity in rats under conditions of experimental tissue hypoxia]. *Фармацевтичний часопис - Pharmaceutical Journal,* 3, 25-28.
[10] Kumar, R., Vijayalakshmi, S., & Nadanasabapathi, S. (2017). Health benefits of quercetin. *Defence Life Science Journal,* 2(2), 142-151. doi: 10.14429/dlsj.2.11359
[11] Li, Y., Yao, J., Han, C., Yang, J., Chaudhry, M. T., Wang, S., ... & Yin, Y. (2016). Quercetin, inflammation and immunity. *Nutrients,* 8(3), 167. doi: 10.3390/nu8030167
[12] Lyashok, A. L. (2013). Передопераційна підготовка хворих з високим кардіальним ризиком [Preoperative preparation of patients with high cardiac risk]. *Медицина транспорту України - Transport Medicine in Ukraine*, 2, 84-89.
[13] Lynda, O. S., Pelykh, V. Ye., Fira, L. S., & Denefil, O. V. (2019). Порівняльний аналіз кардіопротекторних властивостей корвітину та сухого екстракту з хости ланцетолистої листя за умов адреналінового ушкодження серця [A comparative analysis of the cardioprotective properties of corvitin and dry extract from the lanceolate hosta leaves at adrenaline heart injury]. *Медична та клінічна хімія - Medical and Clinical Chemistry,* 4(21), 44-53. doi: 10.11603/mcch.2410-681X.2019.v.i4.10838
[14] Markova, O. O. (1998). *Міокардіодистрофія і реактивність організму [Myocardiodystrophy and Reactivity of the Organism]*. Тернопіль: Укрмедкнига - Ternopil: Ukrmedknyha.
[15] Slabyy, O. B. (2016). Ядерно-цитоплазматичні відношення у кардіоміоцитах та ендотеліоцитах передсердь легеневого серця [Nuclear-cytoplasmic ratios in cardiomyocytes and endotheliocytes of the atria of the pulmonary heart]. *Здобутки клінічної і експериментальної медицини - Achievements of Clinical and Experimental Medicine,* (4), 103-106.
[16] Slavnov, A. A., & Dolgikh, V. T. (2014). Морфологические изменения в стенке аорты после кровопотери (экспериментальное исследование) [Morphological changes in the aortic wall after blood loss (experimental study)] *Общая реаниматология - General Reanimatology*, 10(4), 37-43.
[17] Tretter, L., Szabados, G., Ando, A., & Horvath, I. (1987). Effect of succinate on mitochondrial lipid peroxidation. 2. The protective effect of succinate against functional and structural changes induced by lipid peroxidation. *Journal of Bioenergetics and Biomembranes,* 19(1), 31-44. doi: 10.1007/BF00769730
[18] Turchinskii, M. F., Ainbinder, E. I., Knorre, V. D., & Shcherbo, S. N. (1989). Modification of DNA with dihydrazide of succinic acid for preparation of hybridization probes. *Bioorganicheskaia Khimiia,* 15(10), 1341-1345. PMID: 2534344
[19] Zozulya, I. S., & Zozulya, A. I. (2011). Епідеміологія цереброваскулярних захворювань в Україні [Epidemiology of cerebrovascular diseases in Ukraine]. *Український медичний часопис - Ukrainian Medical Journal,* (5), 38-41.

КІЛЬКІСНА ХАРАКТЕРИСТИКА СТРУКТУРНИХ ЗМІН В МІОКАРДІ БІЛИХ ЩУРІВ ПРИ МОДЕЛЮВАННІ АДРЕНАЛІНОВОЇ МІОКАРДІОДИСТРОФІЇ ТА ЇЇ МЕДИКАМЕНТОЗНІЙ КОРЕКЦІЇ

Герасимюк К. О.

Патологія серцево-судинної системи є однією з основних причин смертності та інвалідизації. В анестезіологічній практиці це найпоширеніший коморбідний стан, котрий призводить до виникнення періопераційних ускладнень та летального результату. Мета дослідження - на основі вивчення морфологічної структури міокарда обгрунтувати кардіопротекторні властивості бурштинової кислоти, оксибутирату натрію і кверцетину при корекції експериментальної серцевої патології. Експерименти проведені на білих щурах, котрим моделювали адреналінову міокардіодистрофію. Корекцію проводили бурштиновою кислотою, оксибутиратом натрію і кверцетином. Морфологічні дослідження проводили через 2 і 24 години після корекції. Через 2 години після введення адреналіну в міокарді спостерігалося виражене венозне і артеріальне повнокров'я. Просвіт судин виглядав розширеним, а їх стінки потоншеними. У тварин, котрим після адреналіну вводили коригуючі середники, відмічений позитивний ефект від їх застосування. Значно меншим було кровонаповнення судин. Стінки артерій були звичайної товщини, внутрішні еластичні мембрани помірно звивисті. Особливих змін зі сторони кардіоміоцитів не спостерігалося. Через 24 години від початку моделювання патології та її медикаментозної корекції зміни у міокарді тварин були значно більшими, ніж у тварин з 2-х годинною експозицією, хоча у тварин із застосуванням коригуючих середників вони були менш вираженими, ніж у тварин без корекції. У щурів, які піддавалися лише впливу адреналіну, відмічені виражені порушення трофіки кардіоміоцитів, які розвивалися на фоні розладів коронарного кровообігу у вигляді потовщення стінок і

звуження просвіту артерій. Вени були повнокровними, зустрічалися крововиливи в інтерстиції. Периваскулярні простори розширювалися за рахунок набряку. У кардіоміоцитах відмічалися зміни дистрофічного характеру: зустрічалися вогнища з просвітленою цитоплазмою, нерідко з її гомогенізацію й каріолізом. Гістологічні дані мали своє морфометричне підтвердження у вигляді відповідної динаміки індекса Вогенворта та ядерно-цитоплазматичних відношень. Отримані результати свідчать про позитивний ефект застосовуваних медикаментозних середників. Дещо більшу ефективність у цьому відношенні проявляв кверцетин.

Ключові слова: *міокардіодистрофія, корекція, кардіоміоцити, артерії, вени.*

DOI: 10.31393/morphology-journal-2023-29(2)-09 Reports of Morphology, Vol. 29, №2, Pages 57-65

ISSN 1818-1295 eISSN 2616-6194

REPORTS OF MORPHOLOGY

Official Journal of the Scientific Society of Anatomists, Histologists, Embryologists and Topographic Anatomists of Ukraine

journal homepage: https://morphology-journal.com

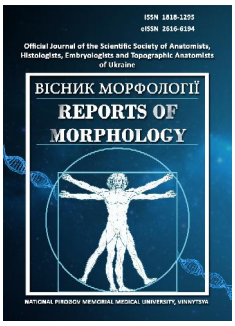

Comparison of temporal cavity indicators when firing "FORT 12R" and "AE 790G1" into a non-biological body simulator

Kusliy Yu. Yu., Shkolnikov V. S., Shevchuk Yu. G., Fomin O. O., Zverkhovska V. F.
National Pirogov Memorial Medical University, Vinnytsia, Ukraine

ARTICLE INFO
Received: 15 March 2023
Accepted: 17 April 2023

UDC: 616-001.45:623.443.35

CORRESPONDING AUTHOR
e-mail: dr.yurus@ukr.net
Kusliy Yu. Y.

CONFLICT OF INTEREST
The authors have no conflicts of interest to declare.

FUNDING
Not applicable.

Gunshot injuries are extremely dangerous due to the extremely unpredictable compliance of ammunition after contact with the body. One of the key elements that takes place in this case is the formation due to high kinetic energy of a temporary cavity, which, despite its existence for a fraction of a second, causes severe damage to the tissues of the human body. The study of this phenomenon is one of the central elements of ballistics and requires an experiment on optically transparent media. The purpose of the study is to compare the parameters of the temporal cavity when fired from the "FORT 12R" and "AE 790G1" pistols into a non-biological simulator of the human body. To achieve the goal, 120 gelatin blocks were produced according to the generally accepted method, which were to be shot at close range, 25 and 50 cm. The blocks were left bare before shooting, or covered with cotton fabric, denim fabric or leatherette. After firing, transverse sections of the blocks were made in order to further measure the parameters of the temporary cavity formed as a result of the firing, according to generally accepted methods. The results of the analysis of the received data regarding the indicators characterizing the dimensions of the temporary cavity at different depths of the wound channel revealed a number of significant differences ($p<0.05$-0.01) between the studied pistols (in almost all cases, "AE 790G1" had larger values), groups of blocks covered with different types of fabrics, bare blocks (in almost all cases, the clothing had protective properties and reduced the size of the temporary cavity) and allowed to establish that during shots from the "FORT 12R" there was a sharp increase in the size of the temporary cavity with its sharp decrease at the end of the wound channel, while with shots from the "AE 790G1" the temporary cavity gradually increases, reaching a maximum at half the depth and then just as gradually decreases. Thus, when comparing the "FORT 12R" and "AE 790G1" pistols, differences in the features of the formation of the temporary cavity were revealed, which in turn is of interest not only for forensics, ballistics and forensic medicine, but also for clinical medicine.

Keywords: *gunshot injury, gunshot wounds, firearm, temporary cavity, imitator of the human body.*

Introduction

Gunshot injury is a common type of injury that often leads to death. The larger the caliber of the weapon, the greater the chance of a fatal outcome [2]. An analysis of the use of firearms in the city of Benin (Nigeria) from 1998 to 2002 showed 210 cases of fatal use of firearms. Most of them (88.1 %) were committed by criminals and a small part (9.0 %) by law enforcement agencies. 88.5 % of lethal use of weapons was murder, 4.3 % accidental and 0.5 % suicide [1]. Data from the National Electronic Injury Surveillance System in the USA showed that the death rate from the use of firearms is a fairly stable indicator and was 22 % in both 2003 and 2012 [5].

In Ukraine, the urgency of gunshot injury research has increased significantly since 2014 [15]. One of the peculiarities of this issue for Ukraine is the extreme urgency of studying gunshot injuries caused by non-lethal weapons, which are more widespread among different strata of the population, which is related to the peculiarity of the legal system.

One of the key tasks of ballistics is the study of projectile handling on the way to the target. We are talking about both pre-wound ballistics - how the projectile behaves when it comes into contact with the body, the impact of obstacles, weather factors, etc., and wound ballistics - the behavior of

the projectile in the object it hit, and first of all - the human body. In wound ballistics, a key place is occupied by the study of temporary cavities, formations that are the result of the transfer of excessive kinetic energy from the projectile to the surrounding tissues and fluids of the human body [4, 14].

One of the most effective and expedient methods of studying the temporal cavity is conducting ballistic experiments using a non-biological imitator of the human body, namely gelatin [3]. Due to the transparency and imitation of the physical characteristics of muscle and fat tissue, this material has become the most common. Also common practice is the use of time-lapse cameras, which allows recording processes lasting a fraction of a second [18] or combining gelatin with biological imitators of the human body [12]. At the same time, there are still ongoing discussions about the influence of various variables on the characteristics of gelatin, such as temperature factors, preparing features, etc. [13].

Taking into account the need to study the features of the temporary cavity for modern models of non-lethal firearms (primarily common in Ukraine), there is a need to conduct an experimental study on gelatin samples, taking into account the presence of obstacles in the form of clothing.

The purpose of the work is to conduct a comparative analysis of the indicators of the temporal cavity during shots from "FORT 12R" and "AE 790G1" pistols from different shooting distances into non-biological simulators of the human body covered and uncovered by various types of clothing.

Materials and methods

The study was performed on 120 gelatin blocks made according to the method of Fackler and Malinowski [6], divided into 2 groups of 60 blocks. Group 1 was subject to shooting using the "FORT 12R" pistol, group 2 - "AE 790G1" (both equipped with 9 mm cartridges, elastic bullets of traumatic effect). In each group, 4 subgroups of 15 blocks were formed: 1st group - bare blocks (BB), 2nd group - blocks covered with cotton fabric (CF), 3rd group - blocks covered with denim fabric (DF), 4th group - blocks covered with leatherette (LB). Shootings were carried out from contact range, 25 and 50 cm. After shooting, the blocks were examined according to The total crack length method [6], The Fackler's wound profile method [16] and The polygon-procedure method [17]. The results were photographed in accordance with the rules of forensic photography using an Alpha A6000 Sony digital camera.

The work was carried out as part of the research work of the National Pirogov Memorial Medical University, Vinnytsia at the expense of state funding of the Ministry of Health of Ukraine: "Characteristics of damage to human body tissue simulators caused by non-lethal weapons' (state registration number 0121U107924).

Committee on Bioethics of National Pirogov Memorial Medical University, Vinnytsya (protocol № 11 From 03.12.2020) found that the studies do not contradict the basic bioethical standards of the Declaration of Helsinki, the Council of Europe Convention on Human Rights and Biomedicine (1977), the relevant WHO regulations and laws of Ukraine.

The statistical analysis of the obtained results was carried out in the licensed statistical package "Statistica 6.0" using non-parametric estimation methods. The reliability of the difference in values between independent quantitative values was determined using the Mann-Whitney U-test, and between qualitative values - according to the Weber E.

Results

TCLM values when fired from the "FORT 12R" and "AE 790G1" pistols have the following features: at a cut depth of 1 cm when fired at *contact range from the "FORT 12R" pistol*, significantly higher values ($p<0.05$-0.01) of the indicator were found at shots in BB, CF or LB compared to DF (87.16±8.09, 85.36±7.52, 87.16±14.45 and 66.16±9.05, respectively); when shooting from a *distance of 25 cm from the "FORT 12R" gun*, significantly higher values ($p<0.01$) of the indicator were found when shooting BBs compared to blocks covered with any types of fabrics (64.68±10.43, 10.42±3.56, 23.50±8.83 and 19.10±6.28, respectively) and significantly lower values ($p<0.05$-0.01) of the indicator when shooting in CF, compared to DF or LB (10.42±3.56, 23.50±8.83 and 19.10±6.28, respectively); when shooting from a *distance of 50 cm from the "FORT 12R" pistol*, significantly higher values ($p<0.05$) of the indicator were found when shooting at DF compared to BB or CF or LB (14.34±3.88, 7.860±2.862, 6.220±3.539 and 6.500±3.434, respectively); when comparing the values of the indicator when shooting from *"FORT 12R"* from different distances, significantly higher values ($p<0.05$-0.01) of the indicator were found when shooting at close range, compared to the shooting distance of 25 cm, 50 cm, and when comparing the indicators at shooting distances 25 and 50 cm for all groups of blocks; when firing at *contact range from the "AE 790G1" pistol*, significantly lower values ($p<0.05$) of the indicator were found when firing at CF compared to DF or LB (75.38±23.23, 124.1±32.0 and 121.6±23.1, respectively); when shooting from a *distance of 25 cm from the "AE 790G1" gun*, significantly higher values ($p<0.05$-0.01) of the indicator were found when shooting BBs compared to blocks covered with fabrics (73.84±18.92, 32.10±19.26, 11.52±6.33 and 34.90±10.77, respectively); when comparing the values of the index when shooting from the *"AE 790G1"* from different distances, significantly lower values ($p<0.01$) of the index were found when shooting BBs from a distance of 50 cm compared to 25 cm and close (6.980±3.238, 73.84±18.92 and 87.22±25.76, respectively), significantly higher ($p<0.05$-0.01) values of the indicator when shooting in CF, DF at close range, compared to 25 and 50 cm (75.38±23.23, 32.10±19.26, 14.14±7.44 and 124.1±32.0, 11.52±6.33, 11.62±6.03

respectively) and significantly higher values (p<0.01) of the indicator at close range shots, compared to the shot distance of 25 cm, 50 cm and when comparing the indicators at the shot distances of 25 and 50 cm in LB (121.6±23.1, 34.90±10.77 and 6.160±3.607 in accordance). When comparing the values of the indicator when fired from the "FORT 12R" and "AE 790G1" pistols, its values were significantly higher (p<0.05-0.01) when fired from the "AE 790G1" when fired at close range in DF, LB and when fired from a distance of 25 cm in LB (124.1±32.0 and 66.16±9.05, 121.6±23.1 and 87.16±14.45, 34.90±10.77 and 19.10±6.28, respectively), and higher values when using "FORT 12R" only when shooting from a distance of 25 cm in DF (23.50±8.83 and 11.52±6.33, respectively);

at a cut depth of 2 cm when *contact shots from the "FORT 12R" pistol* revealed significantly lower values (p<0.05) of the indicator when shooting BB compared to LB (72.48±15.78 and 91.68±8.19 respectively); when fired from a *distance of 50 cm from the "FORT 12R" gun*, significantly lower (p<0.05-0.01) values of the indicator were found when fired at BB, CF and LB blocks, compared to DF (3.360±1.704, 3.300±3.213, 2.860±3.916 and 9.460±2.333, respectively); when comparing the values of the indicator when shooting from *"FORT 12R"* from different distances, significantly higher values (p<0.05-0.01) of the indicator were found when shooting at close range, compared to the shooting distance of 25 cm, 50 cm, and when comparing the indicators at shooting distances 25 and 50 cm for both BB and LB (72.48±15.78, 16.58±10.64, 3.360±1.704 and 91.68±8.19, 9.300±2.570, 2.860±3.916, respectively) and also significantly higher values (p<0.01) of the indicator at close range shots compared to the shot distance of 25 cm, 50 cm for CF and DF (84.02±13.17, 7.760±2.162, 3.300±3.213 and 86.58± 13.57, 11.76±8.19 and 9.460±2.333, respectively); when *contact shots from the "AE 790G1" pistol* revealed significantly higher values (p<0.05-0.01) of the indicator when shooting at DF compared to BB and CF (156.3±22.6, 101.8±19.8 and 121.9±15.5, respectively); when shooting from a *distance of 25 cm from the "AE 790G1" pistol*, significantly higher values (p<0.05) of the indicator were found when shooting at BB or CF compared to DF, LB (35.24±13.75, 27.76±4.75, 15.30±6.89 and 19.84±6.07, respectively); when shooting from a *distance of 50 cm from the "AE 790G1" pistol*, significantly lower values (p<0.05-0.01) of the indicator were found when shooting BBs compared to covered blocks (0.460±1.029, 11.22±4.66, 7.254±8.344 and 5.080±3.235, respectively) and significantly higher values (p<0.05) of the indicator when shooting in CF than LB (11.22±4.66 and 5.080±3.235, respectively); when comparing the values of the indicator when shooting with the *"AE 790G1"* from different distances, significantly higher values (p<0.01) of the indicator were found when shooting at close range, compared to the shooting distance of 25 cm, 50 cm, and when comparing the indicators at the shooting distances of 25 and 50 cm both for BB and CF or LB (101.8±19.8, 35.24±13.75, 0.460±1.029 and 121.9±15.5, 27.76±4.75, 11.22±4.66 and 129.4±34.8, 19.84±6.07, 5.080±3.235, respectively) and significantly higher values (p<0.01) of the indicator when shooting at close range, compared to the shooting distance of 25 cm, 50 cm when shooting in DF (156.3±22.6, 15.30±6.89 and 7.254±8.344, respectively); when comparing the values of the indicator when fired from the "FORT 12R" and "AE 790G1" pistols, it is significantly higher (p<0.05-0.01), its values were found when fired from the "AE 790G1" when fired at close range and 25 cm in BB (101.8±19.8, 35.24±13.75 and 72.48±15.78, 16.58±10.64, respectively), when shooting from all distances in CF (121.9±15.5, 27.76±4.75, 11.22±4.66 and 84.02±13.17, 7.760±2.162, 3.300±3.213, respectively), when shooting at close range in DF (156.3±22.6 and 86.58 ±13.57, respectively) and 25 cm in LB (19.84±6.07 and 9.300±2.570, respectively); significantly higher (p<0.05) values were found when firing "FORT 12R" BBs from a distance of 50 cm (3.360±1.704 and 0.460±1.029, respectively);

at a cut depth of 3 cm when *contact shots from the "FORT 12R" pistol* revealed significantly lower values (p<0.01) of the index when shooting BBs compared to blocks covered with fabrics (25.34±7.69, 88.28±15.13, 76.36±17.24 and 52.70±10.32, respectively) and significantly lower values (p<0.05) of the indicator when shooting at LB compared to CF or DF (52.70±10.32, 88.28±15.13 and 76.36±17.24, respectively); when shooting from a *distance of 25 cm from the "FORT 12R" pistol*, significantly lower values (p<0.05-0.01) of the indicator were found when shooting at BB, LB and CF and DF (0, 0, 5.060±3.159 and 5.340±3.727 in accordance); when comparing the values of the indicator when shooting with *"FORT 12R"* from different distances, significantly higher values (p<0.01) of the indicator were found when shooting at close range, compared to the shooting distance of 25 cm, 50 cm when shooting at BB and LB (25.34±7.69, 0, 0.560±1.252 and 52.70±10.32, 0,0 respectively) and significantly higher values (p<0.05-0.01) of the indicator when shooting at close range, compared to a shot distance of 25 cm, 50 cm and when comparing indicators at shot distances of 25 and 50 cm for both CF and DF (88.28±15.13, 5.060±3.159, 0.860±1.923 and 76.36±17.24, 5.340±3.727 and 0, 0 respectively); when *contact shots from the "AE 790G1" pistol* revealed significantly lower values (p<0.05-0.01) of the indicator when shooting at BB compared to CF or DF (63.50±15.12, 105.0±24.8 and 106.1±16.1, respectively); when comparing the values of the indicator when shooting from the *"AE 790G1"* from different distances, significantly higher values (p<0.01) of the indicator were found when shooting at close range, compared to the shooting distance of 25 cm, 50 cm when shooting at all groups of blocks (63.50±15.12, 0, 0 and 105.0±24.8, 4.540±4.194, 1.620±3.622 and 106.1±16.1, 1.060±2.370, 0 and 87.46±24.29, 0, 0, respectively); when comparing the values of the indicator when fired from

pistols "FORT 12R" and "AE 790G1" significantly higher (p<0.05-0.01), its values were found when fired from "AE 790G1" when fired at close range in BB and DF or LB (63.50±15.12 and 25.34±7.69, 106.1±16.1 and 76.36±17.24, 87.46±24.29 and 52.70±10.32, respectively);

at a cut depth of 4 cm when *contact shots from the "FORT 12R" pistol* revealed significantly lower values (p<0.01) of the index when shooting BBs compared to blocks covered with fabrics (0, 59.98±12.81, 66.80±17.45 and 28.40±6.97, respectively) and significantly lower values (p<0.01) of the indicator when shooting in LB compared to CF or DF (28.40±6.97, 59.98±12.81 and 66.80±17.45, respectively); when comparing the values of the indicator when shooting from *"FORT 12R"* from different distances, significantly higher values (p<0.01) of the indicator were found when shooting at close range, compared to the shooting distance of 25 cm, 50 cm when shooting at all groups of blocks covered with fabrics (59.98±12.81, 0.260±0.581, 0 and 66.80±17.45, 0, 0 and 28.40±6.97, 0, 0, respectively); when *contact shots from the "AE 790G1" pistol* revealed significantly lower values (p<0.05-0.01) of the index when shooting BBs compared to blocks covered with fabrics (19.58±15.00, 60.48±10.73, 63.14±24.44 and 59.48±13.16, respectively); when comparing the values of the indicator when fired from the "AE 790G1" from different distances, significantly higher values (p<0.05-0.01) of the indicator were found when fired at close range, compared to a shot distance of 25 cm, 50 cm when fired at all groups of blocks (19.58±15.00, 0, 0 and 60.48±10.73, 0, 0 and 63.14±24.44, 0, 0 and 59.48±13.16, 0, 0, respectively); when comparing the values of the indicator when fired from "FORT 12R" and "AE 790G1" pistols, significantly higher (p<0.05-0.01) its values were found when fired from "AE 790G1" when fired at close range in BB and LB (19.58±15.00 and 0, 59.48±13.16 and 28.40±6.97, respectively);

at a cut depth of 5 cm when *contact shots from the "FORT 12R" pistol* revealed significantly lower values (p<0.01) of the indicator when shooting at BB or LB compared to CF or DF (0, 0, 24.26±10.75 and 40.16±15.03, respectively); when comparing the values of the indicator when shooting with *"FORT 12R"* from different distances, significantly higher values (p<0.01) of the indicator were found when shooting at close range, compared to the shooting distance of 25 cm, 50 cm when shooting at CF or DF (24.26±10.75, 0, 0 and 40.16±15.03, 0, 0, respectively); when *contact shots from the "AE 790G1" pistol* revealed significantly higher values (p<0.05-0.01) of the indicator when shooting in CF compared to BB and DF or LB (37.80±6.97, 0, 12.58 ±12.39 and 18.78±17.41, respectively); when comparing the values of the indicator when shooting from *"AE 790G1"* from different distances, significantly higher values (p<0.01) of the indicator were found when shooting at close range, compared to the shooting distance of 25 cm, 50 cm when shooting at CF (37.80±6.97, 0 and 0 respectively); when comparing the values of the indicator when fired from "FORT 12R" and "AE 790G1" pistols, its values were significantly higher (p<0.05) when fired at close range from "FORT 12R" in DF (40.16±15.03 and 12.58±12.39, respectively).

The *FWPM* values when fired from the "FORT 12R" and "AE 790G1" pistols have the following features: at a cut depth of 1 cm when fired at *contact range from the "FORT 12R" pistol*, significantly lower values (p<0.05) of the indicator were found when fired at LB compared to with BB and CF (11.60±1.78, 14.88±1.61 and 14.78±0.89, respectively); when shooting from a *distance of 25 cm from the "FORT 12R" pistol*, significantly higher values (p<0.05-0.01) of the indicator were found when shooting at BB compared to CF or LB (14.68±0.40, 5.800±1.528 and 10.42±2.74, respectively); when comparing the values of the indicator when shooting from *"FORT 12R"* from different distances, significantly higher values (p<0.05-0.01) of the indicator were found when shooting at close range, compared to the shooting distance of 25 cm, 50 cm when shooting at CF (14.78±0.89, 5.800±1.528 and 5.840±3.537, respectively), when shooting at close range, 50 cm and 25 and 50 cm in BB and LB (14.88±1.61, 6.960±2.174 and 14.68±0.40, 6.960±2.174, 11.60±1.78, 4.840±2.232 and 10.42±2.74, 4.840±2.232, respectively), when shooting at close range compared to 50 cm when shooting at DF (14.48±2.98 and 7.360±1.679, respectively); when *contact shots from the "AE 790G1" pistol* revealed significantly lower values (p<0.05-0.01) of the indicator when shooting BBs compared to blocks covered with fabric (15.64±2.37, 21.96±3.01, 31.98±3.42 and 30.52±3.50, respectively) and when shot in CF compared to other tissue types (21.96±3.01, 31.98±3.42 and 30.52±3.50 respectively); when shooting from a distance of 25 cm from the *"AE 790G1"* pistol, significantly higher values (p<0.01) of the indicator were found when shooting at BB or LB compared to CF or DF (16.08±0.91, 18.32±2.69 and 9.960±3.807, 6.940±3.190, respectively); when comparing the values of the indicator when shooting from the "AE 790G1" from different distances, significantly higher values (p<0.01) of the indicator were found when shooting at close range, compared to the distance of a shot of 25 cm, 50 cm when shooting at CF and DF (21.96±3.01, 9.960±3.807, 8.360±3.679 and 31.98±3.42, 6.940±3.190, 6.000±2.035, respectively), for close shots compared to 25 cm shot distance, and 25 cm compared to 50 cm shots in BB (15.64±2.37, 6.260±2.422 and 16.08±0.91, 6.260±2.422, respectively), shots at close range, compared to shot distances of 25 cm, 50 cm and when comparing indicators at shot distances of 25 and 50 cm in LB (30.52±3.50, 18.32±2.69 and 4.780±2.084, respectively); when comparing the values of the indicator when fired from the "FORT 12R" and "AE 790G1" pistols, it is significantly higher (p<0.05-0.01), its values were found when fired at close range with the "AE 790G1" into blocks covered with fabrics and blocks covered with LB with distance of 25 cm (21.96±3.01 and 14.78±0.89, 31.98±3.42 and 14.48±2.98, 30.52±3.50 and 11.60±1, 78, 18.32±2.69 and 10.42±2.74,

respectively);

at a cut depth of 2 cm when *contact shots from the "FORT 12R" pistol* revealed significantly higher values ($p<0.05$) of the indicator when shooting at DF compared to BB and CF (7.380±1.633, 3.360±1.704, 2.920±2.699, respectively); when comparing the values of the indicator when shooting from "FORT 12R" from different distances, significantly higher values ($p<0.05$-0.01) of the indicator were found when shooting at close range, compared to the shooting distance of 25 cm, 50 cm, and when comparing the indicators at shooting distances 25 and 50 cm in BB (17.38±2.36, 10.36±3.47 and 3.360±1.704, respectively), when shooting at close range, compared to 25 cm, 50 cm shot distance in CF or LB (14.94±2.00, 6.400±1.075, 2.920±2.699 and 16.94±1.50, 7.320±1.383, 2.860±3.916, respectively), when shooting at close range, compared to 50 cm shooting distance in DF (20.24±4.43 and 7.380±1.633, respectively); when *contact shots from the "AE 790G1" pistol* revealed significantly lower values ($p<0.05$-0.01) of the index when shooting BBs compared to blocks covered with fabric (21.00±2.60, 33.10±4.78, 41.04±1.60 and 39.56±2.35, respectively) and when shot in CF compared to other tissue types (33.10±4.78, 41.04±1.60 and 39.56±2.35 respectively); when fired from a distance of 25 cm from the "AE 790G1" pistol, significantly lower values ($p<0.05$) of the indicator were found when fired at DF compared to blocks covered with other fabrics (10.44±1.79, 14.64±2.02 and 14.80±2.34, respectively); when shooting from a *distance of 50 cm from the "AE 790G1" pistol*, significantly lower values ($p<0.05$-0.01) were found when shooting BBs compared to covered blocks (0.460±1.029, 8.060±3.015, 3.388±3.737 and 4.660±2.528, respectively) and when shooting in DF compared to CF (3.388±3.737 and 8.060±3.015, respectively); when comparing the values of the indicator when shooting with the "AE 790G1" from different distances, significantly higher values ($p<0.05$-0.01) of the indicator were found when shooting at close range, compared to the shooting distance of 25 cm, 50 cm, and when comparing the indicators at the shooting distances 25 and 50 cm in all groups of blocks; when comparing the values of the indicator when fired from the "FORT 12R" and "AE 790G1" pistols, it is significantly higher ($p<0.05$-0.01), its values were found when fired at close range with the "AE 790G1" into blocks covered with fabrics and at a shot distance of 25 cm for CF and LB and for 50 cm only for CF (33.10±4.78 and 14.94±2.00, 41.04±1.60 and 20.24±4.43, 39.56±2.35 and 16.94±1.50, 14.64±2.02 and 6.400±1.075, 14.80±2.34 and 7.320±1.383, 8.060±3.015 and 2.920±2.699, respectively), and significantly greater ($p<0.05$) values found when shooting from a distance of 50 cm in BB with "FORT 12R" (3.360±1.704 and 0.460±1.029, respectively);

at a cut depth of 3 cm when *contact shots from the "FORT 12R" pistol* revealed significantly lower values ($p<0.05$-0.01) of the indicator when shooting BB compared to CF or DF (15.44±3.50, 21.06±1.83 and 27.34±4.88, respectively), and when shooting in LB, compared to DF (20.14±4.04 and 27.34±4.88, respectively); when shooting from a *distance of 25 cm from the "FORT 12R" pistol*, significantly lower values ($p<0.05$-0.01) of the indicator were found when shooting at BB or LB compared to CF and DF (0, 0, 4.360±2.629 and 5.340±3.727 respectively); when comparing the values of the indicator when shooting from "FORT 12R" from different distances, significantly higher values ($p<0.05$-0.01) of the indicator were found when shooting at close range, compared to the shooting distance of 25 cm, 50 cm, and when comparing the indicators at shooting distances 25 and 50 cm in CF or DF (21.06±1.83, 4.360±2.629, 0.860±1.923 and 27.34±4.88, 5.340±3.727, 0 respectively), and when shooting up close, compared to distance shot 25 cm, 50 cm in BB and LB (15.44±3.50, 0, 0.560±1.252 and 20.14±4.04, 0, 0); when *contact shots from the "AE 790G1" pistol* revealed significantly lower values ($p<0.01$) of the indicator when shooting BBs compared to blocks covered with clothing (24.28±2.89, 39.16±5.46, 41.76±5.84 and 42.06±6.90, respectively); when comparing the values of the indicator when shooting with *"AE 790G1"* from different distances, significantly higher values ($p<0.01$) of the indicator were found when shooting at close range, compared to the shooting distance of 25 cm, 50 cm for all groups of blocks (24.28±2.89, 0, 0 and 39.16±5.46, 3.640±3.384, 1.620±3.622 and 41.76±5.84, 1.060±2.370, 0 and 42.06±6.90, 0, 0, respectively); when comparing the values of the indicator when fired from "FORT 12R" and "AE 790G1" pistols, its values were significantly higher ($p<0.01$) when fired at close range with *"AE 790G1"* at all groups of blocks (24.28±2.89 and 15.44±3.50, 39.16±5.46 and 21.06±1.83, 41.76±5.84 and 27.34±4.88, 42.06±6.90 and 20.14±4.04, respectively);

at a cut depth of 4 cm when *contact shots from the "FORT 12R" pistol* revealed significantly lower values ($p<0.01$) of the index when shooting BBs compared to blocks covered with clothing (0, 20.80±2.62, 26.42±3.97, 17.36±3.24, respectively) and significantly higher values ($p<0.05$-0.01) of the indicator when shooting in DF compared to CF and LB (26.42±3.97, 20.80±2.62 and 17.36±3.24, respectively); when comparing the values of the indicator when shooting from *"FORT 12R"* from different distances, significantly higher values ($p<0.01$) of the indicator were found when shooting at close range, compared to the distance of a shot of 25 cm, 50 cm into blocks covered with clothing (20.80±2.62, 0.180±0.402, 0 and 26.42±3.97, 0, 0 and 17.36±3.24, 0, 0, respectively); when *contact shots from the "AE 790G1" pistol* revealed significantly lower values ($p<0.01$) of the indicator when shooting BBs compared to blocks covered with clothing (11.92±7.74, 38.86±2.09, 34.48±6.67 and 39.30±3.71, respectively); when comparing the values of the indicator when shooting from *"AE 790G1"* from different distances, significantly higher values ($p<0.05$-0.01) of the indicator were found when shooting at close range, compared to the shooting distance of 25 cm, 50 cm for all groups of

blocks (11.92±7.74, 0.0 and 38.86±2.09, 0, 0 and 34.48±6.67, 0, 0 and 39.30±3.71, 0, 0, respectively); when comparing the values of the indicator when fired from the "FORT 12R" and "AE 790G1" pistols, it is significantly higher (p<0.05-0.01), its values were found when fired at close range with the "AE 790G1" into all groups of blocks (11.92±7.74 and 0, 38.86±2.09 and 20.80±2.62, 34.48±6.67 and 26.42±3.97, 39.30±3.71 and 17.36±3.24 respectively);

at a cut depth of 5 cm when *contact shots from the "FORT 12R" pistol* revealed significantly lower values (p<0.01) of the indicator when shooting at BB or LB compared to CF and DF (0, 0 and 14.76±5.25, 20.10±4.33, respectively); when comparing the values of the indicator when shooting with *"FORT 12R"* from different distances, significantly higher values (p<0.01) of the indicator were found when shooting at close range, compared to the shooting distance of 25 cm, 50 cm in CF and DF (14.76±5, 25, 0.0 and 20.10±4.33, 0.0, respectively); when *contact shots from the "AE 790G1" pistol* revealed significantly higher values (p<0.05-0.01) of the indicator when shooting in CF compared to other groups of blocks (28.50±2.05, 0, 11.34±11.16 and 15.12±13.84, respectively); when comparing the values of the indicator when shooting with the *"AE 790G1"* from different distances, significantly higher values (p<0.01) of the indicator were found when shooting at close range, compared to the shooting distance of 25 cm, 50 cm for CF (28.50±2.05, 0 and 0 respectively); when comparing the values of the indicator when fired from the "FORT 12R" and "AE 790G1" pistols, its values were significantly higher (p<0.01) when fired at close range with the "AE 790G1" in CF (28.50±2.05 and 14.76±5.25, respectively).

PPM values when fired from "FORT 12R" and "AE 790G1" pistols have the following features: at a cut depth of 1 cm when fired at *contact range from a "FORT 12R" pistol*, significantly lower values (p<0.05) of the indicator were found when fired at DF compared to with LB (64.76±6.98 and 71.98±6.73, respectively); when shooting from a *distance of 25 cm from the "FORT 12R" pistol*, significantly higher values (p<0.01) of the indicator were found when shooting BBs compared to blocks covered with fabrics (53.20±6.37, 20.92±4.46, 28.68±6.11 and 27.72±10.01, respectively); when shooting from a *distance of 50 cm from the "FORT 12R" pistol*, significantly higher values (p<0.05) of the indicator were found when shooting at DF compared to BB and CF (21.44±5.57, 7.380±4.601 and 7.600±4.710, respectively); when comparing the values of the indicator when shooting from *"FORT 12R"* from different distances, significantly higher values (p<0.01) of the indicator were found when shooting at close range, compared to the shooting distance of 25 cm, 50 cm, and when comparing the indicators at the shooting distances of 25 and 50 cm in BB and CF (67.18±3.05, 53.20±6.37, 7.380±4.601 and 66.06±3.58, 20.92±4.46, 7.600±4.710, respectively), when shooting at close range, compared to the shot distance of 25 cm, 50 cm in DF and LB (64.76±6.98, 28.68±6.11, 21.44±5.57 and 71.98±6.73, 27.72±10.01, 15.46±10.42, respectively); when *shooting at contact range from the "AE 790G1" pistol*, significantly lower values (p<0.05-0.01) of the indicator were found when shooting at BB or CF compared to DF or LB (77.70±10.48, 89.82±17.42 and 114.3±10.3, 118.7±10.0, respectively); when shots from *distance 25 cm by "AE 790G1" pistol* revealed significantly higher values (p<0.05-0.01) of the index when shooting BBs compared to blocks covered with clothing (54.22±4.42, 38.98±15.76, 25.92±13.33 and 46.56±10.44, respectively), and LB compared to DF (46.56±10.44 and 25.92±13.33, respectively); when comparing the values of the indicator when shooting with the *"AE 790G1"* from different distances, significantly higher values (p<0.01) of the indicator were found when shooting at close range, compared to the shooting distance of 25 cm, 50 cm, and when comparing the indicators at the shooting distances of 25 and 50 cm in BB and LB (77.70±10.48, 54.22±4.42, 13.22±12.30 and 118.7±10.0, 46.56±10.44, 14.82±9.31, respectively), when shooting at close range, compared to a shot distance of 25 cm, 50 cm in CF or DF (89.82±17.42, 38.98±15.76, 23.18±7.42 and 114.3±10.3, 25.92±13.33, 24.52±11.68, respectively); when comparing the values of the indicator when fired from "FORT 12R" and "AE 790G1" pistols, it is significantly higher (p<0.05-0.01), its values were found when fired at close range with "AE 790G1" into blocks covered with fabrics, at a distance of 25 cm in LB and 50 cm in CF (89.82±17.42 and 66.06±3.58, 114.3±10.3 and 64.76±6.98, 118.7±10.0 and 71.98±6.73, 46.56±10.44 and 27.72±10.01, 23.18±7.42 and 7.600±4.710, respectively);

at a cut depth of 2 cm when *contact shots from the "FORT 12R" pistol* revealed significantly lower values (p<0.05-0.01) of the index when shooting BBs compared to blocks covered with fabrics (67.38±7.23, 77.14±3.73, 81.08±8.86 and 82.70±5.62, respectively), CF compared to LB (77.14±3.73 and 82.70±5.62, respectively); when fired from a *distance of 25 cm from the "FORT 12R" pistol*, significantly lower values (p<0.05) of the indicator were found when fired at CF compared to LB (15.16±7.39 and 27.32±9.28, respectively); when shooting from a *distance of 50 cm from the "FORT 12R" pistol*, significantly higher values (p<0.05-0.01) of the indicator were found when shooting at DF compared to BB and LB (11.92±6.26, 3.360±1.704 and 1.900±3.087, respectively); when comparing the values of the indicator when shooting from *"FORT 12R"* from different distances, significantly higher values (p<0.05-0.01) of the indicator were found when shooting at close range, compared to the shooting distance of 25 cm, 50 cm, and when comparing the indicators at shooting distances 25 and 50 cm in BB and LB (67.38±7.23, 29.12±18.89, 3.360±1.704 and 82.70±5.62, 27.32±9.28, 1.900±3.087, respectively), at close range shots, compared to 25 cm, 50 cm shot distance in CF and DF (77.14±3.73, 15.16±7.39, 8.960±10.31 and 81.08±8.86, 17.40±14.28, 11.92±6.26, respectively); when *contact shots from the "AE 790G1" pistol* revealed significantly lower values (p<0.05-

0.01) of the index when shooting BBs compared to blocks covered with clothing (90.10±5.55, 111.5±12.8, 133.9±11.8 and 161.0±49.7, respectively) and CF compared to DF or LB (111.5±12.8, 133.9±11.8 and 161.0±49.7, respectively); when shooting from a *distance of 25 cm from the "AE 790G1" pistol*, significantly higher values (p<0.05-0.01) of the indicator were found when shooting at BB compared to CF or DF (45.10±4.89, 31.44±16.50 and 19.58±9.88, respectively); when shooting from a *distance of 50 cm from the "AE 790G1" pistol*, significantly lower values (p<0.05-0.01) of the index were found when shooting BBs compared to blocks covered with fabrics (0.460±1.029, 24.50±9.74, 16.43±12.53 and 6.660±4.230, respectively), LB compared to CF (6.660±4.230 and 24.50±9.74, respectively); when comparing the values of the indicator when shooting from the *"AE 790G1"* from different distances, significantly higher values (p<0.01) of the indicator were found when shooting at close range, compared to the shooting distance of 25 cm, 50 cm, and when comparing the indicators at the shooting distances of 25 and 50 cm in BB and LB (90.10±5.55, 45.10±4.89, 0.460±1.029 and 161.0±49.7, 38.30±15.45, 6.660±4.230, respectively), when shooting at close range, compared to the shot distance of 25 cm, 50 cm in CF and DF (111.5±12.8, 31.44±16.50, 24.50±9.74 and 133.9±11.8, 19.58±9.88, 16.43±12.53, respectively); when comparing the values of the indicator when fired from "FORT 12R" and "AE 790G1" pistols, it is significantly higher (p<0.05-0.01), its values were found when fired at close range with "AE 790G1" at all groups of blocks (90.10±5.55 and 67.38±7.23, 111.5±12.8 and 77.14±3.73, 133.9±11.8 and 81.08±8.86, 161.0±49, 7 and 82.70±5.62, respectively) and when fired from a distance of 50 cm with "FORT 12R" in BB (3.360±1.704 and 0.460±1.029, respectively);

at a cut depth of 3 cm when *contact shots from the "FORT 12R" pistol* revealed significantly lower values (p<0.05-0.01) of the index when shooting BBs compared to blocks covered with clothing (32.42±18.64, 79.38±2.30, 85.30±8.74 and 70.22±11.39, respectively) and LB compared to DF (70.22±11.39 and 85.30±8.74, respectively); when shooting from a *distance of 25 cm from the "FORT 12R" pistol*, significantly lower values (p<0.05-0.01) of the indicator were found when shooting at BB or LB compared to CF and DF (0, 0 and 9.180±8.036, 4.440±4,014 respectively); when comparing the values of the indicator when shooting from "FORT 12R" from different distances, significantly higher values (p<0.05-0.01) of the indicator were found when shooting at close range, compared to the shooting distance of 25 cm, 50 cm, and when comparing the indicators at shooting distances 25 and 50 cm in CF and DF (79.38±2.30, 9.180±8.036, 0.860±1.923 and 85.30±8.74, 4.440±4.014, 0, respectively), when shot at close range, compared to a shot distance of 25 cm, 50 cm in BB and LB (32.42±18.64, 0, 0.560±1.252 and 70.22±11.39, 0, 0, respectively); when *contact shots from the "AE 790G1" pistol* revealed significantly lower values (p<0.01) of the indicator when shooting BBs compared to blocks covered with clothing (81.64±5.41, 111.8±10.0, 118.2±11.8 and 119.3±18.6, respectively); when comparing the values of the indicator when shooting with *"AE 790G1"* from different distances, significantly higher values (p<0.01) of the indicator were found when shooting at close range, compared to the shooting distance of 25 cm, 50 cm for all groups of blocks (81.64±5.41, 0, 0 and 111.8±10.0, 6.500±6.398, 1.620±3.622 and 118.2±11.8, 1.040±2.326, 0 and 119.3±18.6, 0, 0 respectively); when comparing the values of the indicator when fired from "FORT 12R" and "AE 790G1" pistols, its values were significantly higher (p<0.01) when fired at close range with "AE 790G1" in all groups of blocks (81.64±5.41 and 32.42±18.64, 111.8±10.0 and 79.38±2.30, 118.2±11.8 and 85.30±8.74, 119.3±18.6 and 70, 22±11.39, respectively);

at a cut depth of 4 cm when *contact shots from the "FORT 12R" pistol* revealed significantly lower values (p<0.01) of the index when shooting BBs compared to blocks covered with clothing (0, 70.60±7.19, 80.24±6.39 and 44.84±11.32, respectively) and LB compared to CF or DF (44.84±11.32, 70.60±7.19, 80.24±6.39, respectively); when comparing the values of the indicator when shooting with "FORT 12R" from different distances, significantly higher values (p<0.01) of the indicator were found when shooting at close range, compared to the shooting distance of 25 cm, 50 cm in groups of blocks covered with clothing (70.60±7.19, 2.040±4.562, 0 and 80.24±6.39, 0, 0 and 44.84±11.32, 0, 0, respectively); when *contact shots from the "AE 790G1" pistol* revealed significantly lower values (p<0.01) of the indicator when shooting BBs compared to blocks covered with clothing (35.96±25.45, 96.32±12.52, 85.92 ±17.00 and 95.90±15.64, respectively); when comparing the values of the indicator when shooting with *"AE 790G1"* from different distances, significantly higher values (p<0.05-0.01) of the indicator were found when shooting at close range, compared to the shooting distance of 25 cm, 50 cm for all groups of blocks (35.96±25.45, 0, 0 and 96.32±12.52, 0, 0 and 85.92±17.00, 0, 0 and 95.90±15.64, 0, 0, respectively); when comparing the values of the indicator when fired from "FORT 12R" and "AE 790G1" pistols, significantly higher (p<0.05-0.01) its values were found when fired at close range with "AE 790G1" in groups of BB, CF and LB blocks (35.96±25.45 and 0, 96.32±12.52 and 70.60±7.19, 95.90±15.64 and 44.84±11.32, respectively);

at a cut depth of 5 cm when *contact shots from the "FORT 12R" pistol* revealed significantly lower values (p<0.01) of the indicator when shooting at BB or LB compared to CF and DF (0, 0 and 35.12±9.92, 49.56±19.01, respectively); when comparing the values of the indicator when shooting from *"FORT 12R"* from different distances, significantly higher values (p<0.01) of the indicator were found when shooting at close range, compared to the shooting distance of 25 cm, 50 cm in CF or DF (35.12±9.92, 0, 0 and 49.56±19.01, 0, 0, respectively); when *contact shots*

from the "AE 790G1" pistol revealed significantly lower values ($p<0.01$) of the indicator when shooting BBs compared to CF (0 and 42.58±19.78, respectively); when comparing the values of the indicator when shooting from the *"AE 790G1"* from different distances, significantly higher values ($p<0.01$) of the indicator were found when shooting at close range, compared to the shooting distance of 25 cm, 50 cm for CF (42.58±19.78, 0 and 0 respectively); when comparing the values of the indicator when fired from the "FORT 12R" and "AE 790G1" pistols, its values were significantly higher ($p<0.05$) when fired at close range from the "FORT 12" in DF (49.56±19.01 and 17.06±18.04, respectively).

Since the cut depth of 6 cm was reached only by ammunition when fired at contact range with "FORT 12R" in DF, it was not possible to conduct any comparative analysis for *TCLM, FWPM* and *PPM* indicators.

Discussion

The results obtained by us agree quite well with the conclusions of the previous work, which also noted mainly higher damage values when fired from the "AE 790G1" pistol compared to the "FORT 12R" [9].

At the same time, the difference in the indicators of the temporary cavity when firing from "FORT 12R" draws attention. In contrast to the data of our research, the team of authors led by V. Gunas [7] established that "FORT 12R" forms an amphora-like profile of the temporary cavity, which is more reminiscent of the data obtained when fired with "AE 790G1". The explanation of this phenomenon can be both the design features of the "FORT 12RM" or the cartridges for it (this gun is produced with specific 45 Rubber bullets), and the features of the experimental model performed in the study (instead of blocks, shots were fired into torso simulators).

V. V. Shcherbak [20, 21] in his publications investigated the parameters of the temporary cavity formed during the firing of the combat pistols "FORT 12" and "FORT 12TP". At the same time, he noted the differences between the parameters of the cavities in the cases of the use of pistols: when fired with "FORT 12", the parameters of the cavity had a wave-like character (high indicators within the depth range of 6-10 cm) and reached a maximum at a depth of 15-23 cm, while "FORT 12TP" high cavity indicators were observed at depths of 4-10 cm and maximum at 16-24 cm.

As for the influence of layers of clothing on the parameters of gunshot damage, the opinion of the general public of scientists is unequivocal regarding the importance of taking into account the results of experimental ballistic studies using covering material on targets. Such conclusions were proved as a result of experimental studies by T. Stevenson [22] with co-authors in the study of military clothing, D. C. Kieser [8] and colleagues in the study of denim fabric and P. F. Mahoney [11] and others in the study of helmets.

The continuation of discussions regarding the optimal model for conducting a ballistic experiment was also noted. Thus, data on greater consistency of results when using a biological imitator of the human body and 20 % but not 10 % gelatin solutions were found [10], and the high value of using a support for the target during ballistic studies, especially if the target is small, was noted [19].

Conclusions

1. The use of the "AE 790G1" gun leads to the formation of a larger temporary cavity compared to the "FORT 12R".

2. All types of clothing used in the study contributed to the reduction of the temporary cavity indicators, thus showing protective properties that were most noticeable when fired from a distance of 25 cm.

3. When firing from "FORT 12R", the formation of a temporary cavity is noted, resembling in shape a jug with a wide base, which narrows sharply at the end, while when firing from "AE 790G1" a temporary cavity is formed, resembling an amphora with a thin base, which then expands and gradually narrows at the end.

References

[1] Akhiwu, W. O., & Igbe, A. P. (2013). Fatal gunshot injuries in Benin city, Nigeria. *Medicine, Science and the Law*, 53(4), 199-202. doi: 10.1177/0025802413483718

[2] Braga, A. A., & Cook, P. J. (2018). The association of firearm caliber with likelihood of death from gunshot injury in criminal assaults. *JAMA Network Open,* 1(3), e180833. doi: 10.1001/jamanetworkopen.2018.0833

[3] Carr, D. J., Stevenson, T., & Mahoney, P. F. (2018). The use of gelatine in wound ballistics research. *International Journal of Legal Medicine,* 132, 1659-1664. doi: 10.1007/s00414-018-1831-7

[4] Caudell, J. N. (2013). Review of wound ballistic research and its applicability to wildlife management. *Wildlife Society Bulletin,* 37(4), 824-831. doi: 10.1002/wsb.311

[5] Cook, P. J., Rivera-Aguirre, A. E., Cerda, M., & Wintemute, G. (2017). Constant lethality of gunshot injuries from firearm assault: United States, 2003-2012. *American Journal of Public Health*, 107(8), 1324-1328. doi: 10.2105/AJPH.2017.303837

[6] Fackler, M. L., & Malinowski, J. A. (1985). The wound profile: a visual method for quantifying gunshot wound components. *The Journal of Trauma,* 25(6), 522-529. PMID: 4009751

[7] Gunas, V. I., Nepryliuk, R. H., Khomuk, N. M., Tovbukh, L. P., & Ryzhak, Y. V. (2020). Features of formation of a temporary pulsating cavity at a contact shot from the "FORT-12RM" pistol in the dressed simulator of a human torso. *Forensic Medical Examination,* (2), 45-52. doi: 10.24061/2707-8728.2.2020.7

[8] Kieser, D. C., Carr, D. J., Leclair, S. C., Horsfall, I., Theis, J. C., Swain, M. V., & Kieser, J. A. (2013). Clothing increases the risk of indirect ballistic fractures. *Journal of Orthopaedic Surgery and Research,* 8, 1-7. doi: 10.1186/1749-799X-8-42

[9] Kusliy, Yu., Shevchuk, Yu., Fomin, O., Adamchuk, O., & Konopelniuk, O. (2022). Peculiarities of soot deposition, tearing of clothing and human body simulator during shootings from "ORT 12R" and "AE 790G1" pistols. *Forensic Medical Examination,* (2), 36-42. doi: 10.24061/2707-8728.2.2022.5

[10] Mabbott, A., Carr, D. J., Champion, S., & Malbon, C. (2016).

Comparison of porcine thorax to gelatine blocks for wound ballistics studies. *International Journal of Legal Medicine*, 130, 1353-1362. doi: 10.1007/s00414-015-1309-9

[11] Mahoney, P. F., Carr, D. J., Miller, D., & Teagle, M. (2017). The effect of helmet materials and simulated bone and tissue layers on bullet behaviour in a gelatine model of overmatch penetrating head injury. *International Journal of Legal Medicine*, 131, 1765-1776. doi: 10.1007/s00414-017-1665-8

[12] Mahoney, P., Carr, D., Arm, R., Gibb, I., Hunt, N., & Delaney, R. J. (2018). Ballistic impacts on an anatomically correct synthetic skull with a surrogate skin/soft tissue layer. *International Journal of Legal Medicine,* 132, 519-530. doi: 10.1007/s00414-017-1737-9

[13] Maiden, N. R., Fisk, W., Wachsberger, C., & Byard, R. W. (2015). Ballistics ordnance gelatin-how different concentrations, temperatures and curing times affect calibration results. *Journal of Forensic and Legal Medicine,* 34, 145-150. doi: 10.1016/j.jflm.2015.05.019

[14] Milner, M. P., & Hutchens, S. B. (2021). Dynamic fracture of expanding cavities in nonlinear soft solids. Journal of Applied Mechanics, 88(8), 081008. doi: 10.1115/1.4051431

[15] Mishalov, V. D., Petroshak, O. Y., Hoholyeva, T. V., Gurina, O. O., & Gunas, V. I. (2019). Forensic assessment of gunshot injuries in Maidan Nezalezhnosti protesters. *World of Medicine and Biology,* 15(3), 118-122. doi: 10.26724/2079-8334-2019-3-69-118-122

[16] Ragsdale, B. D., & Josselson, A. (1988). Predicting temporary cavity size from radial fissure measurements in ordnance gelatin. *The Journal of Trauma*, 28(1 Suppl), S5-S9. doi: 10.1097/00005373-198801001-00003

[17] Schyma, C., & Madea, B. (2012). Evaluation of the temporary cavity in ordnance gelatine. *Forensic Science International,* 214(1-3), 82-87. doi: 10.1016/j.forsciint.2011.07.021

[18] Schyma, C., Baumann, F., Madea, B., & Gotsmy, W. (2021). Study of backspatter using high-speed video of experimental gunshots. *Forensic Science, Medicine and Pathology,* 17, 36-46. doi: 10.1007/s12024-020-00326-0

[19] Schyma, C., Herr, N., Brunig, J., Brencicova, E., & Muller, R. (2017). The influence of the counterfort while ballistic testing using gelatine blocks. *International Journal of Legal Medicine,* 131, 1325-1332. doi:10.1007/s00414-017-1623-5

[20] Shcherbak, V. V. (2015). Determination of the characteristics of the temporary pulsating cavity during shots from the Fort-12 pistol. *Theory and Practice of Forensic Examination and Criminology*, (15), 388-394.

[21] Shcherbak, V. V. (2019). Peculiarities of the formation of a temporary pulsating cavity during shots from Fort pistols. *Ukrainian Journal of Medicine, Biology and Sports,* 4(1), 225-229. doi: 10.26693/jmbs04.01.225

[22] Stevenson, T., Carr, D. J., & Stapley, S. A. (2019). The effect of military clothing on gunshot wounding patterns in gelatine. *International Journal of Legal Medicine,* 133, 1121-1131. doi: 10.1007/s00414-018-1972-8

ПОРІВНЯННЯ РОЗМІРІВ ТИМЧАСОВОЇ ПОРОЖНИНИ ПРИ ПОСТРІЛАХ З ПІСТОЛЕТІВ "FORT 12R" ТА "AE 790G1" В НЕБІОЛОГІЧНИЙ ІМІТАТОР ТІЛА

Куслій Ю. Ю, Школьніков В. С., Шевчук Ю. Г., Фомін О. О., Зверховська В. Ф.

Вогнепальні ушкодження є вкрай небезпечними за рахунок непередбачуваного поводження боєприпасу після контакту з тілом. Одним із ключових елементів, що має місце при цьому, це утворення за рахунок високої кінетичної енергії тимчасової порожнини, що, незважаючи на своє існування на лічені долі секунди, призводить до важких ушкоджень тканин тіла людини. Дослідження цього явища є одним із центральних елементів балістики і вимагає проведення експерименту на оптично прозорих середовищах. Метою дослідження є порівняння показників тимчасової порожнини при пострілах із пістолетів "FORT 12R" та "AE 790G1" у небіологічний імітатор тіла людини. Для досягнення поставленої мети за загальноприйнятою методикою були виготовлені 120 желатинових блоків, які підлягали відстрілу з відстаней впритул, 25 та 50 см. Блоки перед відстрілом залишали ненакритими, або покривали бавовняною тканиною, джинсовою тканиною чи шкірозамінником. Після проведення відстрілу виконували поперечні розрізи блоків з метою подальшого вимірювання показників тимчасової порожнини, що утворилася в результаті прострілу, за загальноприйнятими методиками. Результати аналізу отриманих даних щодо показників, що характеризують розміри тимчасової порожнини на різних глибинах ранового каналу, виявили цілий ряд достовірних відмінностей (p<0,05-0,01) між досліджуваними пістолетами (практично в усіх випадках більші значення мав "AE 790G1"), групами блоків, вкритих різними видами тканин, ненакритими блоками (практично у всіх випадках одяг мав захисні властивості і зменшував розмір тимчасової порожнини) та дозволили встановити, що при пострілах з "FORT 12R" відмічається різке збільшення розмірів тимчасової порожнини з її різким зменшенням наприкінці ранового каналу, в той час як при пострілах з "AE 790G1" тимчасова порожнина поступово збільшувалась, сягаючи максимуму на половині своєї глибини і поступово зменшувалась. Таким чином, при порівнянні результатів пострілів пістолетів "FORT 12R" та "AE 790G1" виявлено відмінності в особливостях формування тимчасової порожнини, що в свою чергу становить інтерес не тільки для криміналістики, балістики та судової медицини але й для клінічної медицини.

Ключові слова: *вогнепальна травма, вогнепальні ушкодження, вогнепальна зброя, тимчасова порожнина, імітатор тіла людини.*

DOI: 10.31393/morphology-journal-2023-29(2)-10 Reports of Morphology, Vol. 29, №2, Pages 66-79

ISSN 1818-1295 eISSN 2616-6194

REPORTS OF MORPHOLOGY

Official Journal of the Scientific Society of Anatomists, Histologists, Embryologists and Topographic Anatomists of Ukraine

journal homepage: https://morphology-journal.com

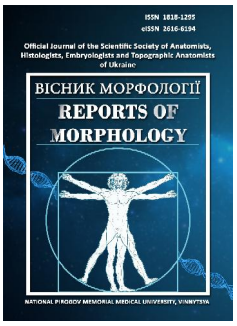

Morphological structure of testicles under conditions of experimental gonadopathy and after the administration of cholecalciferol in comprehensive correction schemes

Marakhovskyi I. O., Korenieva Ye. M., Laryanovska Yu. B., Smolienko N. P., Belkina I. O., Velychko N. F., Chystiakova E. Ye., Misiura K. V., Bondarenko V. O.

S I "V. Danilevsky Institute for Endocrine Pathology Problems of NAMS of Ukraine", Kharkiv, Ukraine

ARTICLE INFO

Received: 03 April 2023

Accepted: 05 May 2023

UDC: 612.616.3;591.147.8

CORRESPONDING AUTHOR

e-mail: ihor1marahovskiy@gmail.com

Marakhovskyi I. O.

CONFLICT OF INTEREST

The authors have no conflicts of interest to declare.

FUNDING

Not applicable.

The problem of male infertility is relevant and calls for a solution. The use of the D_3 vitamin in infertility treatment schemes has a potentially positive effect on reproductive health in male individuals. The present study aims to examine the effect of vitamin D_3, administered alone or in combination with a preparation containing the extract of Tribulus terrestris on the changes in the histological picture of testicular morphology in rats with experimental gonadopathy. Male rats with modeled reproductive function pathology (Serotonin-induced gonadopathy) were divided into groups receiving correction using cholecalciferol alone or in combination with the reference drug Tribestan (Tr), which contains an extract of Tribulus terrestris. In addition to observational microscopy, morphometric evaluation of spermatogenesis was performed on sections of the testicles stained with hematoxylin and eosin. The statistical analysis was performed using the standard software package "Statistica 6.0" with the utilization of the Student's t-test and its nonparametric counterpart, the Kruskal-Wallis test for one-way analysis of variance, followed by the Mann-Whitney test. It was found that the seminiferous tubules of rats with Serotonin-induced gonadopathy are significantly reduced in size, and their tunica propria is thickened. Sertoli cells are often destructively altered, and the uniformity of their arrangement is disrupted. A decrease in the weight of the gonads, epididymis, prostate gland, and hypoandrogenization was observed as well as a decline in spermatogenesis indicators. An improvement in the morphological characteristics of the gonads was noted following the administration of vitamin D_3 in the presence of pathology. The seminiferous tubules had a normal histological structure. The germ cells were arranged in concentric rows according to their developmental stages, and the Sertoli cells appeared visually unchanged. The population of Leydig cells appeared visually more heterogeneous than in the control animals. However, occasionally seminiferous tubules with focal necrobiosis of germ cells and dystrophy of Sertoli cells, as well as a reduction in rows of germ cells, were observed. Overall, the quantitative indicators of spermatogenesis improved after the administration of vitamin D_3 compared to rats with experimental gonadopathy, although they did not reach the levels of the intact control. The administration of a combination of vitamin D_3 and Tribestan in the presence of gonadopathy resulted in a greater positive effect compared to their individual use. The microscopic condition of the testicular tissue in rats was fully recovered. The combined use of vitamin D_3 with Tribestan normalized the weight of the gonads and their appendages, significantly reduced the manifestations in the histological sections of degeneration and damage in the reproductive cells during the period of growth and differentiation, improved the relative level of androgen status in the organism and had a positive effect on spermatogenesis in the gonads. Thus, we have established that the combined use of Cholecalciferol and Tribestan for correcting experimental gonadopathy was more effective than either of the mentioned components alone.

Keywords: *histological structure of the testis, gonadopathy, vitamin D, cholecalciferol, spermatogenesis.*

Introduction

Over 48.5 millions of couples worldwide suffer from infertility due to reproductive dysfunction [25]. After 12 months or more of regular unprotected sexual intercourse without successful conception, the male factor alone or in combination with the female factor may be the cause of infertility in at least half of all cases. According to estimates, there are over 30 million infertile men worldwide [9]. Despite the alarming prevalence, the causes of male infertility remain in a significant percentage of cases undetermined. For instance, a prospective study of 1.737 infertile patients with abnormal semen parameters revealed the etiology of infertility in only 40 % of men [22]. The lack of a definitive diagnosis is particularly common among men with oligozoospermia. Approximately 75 % of oligozoospermia patients are diagnosed with idiopathic hypofertility [22], and this condition can be caused by gonadopathy of various origins. The impairment of the gonads causes a decrease in testicular function, accompanied by or resulting in changes in the morphostructure of the male reproductive glands, it causes hypofertility and results in a deficiency in the secretion of androgens, inhibin B, anti-Mullerian hormone, and spermatogenic insufficiency [9, 21].

Various correction methods are typically used in the treatment of male infertility, including hormonal and herbal remedies, cytomedines, essential amino acids, vitamins, etc [13]. However, despite significant advancements in pharmacotherapy for disorders of the reproductive glands, the issue of male infertility remains relevant and requires a solution, considering, in particular, the fact that its treatment improves the quality of life, holds high social significance, and reduces healthcare costs [17]. This prompts further research and exploration of new approaches, means, and strategies for the management of hypofertility. Recently, the use of vitamin D_3 for this purpose has been attracting the attention of researchers. Despite the prevalent occurrence of vitamin D_3 deficiency, the question of its impact on the reproductive function of the male body, specifically the morphological structure of the gonads and the germ cell formation within them, remains up for debate. The results of clinical and experimental data show that the deficiency of this vitamin-hormone negatively affects the development of testes and the process of spermatogenesis [11], determining the qualitative and quantitative parameters of the ejaculate [8, 19]. There is evidence that the use of vitamin D_3 can affect sperm motility in men with asthenozoospermia and low serum levels of $25(OH)D_3$ [18]. There is an increasing number of publications highlighting the importance of vitamin D in sperm maturation [1, 12].

Vitamin D_3 deficiency in animals can lead to impaired maturation of seminal ducts, reduced testicular mass, and decreased sperm concentration [7], resulting in compromised reproductive ability in males.

At the same time, effective correction of gonadal morphology and testosterone levels in rats with induced aging, which leads to decreased fertility, has been reported [14]. The addition of cholecalciferol (vitamin D_3) to the correction of reproductive pathology using linagliptin leads to significant recovery of testicular histoarchitectonics, normalization of steroidogenesis and spermatogenesis following experimental damage to testicular tissue by cisplatin [10].

Based on the above, *the aim of our study* was to determine the impact of vitamin D_3 used alone or in combination with a preparation containing an extract of Tribulus terrestris, on the histological changes in the morphological structure of rat testes with experimental gonadopathy.

Materials and methods

The study involved 30 sexually mature seven-month-old rats weighing 250-350 g. The animals involved in the study were collected from the experimental vivarium SI "V.Danilevsky Institute for Endocrine Pathology Problems of the NAMS of Ukraine". The work was carried out following the national "General ethical principles of animal experimentation" (Ukraine, 2001), which are aligned with the provisions of the "European Convention for the Protection of Vertebrate Animals used for Experimental and other Scientific Purposes" (Strasbourg, 1985) [23]. The Wistar rat population was kept under standard vivarium conditions with natural lighting, a diet recommended for this species of animal, and unlimited access to water [15].

To model the pathology of reproductive function due to gonad impairment, a Serotonin model accompanied by impaired spermatogenesis was used.

The sexually active males were randomized into groups for this purpose: S-model group (animals with an experimental model of Serotonin-induced gonadal damage, gonadopathy (EGP)); S+vehicle (rats that received the vehicle (kernel oil) alongside the modeling of EGP) (for data analysis, these two groups were combined into one S group as they did not display any differences); S+vit. D_3 (animals that received vitamin D_3 orally alongside the modeling of Serotonin-induced testicular damage); S + Tribestan (Tr) (rats that received Tr as a reference drug alongside EGP); S+vit. D_3+Tr (animals that received both drugs orally: cholecalciferol and Tr alongside the modeling of EGP). The intact males were considered the control group.

The testicular pathology was induced by subcutaneous administration of Serotonin hydrochloride (ShanDong Octagon Chemicals Limited, China), for 14 days at a dose of 3.3 mg/kg body weight [26].

The reference drug Tribestan (Tr) was administered orally at a dose of 68 mg/kg body weight three days before the start of the Serotonin hydrochloride (SH) course, during the administration of Serotonin (14 days), and for three days after the last injection of Serotonin once a day. The dosage of the drug for the research was calculated using the species conversion factor based on the human daily

dose. Cholecalciferol (D_3) was administered following the same protocol, at a volume of 0.5 ml with a dose of 4000 IU (*per os*). The solutions made from kernel oil were prepared using vitamin D_3 (powder, China, batch CHG20062009, which complies with the quality standard GB 9840-2017).

At the end of the treatment period, the animals were euthanized by rapid decapitation, and their organs (testes, epididymides, ventral part of the prostate gland) were examined during autopsy to assess their condition and determine their weight.

The testes were removed and fixed in 10 % formalin for further histological investigations. According to the method described by B. A. Vartopetov and O. M. Demchenko (1975), the type of crystallization of the prostatic fluid (PF) was determined from prostatic imprints, the assessment of the "fern leaf" phenomenon allows evaluating the level of androgenic saturation in the animals' bodies [5]. To *study the morphological structure*, the fixed testes were dehydrated in progressively stronger alcohols and embedded in paraffin. Sections with a thickness of 6-7 μm were obtained from the paraffin blocks using a sliding microtome MS-1, which were subsequently mounted on glass slides and stained with hematoxylin and eosin. Morphometric evaluation of spermatogenesis was performed in addition to the microscopic examination of testicular sections [2, 3].

The specimens were examined under the Granum L 30(03) light microscope, and microscopic images were captured using the Granum DCM 310 digital video camera.

The photographs were processed on a Pentium 2.4 GHz computer using the ToupView software.

The statistical analysis was performed using the standard software package "Statistica 6.0" with the utilization of the Student's t-test and its nonparametric counterpart, the Kruskal-Wallis test for one-way analysis of variance, followed by the Mann-Whitney test [16].

Results

Table 1 presents data on the organ weights of males with testicular injury induced with SH before and after correction. This pathology in males (group S) caused a decrease in the absolute weight of the testes by 20 % ($p<0.05$), their appendages (epididymides) by 16 % ($p<0.05$), and the ventral part of the prostate gland by 28 % ($p<0.05$) compared to those in the animals of the control group. The oral administration of vitamin D3 or Tr (groups S+vit. D_3 and S+Tr) as monotherapy did not significantly alter the state of the investigated organs compared to the data of the animals in group S, indicating the continuation of the pathological process in them.

The combined use of vitamin D_3 with the baseline treatment (group S+vit. D_3+Tr) as a correction for the pathological condition induced by experimental gonadopathy (EGP) increased absolute testes weight by 21 % ($p<0.05$) compared to animals in group S and even its normalization (see Table 1).

Table 1. Indicators of the absolute weight of the reproductive organs and pituitaries of male rats in the experimental groups (M±m).

Group	Testes, mg	Epididymides, mg	The ventral part of the prostate gland, mg
Control, n=5	3229±186	1139±38	500.6±38.2
S, n=12	2582±2051	953.5±40.9[1]	362.0±24.8[1]
S+vit. D_3, n=8	2767±223	988.4±35.0[1]	402.4±28.5[1]
S+Tr, n=9	2932±141	1041±42	400.1±27.8[1]
S+vit. D_3+Tr, n=12	3123±1022	1033±46	397.5±40.5[1]

Notes: [1] - Statistically significant differences compared to the control group, $p<0.05$; [2] - statistically significant differences compared to the S group, $p<0.05$; [3] - statistically significant differences compared to the S+vit. D_3 group, $p<0.05$; [4] - statistically significant differences compared to the S+Tr group, $p<0.05$.

It can be assumed, therefore, that the combined use of vitamin D_3 and Tr led to a reduction in the intensity of the pathological process in the testes, accompanied by the normalization of the weight of the gonads and their appendages, but did not affect the weight of the ventral part of the prostate gland. The effect of the mentioned composition on the weight of the testes, their appendages, and the prostate gland was comparable to that of the reference medication in rats.

Subsequently, the histological structure of the gonads in male rats, whose reproductive function was impaired by SH, as well as those receiving corrective therapy, was studied.

The testes of intact rats served as a general control in our studies on the effects of vitamin D_3 (Fig. 1) [4], administered both independently and in various correction schemes for experimental reproductive disorders, their morphological structure and morphometric indicators corresponded to normal values (Table 2).

As demonstrated by light microscopy on sections of intact rat testes, convoluted seminiferous tubules (T) were observed, cut in a transverse or oblique direction, and had an oval or round shape. The diameter of the T was normal, and the tunica propria of the T, as well as the proteinaceous and vascular membranes, were within normal limits. The wall of the seminiferous T consisted of germ cells. In the basal compartment, spermatogonia of the seminiferous epithelium were located. Among them, there are distinguishable cells with chromatin in the nucleus of condensed type, referred to as type B, and uncondensed type, known as type A. Type A spermatogonia present as both so-called "pale" (renewing) cells and "dark" (reserve) cells. Occasionally, mitosis can be observed in spermatogonia. In the intermediate compartment of the seminiferous tubule wall, spermatocytes are located. The majority of first-order spermatocytes were in the pachytene stage. In some tubules, metaphases of the first and (less frequently) second meiotic divisions, as well as anaphase of these divisions, were well evident. In the adluminal

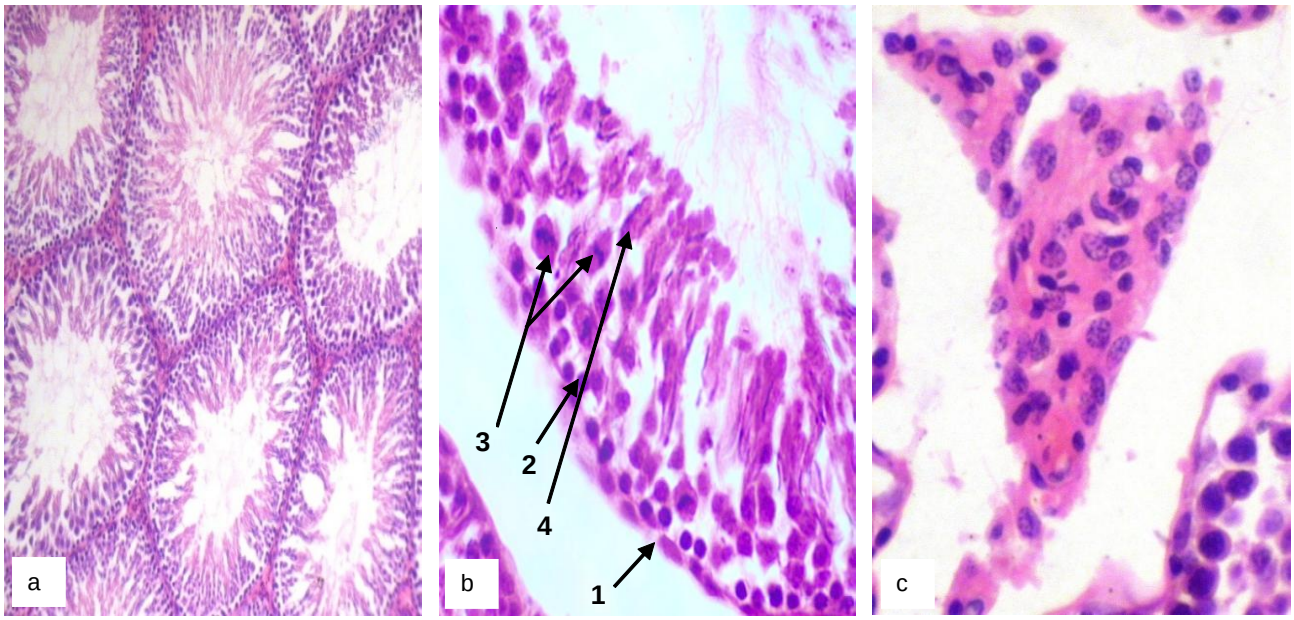

Fig. 1. The testes of intact rats: a - general view of seminiferous tubules (x100); b - in the epitheliospermatogenic layer of the tubule, Sertoli cells (1), spermatogonia (2), spermatocytes in metaphase I and II (3), and spermatids (4) can be observed (x250); c - normochromic Leydig cells in the intertubular space (x400). Hematoxylin-eosin [4].

Table 2. The impact of vitamin D3 on quantitative indicators of spermatogenesis in Serotonin-induced testicular pathology in rats (M±m).

Group	Indicators			
	Number of normal spermatogonia in the seminiferous tubule	Number of tubules in the 12th stage of meiosis, %	Number of tubules with exfoliated epithelium, %	Spermatogenesis index, scores
Control, n=4	61.08±0.48	4.000±0.413	0.000±0.000	3.331±0.002
S, n=8	23.46±4.26[1]	0.748±0.252[1]	5.253±0.371[1]	1.652±0.344[1]
S+vit. D_3, n=4	49.06±1.86[1 2]	3.253±0.247[2]	2.002±0.410[1 2]	3.022±0.131[2]
S+Tr, n=4	50.63±3.16[1 2]	2.501±0.292[1 2]	2.249±0.481[1 2]	3.001±0.183[2]
S+vit. D_3+Tr, n=4	60.09±0.33[2 3 4]	3.748±0.249[2 4]	0.503±0.289[2 3 4]	3.332±0.001[2]

Notes: [1] - statistically significant differences compared to the data of the control group, $p<0.05$; [2] - statistically significant differences compared to the data of the S group, $p<0.05$; [3] - statistically significant differences compared to the data of the S+vit. D_3 group, $p<0.05$; [4] - statistically significant differences compared to the data of the S+Tr group, $p<0.05$.

compartment of the seminiferous T, numerous spermatids and fully formed spermatozoa are visible. Germ cells at different stages of development are arranged in a strict order, forming concentric layers corresponding to the stages of the spermatogenic cycle. Associations of germ cells are clearly demarcated, and in different regions of the same T, only one specific combination of cells can be observed. In various tubules, not only spermatogenesis (the process of sequential transformation of germ cells: spermatogonia ® spermatozoa) but also spermiogenesis can be clearly traced - the stages of cellular transformation from spermatids to spermatozoa. The strip of seminiferous epithelium contained at least 4-6 rows of cells. Numerous Sertoli cells (supporting cells) were located between the spermatogonia on the basal membrane. Their light pear-shaped nucleus with a nucleolus was clearly visible. The cytoplasmic extensions of these cells are masked by the germ cells at later stages of development. The interstitial connective tissue was very limited. Clusters of Leydig cells (up to 7-20 cells), along with a few fibroblasts, were observed near the blood vessels within the interstitial spaces. The nuclei were mostly round to oval in shape, relatively large in volume, well-defined, normochromic, with noticeable evenly distributed chromatin granularity, and typically contained a single nucleolus. The cytoplasm of the cells was intensely eosinophilic, with weak peripheral vacuolization in some cells, and the cell boundaries were not clearly defined. The described state of Leydig cells indicates their normal functional activity (see Fig.1).

The morphometric characteristics of spermatogenesis in intact rats corresponded to the physiological norm for these animals (see Table 2).

After inducing gonadopathy by administering SH (group S) to 25 % of the rats, histological examination of the testes revealed a significant reduction in the size of seminiferous tubules, thickening, and swelling of their tunica propria. Sertoli cells were observed in the tubular wall (often with destructive changes, most of which appeared swollen, the

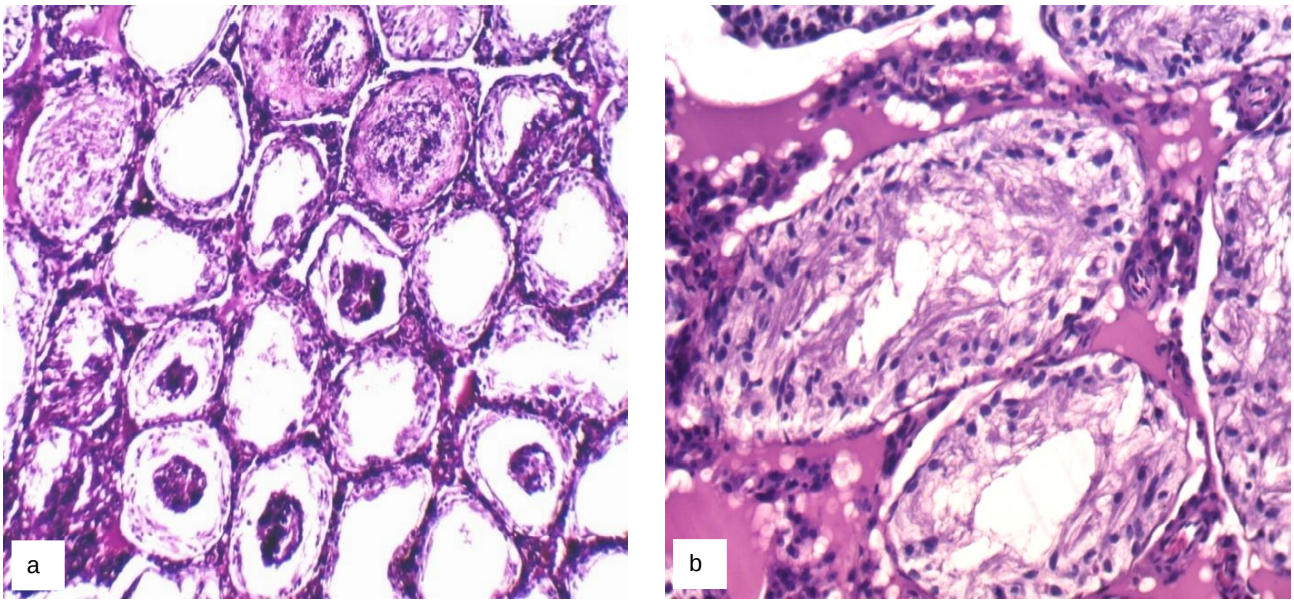

Fig. 2. Rat testis after administration of Serotonin hydrochloride: a - seminiferous tubules significantly reduced in size, the epitheliospermatogenic layer pathologically altered, some tubules filled with necrotic debris (x100); b - disordered arrangement of undifferentiated cells in the tubular wall, protein infiltration in the interstitial stroma (x250). Hematoxylin-eosin.

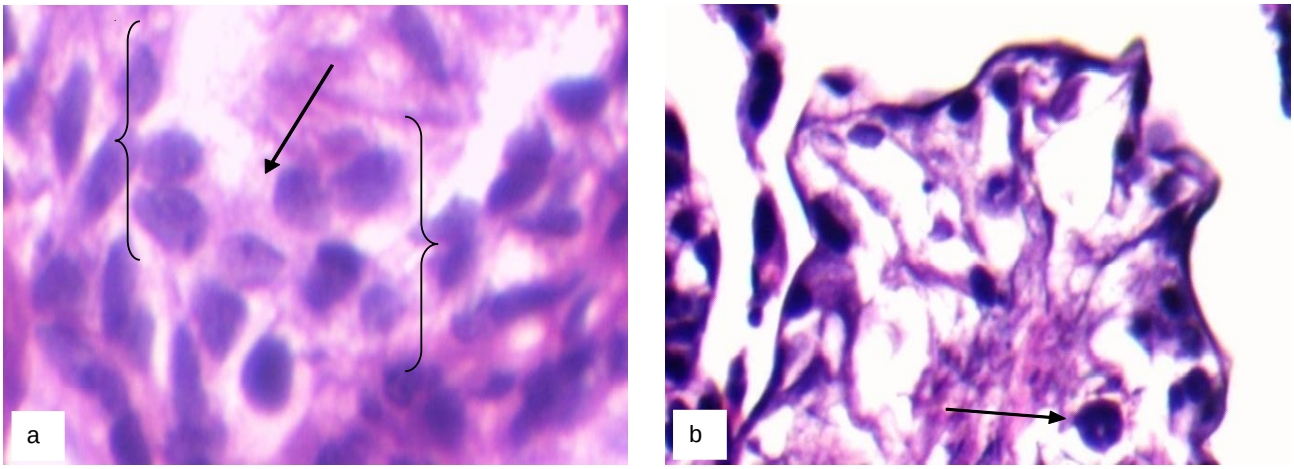

Fig. 3. Rat testis after administration of Serotonin hydrochloride: a - group arrangement of Sertoli cells; b - individual spermatid clumps in seminiferous tubules. Hematoxylin-eosin. x400.

nuclei sharply displaced or absent altogether, the regular arrangement of these cells was disrupted, with either individual cells or clusters present) and irregularly distributed undifferentiated cells of varying number. Some tubules were filled with necrotic debris. Accumulations of remnants of dystrophic germ cells were visible in the lumen of many tubules, while individual tubules exhibited "seminiferous syncytia" or cell clusters, characterized by giant multinuclear formations mainly containing spermatids. The intercellular stroma was extensively infiltrated with proteinaceous exudate (see Fig.2, Fig.3).

In the remaining 75 % of rats, a lesser degree of atrophy signs were found, and they exhibited significant variation. In the majority of those rats, the seminiferous tubules exhibited more or less preserved spermatogenic epithelium and complete destruction of the epitheliospermatogenic layer was observed only in individual tubules or within the same tubule in a patchy pattern (the germ cells present in these foci appeared as shadow cell or were in a necrobiotic state). Frequently, in the seminiferous tubules, reduction of the germ cell rows, stratification of layers, and epithelial desquamation (disorganized displacement of structural elements into the lumen of the tubule) are observed, indicating a weakening of the intercellular connections between spermatocytes and spermatids with sustentocytes (see Fig. 3). In some tubules, there is a visually reduced presence of spermatogonia (including dark type A), very rare figures of mitosis in spermatocytes. There was a decreased presence of tubules with mature spermatozoa. There is a visually increased number of tubules in which a significant amount of residual bodies was observed in the lumen (remnants of cytoplasm shed by differentiating spermatids), indicating a weakened

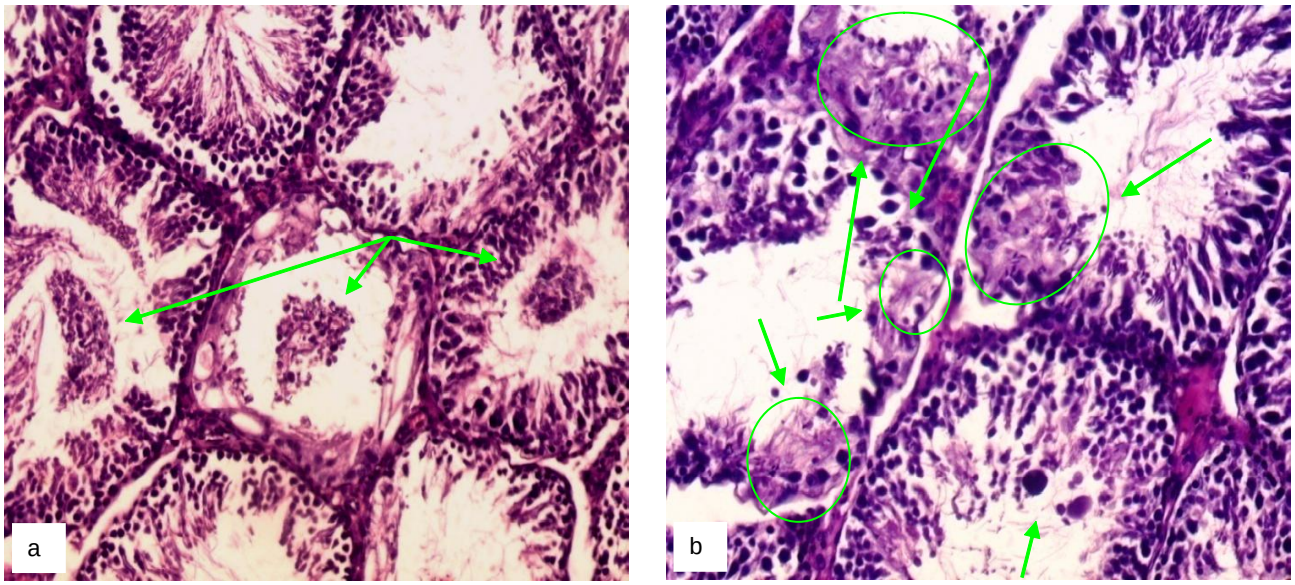

Fig. 4. Testes of rats after administration of Serotonin hydrochloride: against the background of tubules with relatively well-preserved epitheliospermatogenic layer, tubules with epithelial desquamation (a), nest-like destruction of the epithelium, and individual cell clusters were observed (b). Hematoxylin-eosin. x250.

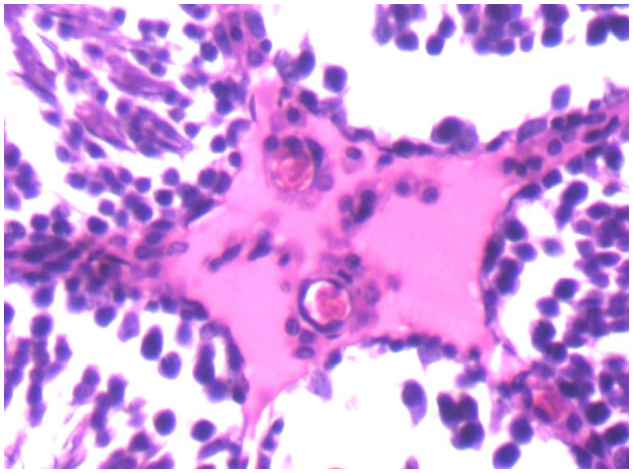

Fig. 5. Testes of rats after administration of Serotonin hydrochloride: decreased number of activated hormone-producing Leydig cells in the interstitial tissue, which is extensively infiltrated with protein. Hematoxylin-eosin. x400.

Table 3. The effect of vitamin D3 on the phenomenon of crystallization of the prostate gland secretion in Serotonin-induced testicular pathology in rats, scores (M±m).

Group	Crystallization of the prostate gland secretion
Control, n=8	3.612±0.231
S, n=10	1.743±0.262[1]
S+vit. D_3, n=7	2.448±0.030[1 2]
S+Tr, n=7	2.124±0.061[1]
S+vit. D_3+Tr, n=8	2.669±0.024[1 2 3 4]

Notes: [1] - statistically significant differences compared to the control group, $p<0.05$; [2] - statistically significant differences compared to the S group, $p<0.05$; [3] - statistically significant differences compared to the S+vit. D_3 group, $p<0.05$; [4] - statistically significant differences compared to the S+Tr group, $p<0.05$.

function of their clearance by supporting cells. Syncytia are occasionally visible (Fig. 4, Fig. 5).

The quantitative assessment of spermatogenesis in Serotonin-exposed rats revealed changes in all its characteristic parameters: reduced number of normal spermatogonia in tubules, decreased number of tubules containing second-order spermatocytes in metaphase II of maturation (meiotic stage 12), increased frequency of tubules with sloughed epithelium. As a result, there is a significant decrease in the spermatogenesis index (see Table 2). It should be noted that the scoring of each cell layer in the tubular wall was conducted only if it contained at least 7 cells.

Androgen saturation of the organism, determined by the crystallization type of the prostate gland secretion, was significantly reduced in 25 % of rats. The phenomenon of "fern leaf" was not observed in the impression of the secretion, but isolated thick coarse cross-shaped crystals were detected against a structureless mass with small areas of "remnants" of distorted crystal branches. In the remaining 75 % of animals, the pattern of "fern leaf" was observed in the impressions, but the crystal branches were shortened, and less numerous, and the angle of divergence from the stems was significantly increased, indicating a considerable decrease in the level of androgen saturation in the organism. Overall, the assessment of crystallization of the prostate gland secretion was 1.76 scores for the group (see Table 3).

In animals with EGP after administration of the Serotonin hydrochloride and kernel oil, the microscopic picture of testicular tissue, spermatogenesis indicators, and level of androgenization based on the type of crystallization of the prostate gland secretion showed practically identical characteristics to the previously presented indicators,

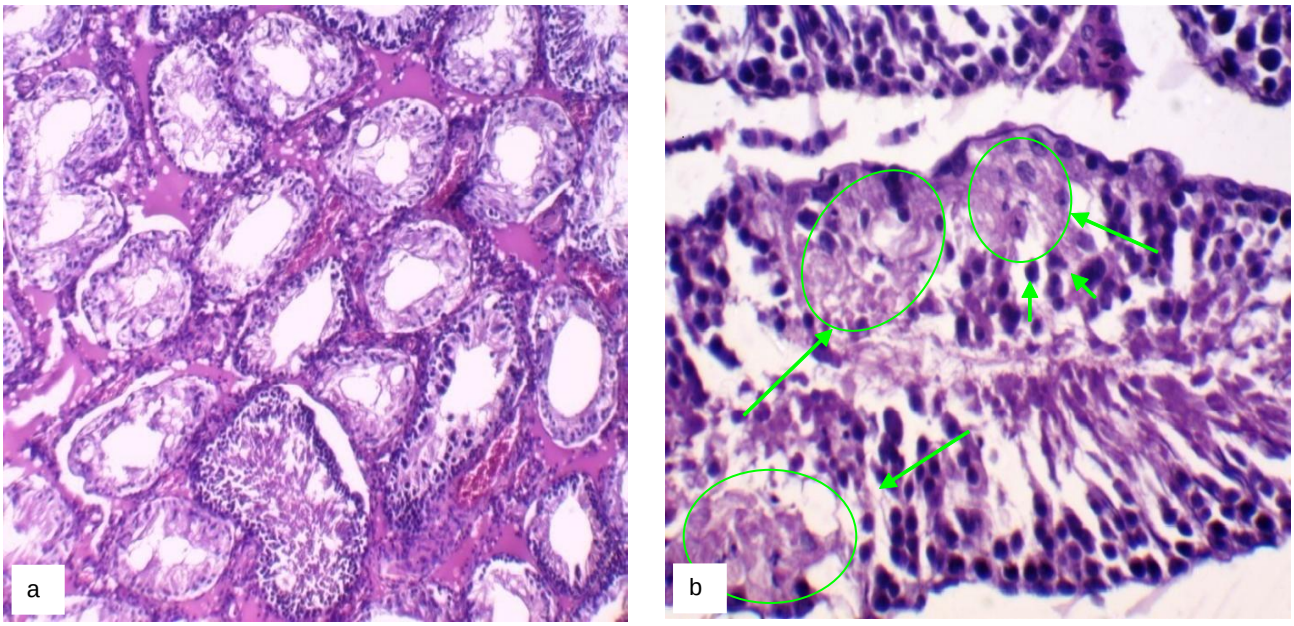

Fig. 6. Testes of rats after administration of Serotonin hydrochloride and kernel oil: a - decrease in the size of seminiferous tubules, atrophy of the spermatogenic epithelium, protein infiltration of the interstitial stroma (x100); b - nesting destruction of germ cells (x250). Hematoxylin-eosin.

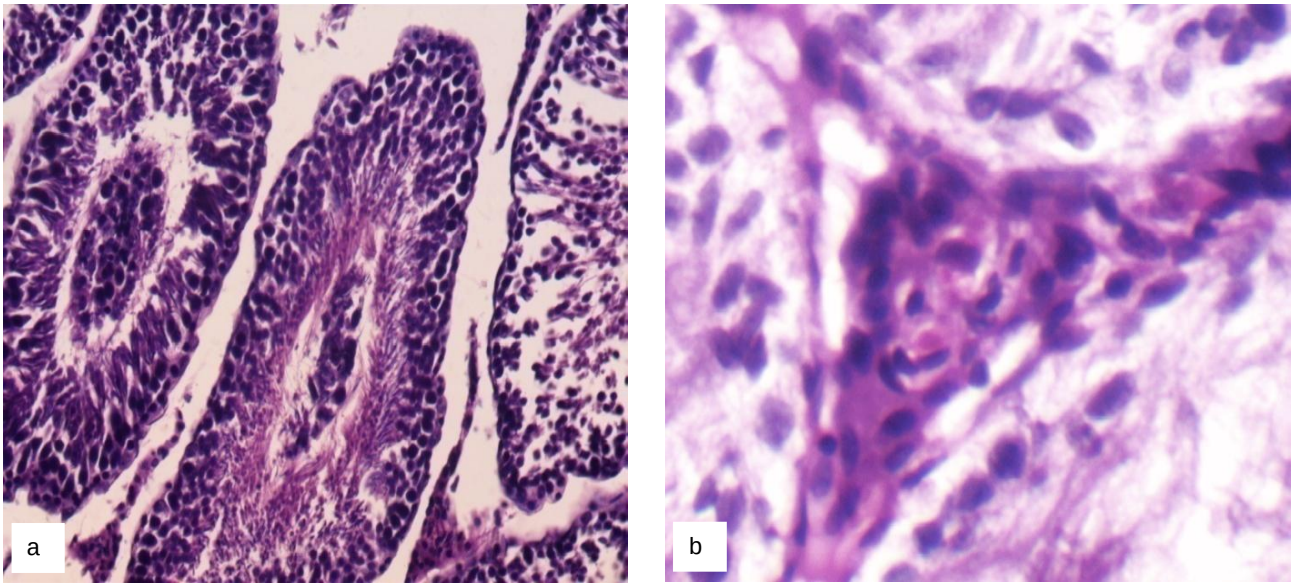

Fig. 7. Testes of rats after administration of Serotonin hydrochloride and kernel oil: a - desquamation of the epithelium into the lumen of seminiferous tubules (x200); b - monomorphic, less active Leydig cells in the interstitial tissue (x400). Hematoxylin-eosin.

including the distribution of animals according to the severity of pathology (see Fig. 6, Fig. 7, Table 3).

After the administration of D_3 in rats with the development of pathology, an improvement in the morphological picture of testicular tissue was observed. Seminiferous T were visually of normal size and had a normal histological structure. The epitheliospermatogenic layer contained germ cells arranged in concentric rows according to their developmental stages (including spermatozoa). The number of T with metaphase of the second meiotic division was increased (see Fig. 8). Sertoli cells were visually unchanged. The population of Leydig cells appeared visually more heterogeneous than in the control animals. The majority of Leydig cells were activated, as evidenced by the presence of large round normochromic nuclei with distinct nucleoli. The cytoplasm of these cells had a larger volume (see Fig. 9). However, in all animals with fully restored spermatogenesis, there were areas of focal necrobiosis of germ cells, dystrophy of supporting cells specifically in the regions of destruction (see Fig. 10), reduction of germ cell rows, layer disorganization, epithelial desquamation, and the presence of few cell

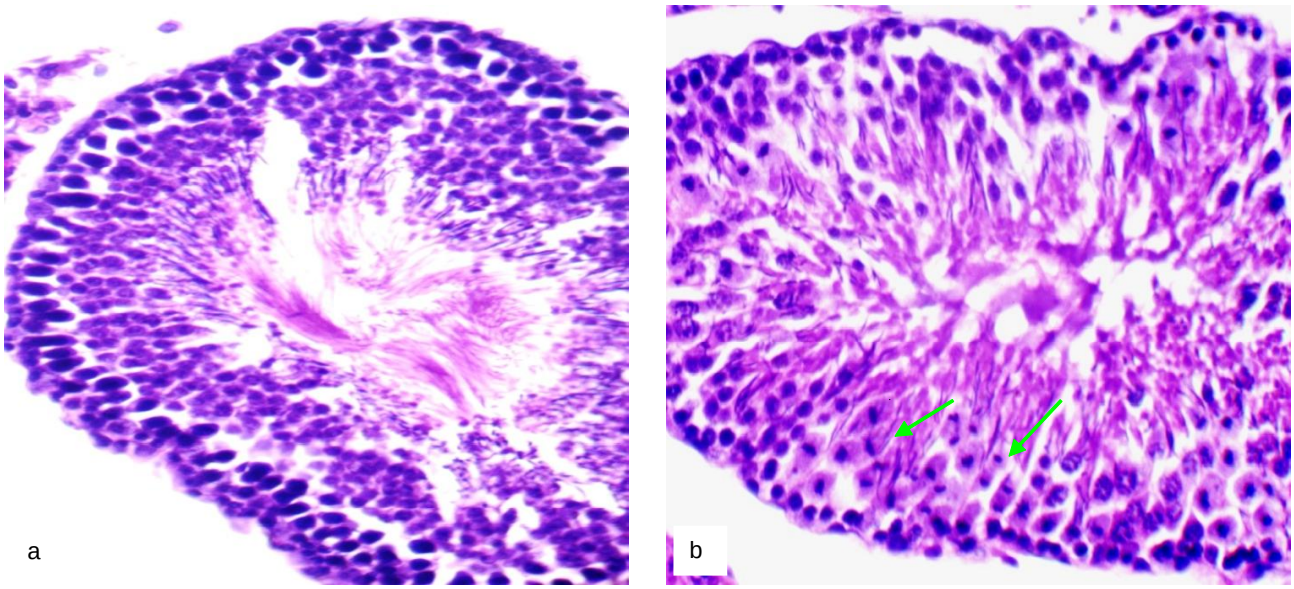

Fig. 8. The testes of rats after administration of Serotonin hydrochloride and vitamin D_3: a - a complete pool of germ cells in the seminiferous tubule (x200); b - numerous secondary spermatocytes in the metaphase of the second division (x250). Hematoxylin-eosin.

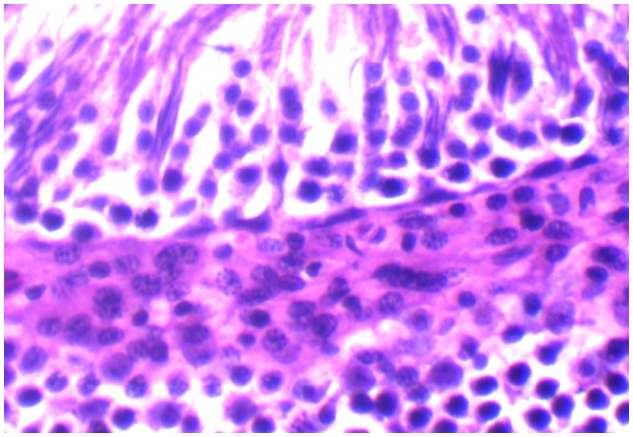

Fig. 9. The testes of rats after administration of Serotonin hydrochloride and vitamin D_3. The majority of Leydig cells are in an active functional state. Hematoxylin-eosin. x400.

clusters (see Fig.11). The severity of these impairments varied among different males within the group, but overall, they were more pronounced in animals from the EGP group, as confirmed morphometrically: the quantitative indicators of spermatogenesis improved after D_3 administration compared to rats with S-GP, although they did not reach the levels of intact control. For instance, the number of normal spermatogonia in the seminiferous tubules increased by 2.1 times. As a result, a significantly greater number of secondary spermatocytes were able to undergo division, and the number of tubules with the 12th stage of meiosis increased. The spermatogenesis index increased by 1.95 times (see Table 2).

The reference drug Tr, administered following a similar scheme, exerted a sufficiently pronounced positive effect on the state of the testicular tissue in rats with EGP. In 50 % of the animals, cross-sections of the seminiferous tubules

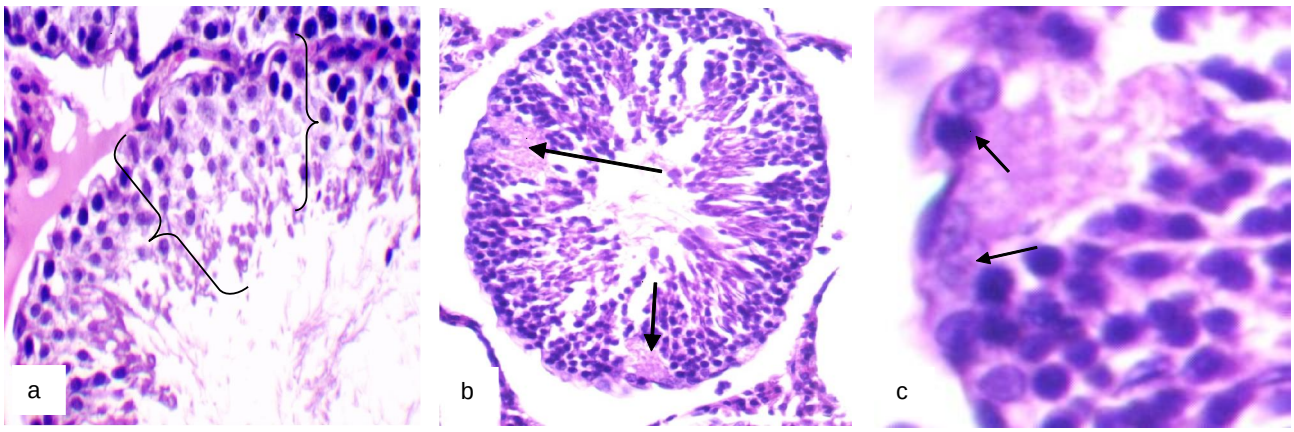

Fig. 10. The testes of rats after administration of Serotonin hydrochloride and vitamin D_3. Varying degrees of destruction of germ cells at various stages of development in the seminiferous tubules (a - b, x250, x200), dystrophy of Sertoli cells in the area of epithelial destruction (c, x400). Hematoxylin-eosin.

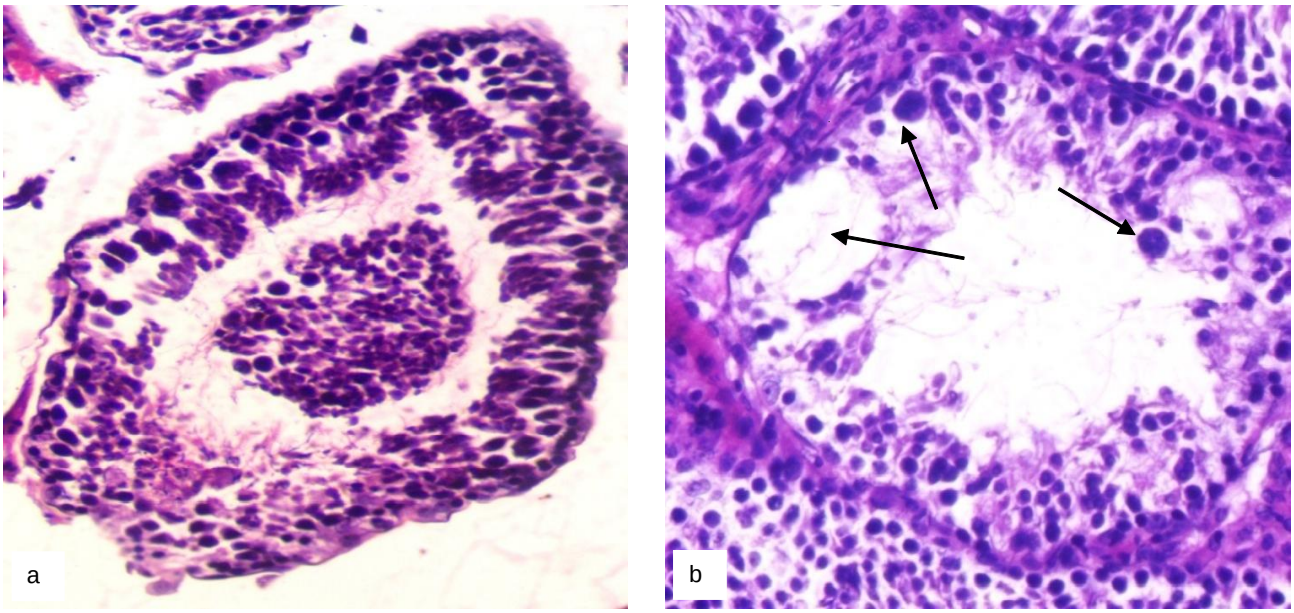

Fig. 11. The testes of rats after administration of Serotonin hydrochloride and vitamin D_3: a - desquamation of epithelium, focal layering of cell layers; b - focal reduction of germ cell rows, syncytia. Hematoxylin-eosin. x250.

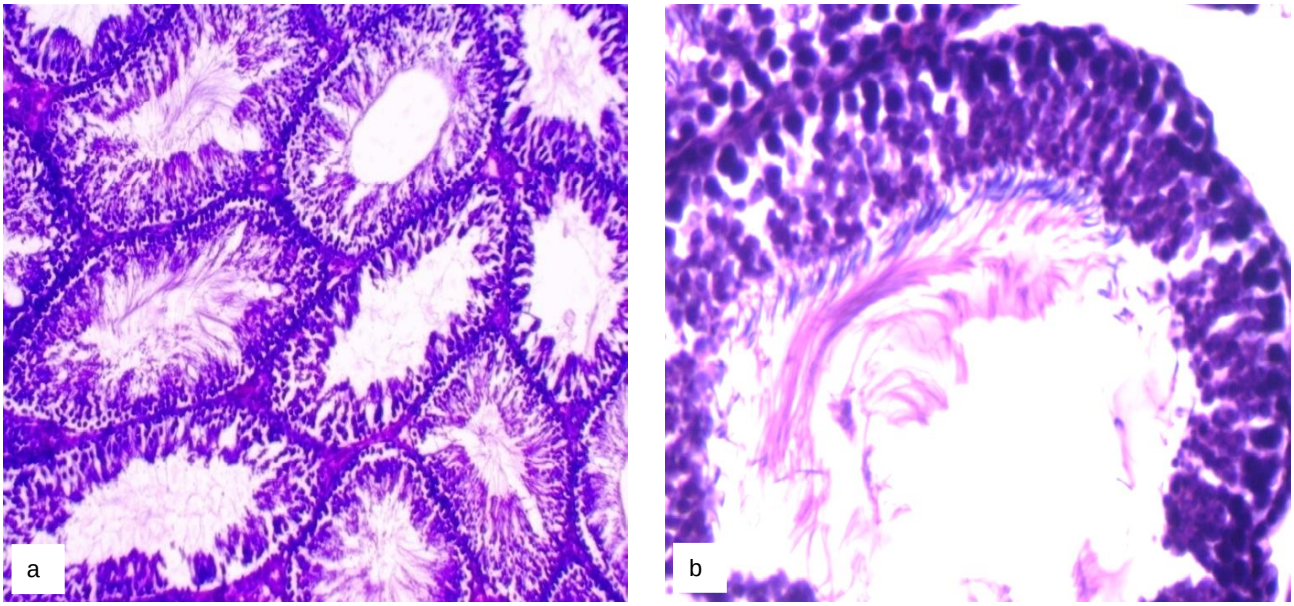

Fig. 12. Rat testis after Tribestan administration in combination with Serotonin hydrochloride: a - the normal state of seminiferous tubules (x200); b - the full spectrum of germ cells (x250). Hematoxylin-eosin.

revealed an unchanged strip of the spermatogenic epithelium, characterized by its width, organization, and completeness of the represented pool of germ cells.

In the rest of the rats, seminiferous tubules of varying number with areas of epithelial disorganization were found, reduction in rows of germ cells, and their stratification. The typical combination of different cell types was not disrupted (Fig. 12).

The areas varied in size, clearly showing a decrease in the number of spermatogonia. The nuclei of Sertoli cells acquired a rounded shape, with displaced nuclei (Fig. 13). The glandular cells varied in number, size, and nuclear status, with an increased presence of inactive forms in rats with changes (Fig.14).

The quantitative indicators of spermatogenesis after administration of Tr overall confirmed the visual assessment of the testicular tissue condition: the number of normal spermatogonia was significantly increased compared to the pathological control, there was an increased meiotic activity in the seminiferous tubules, minimal epithelial desquamation was observed, and the spermatogenesis index was increased. However, all these indicators did not reach the level of intact control (see Table 2).

The administration of a combination of vitamin D_3 and

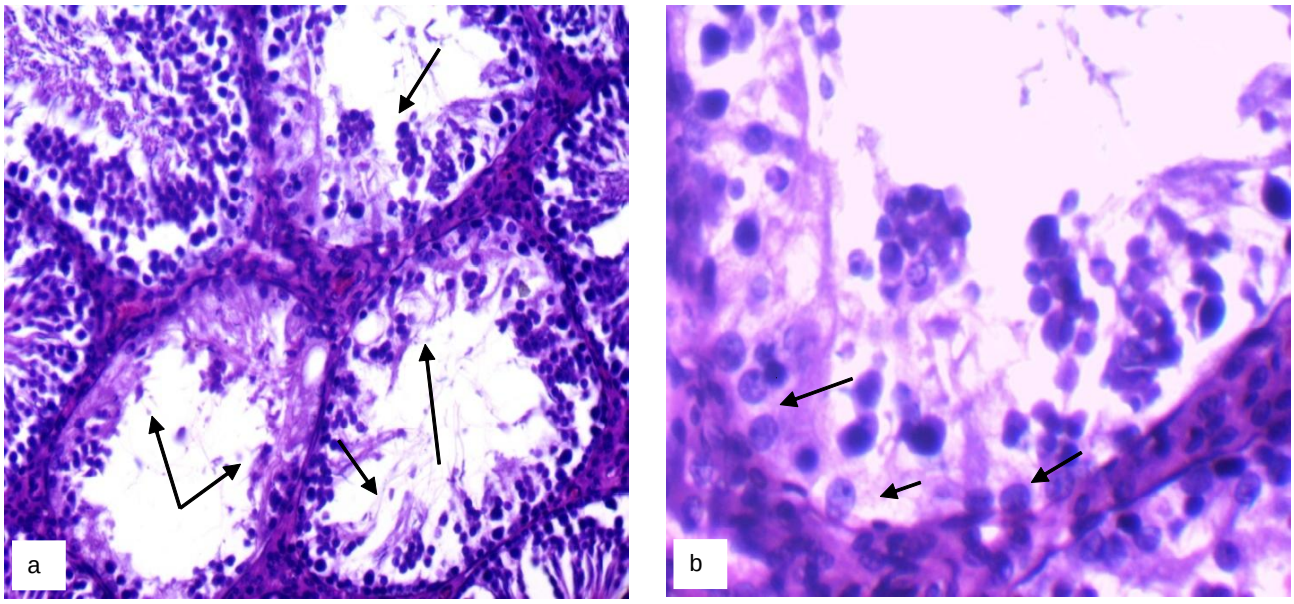

Fig. 13. Rat testis after Tribestan administration in combination with Serotonin hydrochloride: a - necrobiosis of germ cells, reduction of rows, the appearance of "windows" in the epitheliospermatogenic layer of the tubules (x250); b - dystrophic changes in Sertoli cells (x400). Hematoxylin-eosin.

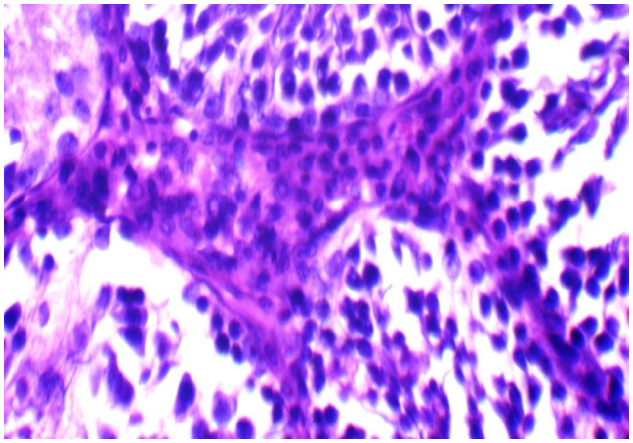

Fig. 14. Rat testis after Tribestan administration in combination with Serotonin hydrochloride. Increase in inactive forms of Leydig cells in the interstitial space. Hematoxylin-eosin. x250.

Tr on the background of EGP potentiates the positive effect of each component when used alone. In all 100 % of rats, the microscopic condition of the testicular tissue was completely restored. The size of the seminiferous tubules, the width of the epithelial spermatogenic layer, the presence of germ cells, their arrangement, and the typical combination of cell types corresponded to the norm. Seminiferous tubules with spermatogenic cells showing dystrophic changes or in a state of necrobiosis were not observed in all animals, and they were sporadic (see Fig. 15). There were no visually identifiable changes in Sertoli cells (see Fig. 16).

Leydig cells and quantitative characteristics of spermatogenesis have been restored nearly to the intact level in these rats (see Table 2).

As for the level of androgen saturation in their organisms, in all rats of this group, the "fern leaf" pattern has been practically fully restored. Only small areas with contracted, reduced branching, and increased angle of departure from the main stem have remained. The evaluation of the pattern was 2.67 points (see Table 3).

Discussion

Summarizing the obtained results, the following observations can be made: long-term administration of Serotonin hydrochloride in a dose of 3 mg/kg leads to the development of gonadopathy, accompanied by a decrease in the mass of testes, their appendages, and the ventral part of the prostate gland, and the occurrence of pathological changes in the testicular tissue of rats, characterized by destructive alterations of Sertoli cells (which are responsible for nourishing the germ cells [20]), varying degrees of destruction of seminiferous tubules, dystrophy and necrobiosis of germ cells, as a result, the spermatogenesis is suppressed, including a reduction in the number of stem cells (spermatogonia), delayed differentiation of germ cells (spermatids ® spermatozoa), and a decrease in the spermatogenic index. The obtained results are supported by the literature data on the histological structure of the testes and the submicroscopic architecture of Sertoli cells after the use of Serotonin hydrochloride [6, 26]. Under the influence of Serotonin hydrochloride, the number of activated hormone-producing Leydig cells decreases, as observed in our study and reported in the literature, which leads to a decrease in the androgen status of the animals' bodies, and is confirmed not only indirectly by the test of crystallization of the prostate gland secretion (see Table 3) but also by a decrease in the

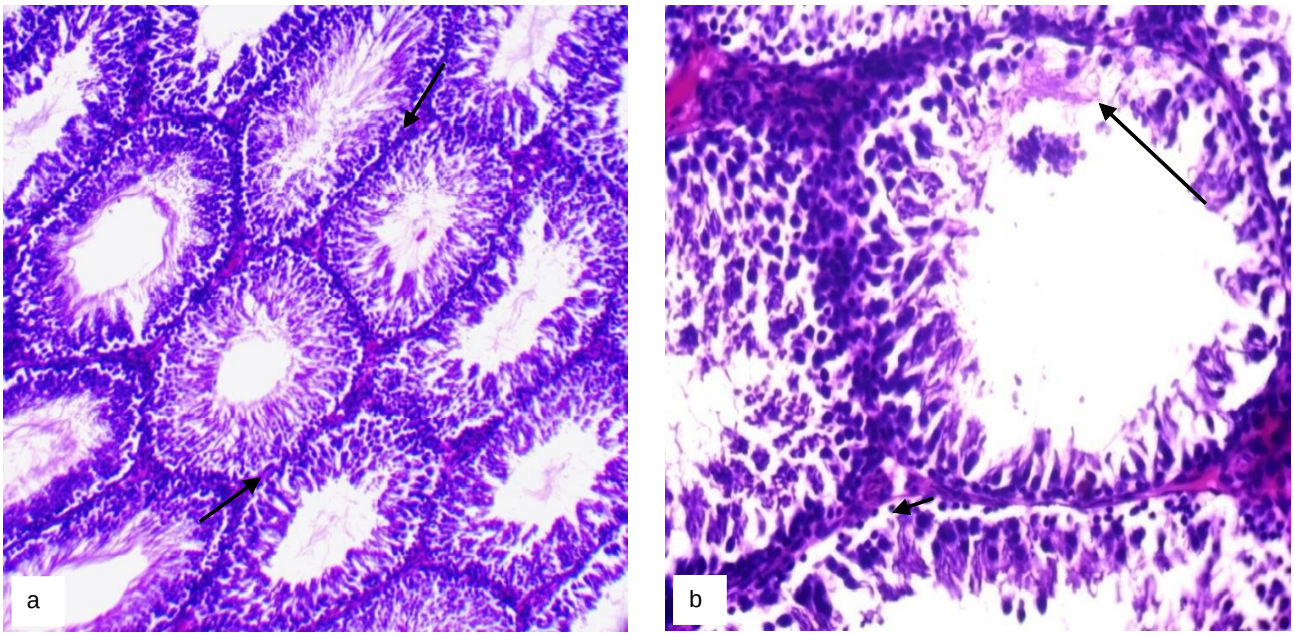

Fig. 15. Rat testis after administration of a combination of vitamin D_3 and Tribestan on the background of Serotonin hydrochloride: a - normal state of testicular tissue (x100); b - individual seminiferous tubule with focal destruction of germ cells (x200). Hematoxylin-eosin.

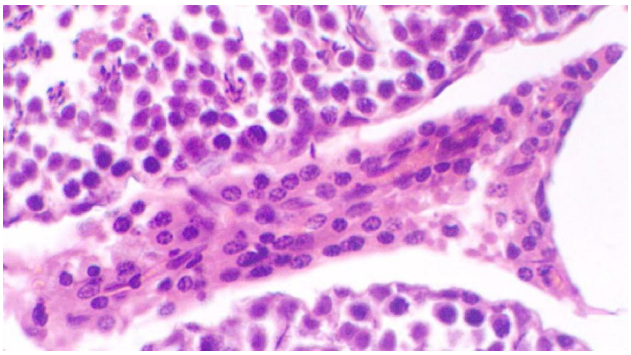

Fig. 16. Rat testis after administration of a combination of vitamin D_3 and Tribestan on the background of Serotonin hydrochloride. Prevalence of active forms of Leydig cells. Hematoxylin-eosin. x400.

level of male sex hormone associated with experimental gonadopathy [4].

The administration of vitamin D_3 does not affect the mass indicators of the reproductive organs. However, in the gonads of animals in this group, the number of normal spermatogonia increases, the percentage of seminiferous tubules with exfoliated epithelium decreases compared to the pathology but does not reach the level of intact animals, while the percentage of tubules in the 12th stage of meiosis and the spermatogenesis index normalize. After the administration of cholecalciferol in EGP, the condition of Sertoli cells improves, which patently contributes to the improvement of trophic support for germ cells, resulting in reduced dystrophic and destructive manifestations in germ cells during growth and differentiation, which in turn leads to increased reserve of spermiogenesis, an elevated spermatogenesis index, and noticeable activation of hormone-producing Leydig cells, which is the most likely cause of an increase in the androgen status of the animals' bodies [6]. In terms of the positive effects on the morphological state of the testes, spermatogenesis in the gonads, and the androgen status of the organism, vitamin D_3 when administered separately, is practically equal to the reference drug Tr, and when used in combination with the investigated preparations, the effect is potentiated. Positive changes in the morphological structure of the rat testes, observed in the group receiving combined correction ($S+D_3+Tr$), contribute to the increase in the level of spermatogenesis [24] and improvement of the reproductive potential of animals with Serotonin-induced gonadopathy.

Conclusion

1. Modeling testicular hypofunction using Serotonin hydrochloride leads to the development of pathological changes in the testicular tissue of rats. Histological examination of the testes reveals a significant reduction in the size of seminiferous tubules, thickening and swelling of their tunica propria. Sertoli cells are frequently destructively altered, and the uniformity of their arrangement is disrupted. The interstitial stroma is abundantly infiltrated with proteinaceous exudate. A decrease in the weight of the testes, epididymides, and prostate gland is observed compared to intact rats, along with hypoandrogenization and a decrease in all indicators of the spermatogenesis process.

2. After the administration of D_3 in the presence of pathological changes, an improvement in the morphological picture of the testicular tissue was noted. The seminiferous tubules exhibited a normal histological

structure. The epitheliospermatogenic layer contained germ cells arranged in concentric rows according to their developmental stages, including spermatozoa. The number of tubules with metaphase of the second division of maturation was increased, and Sertoli cells appeared visually unchanged. The population of Leydig cells was visually more heterogeneous than in control animals. The majority of Leydig cells were activated, as indicated by the presence of large round normochromic nuclei with distinct nucleoli. However, in all animals, alongside tubules with fully restored spermatogenesis, there were also tubules showing focal necrobiosis of germ cells and Sertoli cell dystrophy, accompanied by a reduction in the germ cell rows. Overall, the quantitative indicators of spermatogenesis improved after the administration of D_3 compared to rats with experimental gonadopathy, although they did not reach the levels of the intact control. The weight of the reproductive organs did not differ from the measurements of animals with pathology.

3. The reference drug, when administered according to a similar scheme, had a pronounced positive effect on the state of the testicular tissue in rats with experimental gonadopathy. In 50 % of the animals, cross-sections of the seminiferous tubules showed an unchanged strip of spermatogenic epithelium in terms of width, organization, and completeness of the represented pool of germ cells. The quantitative parameters of spermatogenesis in the tubules increased compared to rats with pathology, and the spermatogenic index in the gonads normalized. The typical combination of different cell types remained intact. Under conditions of Serotonin-induced gonadopathy in rats, the weight of the testes and epididymides normalized, and the weight of the prostate gland was equal to that in rats with pathology.

4. The combined use of vitamin D_3 together with Tribestan in experimental Serotonin-induced gonadopathy is accompanied by the normalization of gonad and appendage weights, it reduces histological manifestations of dystrophic and destructive changes in germ cells during growth and differentiation, improves the relative level of androgen status in the body, and has a positive effect on spermatogenesis in the gonads. Correction of Serotonin-induced gonadopathy with a combination of vitamin D3 and Tribestan yields better results than using either of the mentioned components alone.

References

[1] Aquila, S., Guido, C., Middea, E., Perrotta, I., Bruno, R., Pellegrino, M., & Ando, S. (2009). Human male gamete endocrinology: 1α,25-dihydroxyvitamin D3 (1,25(OH)$_2$D$_3$) regulates different aspects of human sperm biology and metabolism. *Reproductive Biology and Endocrinology*, 7, 1-13. doi: 10.1186/1477-7827-7-140

[2] Bahriy, M. M., Dibrova, V. A., Popadynets, O. H., & Hryshchuk, M. I. (2016). *Методики морфологічних досліджень: Монографія [Methods of morphological research: Monograph].* Вінниця: Нова книга - Vinnytsya: A new book.

[3] Barylyak, I. R., Neumerzhyts'ka, L. V., Byshovets', T. F., & Danylenko, V. S. (2000). *Вивчення гонадотоксичної дії нових лікарських засобів та їх впливу на репродуктивну функцію тварин. Методичні рекомендації [Study of gonadotoxic effects of new drugs and their effects on reproductive function of animals. Guidelines].* Київ: Авіцена - Kyiv: Avicenna.

[4] Bielkina, I., Velychko, N., Marakhovskyi, I., Korenieva, Y., Smolienko, N., Chystiakova, E., ... & Bondarenko, V. (2023). The impact of cholecalciferol on the sex hormones level and serum biochemical indices in rat males with experimental gonadopathy. *Problems of Endocrine Pathology,* 80(1), 54-63. doi: 10.21856/j-PEP.2023.1.07

[5] Brechka, N. M. (2019). Показники гормонального статусу самців щурів після застосування препаратів природного походження в умовах доброякісної гіперплазії передміхурової залози [Indicators of the hormonal status of male rats after the use of drugs of natural origin in conditions of benign prostatic hyperplasia]. *Український журнал медицини, біології та спорту - Ukrainian Journal of Medicine, Biology and Sports,* 4(5), 325-331. doi: 10.26693/jmbs04.05.325

[6] Brechka, N. M., Nevzorov, V. P., Bondarenko, V. A., Malova, N. G., & Selyukova, N. Yu. (2015) Дослідження субмікроскопічної архітектоніки клітин Сертолі й Лейдіга після впливу гідрохлориду серотоніну та можливості корекції метаботропними засобами [Investigation of the submicroscopic architectonics of Sertoli and Leydig cells after exposure to Serotonin hydrochloride and the possibility of correction with metabotropic agents]. *Фізіологічний журнал - Physiological Journal,* 61(4), 93-99. doi: 10.15407/fz61.04.085

[7] Chen, Y., & Zhi, X. (2020). Roles of vitamin D in reproductive systems and assisted reproductive technology. *Endocrinology,* 161(4). doi: 10.1210/endocr/bqaa023

[8] Ciccone, I. M., Costa, E. M., Pariz, J. R., Teixeira, T. A., Drevet, J. R., Gharagozloo, P., ... & Hallak, J. (2021). Serum vitamin D content is associated with semen parameters and serum testosterone levels in men. *Asian Journal of Andrology,* 23(1), 52. doi: 10.4103/aja.aja_9_20

[9] Crafa, A., Calogero, A. E., Cannarella, R., Mongioi', L. M., Condorelli, R. A., Greco, E. A., ... & La Vignera, S. (2021). The burden of hormonal disorders: a worldwide overview with a particular look in Italy. *Frontiers in Endocrinology,* 12, 694325. doi: 10.3389/fendo.2021.694325

[10] Elrashidy, R. A., Zakaria, E. M., Elmaghraby, A. M., Abd El Aziz, R. E., Abdelgalil, R. M., Megahed, R. M., ... & Ibrahim, S. E. (2022). Linagliptin and Vitamin D3 Synergistically Rescue Testicular Steroidogenesis and Spermatogenesis in Cisplatin-Exposed Rats: The Crosstalk of Endoplasmic Reticulum Stress with NF-kB/iNOS Activation. *Molecules*, 27(21), 7299. doi: 10.3390/molecules27217299

[11] Fu, L., Chen, Y. H., Xu, S., Ji, Y. L., Zhang, C., Wang, H., ... & Xu, D. X. (2017). Vitamin D deficiency impairs testicular development and spermatogenesis in mice. *Reproductive Toxicology,* 73, 241-249. doi: 10.1016/j.reprotox.2017.06.047

[12] Hirai, T., Tsujimura, A., Ueda, T., Fujita, K., Matsuoka, Y., Takao, T., ... & Okuyama, A. (2009). Effect of 1,25-dihydroxyvitamin D on testicular morphology and gene expression in experimental cryptorchid mouse: testis specific cDNA microarray analysis and potential implication in male infertility. *The Journal of urology,* 181(3), 1487-1492. doi: 10.1016/

j.juro.2008.11.007

[13] Horpynchenko, I. I., Hurzhenko, Yu. M., & Imshynets'ka, L. P. (2019). Надання медичної допомоги хворим з чоловічим фактором безпліддя подружньої пари [Providing medical care to patients with a male infertility factor in a married couple]. *Здоровье мужчины - Men's Health*, (2), 23-35. doi: 10.30841/2307-5090.2.2019.179446

[14] Jeremy, M., Gurusubramanian, G., & Roy, V. K. (2019). Vitamin D3 mediated regulation of steroidogenesis mitigates testicular activity in an aged rat model. *The Journal of Steroid Biochemistry and Molecular Biology,* 190, 64-75. doi: 10.1016/j.jsbmb.2019.03.016

[15] Kozhemiakin, Yu. M., Khromov, O. S., Filonenko, M. A., & Saifetdinova, G. A. (2002). *Науково-практичні рекомендації з утримання лабораторних тварин та роботи з ними [Scientific and Practical Recommendations for Keeping Laboratory Animals and Working with Them].* Київ: Авіцена - Kyiv: Avicenna.

[16] Lapach, S. N., Gubenko, A. V., & Babich, P. N. (2000). *Статистические методы в медико-биологических исследованиях с использованием Excel [Statistical Methods in Biomedical Research Using Excel].* Киев: Морион - Kiev: Morion.

[17] Livingston, M., Kalansooriya, A., Hartland, A. J., Ramachandran, S., & Heald, A. (2017). Serum testosterone levels in male hypogonadism: Why and when to check - A review. *International Journal of Clinical Practice,* 71(11), e12995. doi: 10.1111/ijcp.12995

[18] Maghsoumi-Norouzabad, L., Zare Javid, A., Mansoori, A., Dadfar, M., & Serajian, A. (2021). The effects of Vitamin D3 supplementation on Spermatogram and endocrine factors in asthenozoospermia infertile men: a randomized, triple blind, placebo-controlled clinical trial. *Reproductive Biology and Endocrinology,* 19(1), 1-16. doi: 10.1186/s12958-021-00789-y

[19] Nasreen, K., Ishrat, S., Banu, J., Fatima, P., Ansary, S. A., Jahan, I., ... & Islam, M. K. (2021). Comparison of vitamin D (25OHD) status between fertile and infertile men. *International Journal of Reproduction, Contraception, Obstetrics and Gynecology,* 10(4), 1303-1310. doi: 10.18203/2320-1770.ijrcog20211104

[20] O'Shaughnessy, P. J. (2014). Hormonal control of germ cell development and spermatogenesis. In *Seminars in Cell & Developmental Biology*, 29, 65. doi: 10.1016/j.semcdb.2014.02.010

[21] Ostrovska, S. S., Abramov, S. V., Pisarevska, I. A., Trushenko, O. S., Zherzhova, T. A., Pervysherst, K. Yu., ... & Zakharyev, A. V. (2021). Токсичний вплив кадмію на репродуктивну функцію чоловіків [Toxic effect of cadmium on male reproductive function]. *Український журнал медицини, біології та спорту - Ukrainian Journal of Medicine, Biology and Sports,* 6(6/34), 275-281. doi: 10.26693/jmbs06.06.275

[22] Punab, M., Poolamets, O., Paju, P., Vihljajev, V., Pomm, K., Ladva, R., ... & Laan, M. (2017). Causes of male infertility: a 9-year prospective monocentre study on 1737 patients with reduced total sperm counts. *Human Reproduction*, 32(1), 18-31. doi: 10.1093/humrep/dew284

[23] Reznikov, O. H. (2003). Загальні етичні принципи експериментів на тваринах [General ethical principles of animal experiments]. *Ендокринологія - Endocrinology,* 8(1), 142-145.

[24] Smolienko, N. P., Korenieva, E. M., Marakhovskyi, I. O., Chistyakova, E. E., Velichko, N. F., Bielkina, I. O., & Bondarenko, V. O. (2022). Статева поведінка самців щурів із гонадопатією після корекції вітаміном D3 та Трібестаном [Sexual behavior of male rats with gonadopathy after correction with vitamin D3 and Tribestan]. *Вісник проблем біології і медицини - Herald of Problems of Biology and Medicine,* 2(1/164), 240-248. doi: 10.29254/2077-4214-2022-2-1-164-240-248

[25] World Health Organization. (2018). International Classification of Diseases, 11th Revision (ICD-11). Geneva: Switzerland.

[26] Zaichenko, H. V., Yakovleva, L. V., Butenko, I. G., & Laryanovskaya, Yu. B. (2008). Вплив глюкозаміну гідрохлориду на сперматогенез щурів при його порушенні серотоніном [Effect of glucosamine hydrochloride on spermatogenesis in rats when it is disturbed by Serotonin]. *Фармакологія та лікарська токсикологія - Pharmacology and Medicinal Toxicology,* 1(3), 74-79.

МОРФОЛОГІЧНА БУДОВА СІМ'ЯНИКІВ ЗА УМОВ ЕКСПЕРИМЕНТАЛЬНОЇ ГОНАДОПАТІЇ ТА ПІСЛЯ ЗАСТОСУВАННЯ ХОЛЕКАЛЬЦИФЕРОЛУ У КОМПЛЕКСНИХ СХЕМАХ КОРЕКЦІЇ

Мараховський І. О., Коренєва Є. М., Лар'яновська Ю. Б., Смолєнко Н. П., Бєлкіна І. О., Величко Н. Ф., Чистякова Е. Є., Місюра К. В., Бондаренко В. О.

Проблема чоловічого безпліддя є актуальною та потребує вирішення. Застосування вітаміну D_3 (віт. D_3) у схемах лікування безпліддя може позитивно впливати на репродуктивну здатність особин чоловічої статі. Мета даного дослідження - визначити вплив вітаміну D_3, застосованого самостійно або разом із препаратом, що містить екстракт якірців сланких, на зміни гістологічної картини морфологічної будови сім'яників щурів із експериментальною гонадопатією. Самців щурів зі змодельованою патологією репродуктивної функції (серотоніновою гонадопатією) розподіляли на групи, котрі отримували корекцію за допомогою холекальциферолу окремо або разом із референтним препаратом Трібестаном (Тр), що містить екстракт якірців сланких. На зрізах сім'яників (забарвлення гематоксиліном та еозином) окрім оглядової мікроскопії проводили морфометричну оцінку сперматогенезу. Статистичну обробку проводили в стандартному пакеті програм "Statistica 6.0" з використанням t-критерію Стьюдента та непараметричного аналогу однофакторного дисперсійного аналізу - критерій Краскела-Уоліса, після чого застосовували критерій Мана-Уітні. Встановлено, що сім'яні канальці сім'яників щурів зі серотоніновою гонадопатією виразно зменшені у розмірі, власна їхня оболонка потовщена. Клітини Сертолі часто деструктивно змінені, порушена рівномірність їх розташування. Спостерігалось зниження маси гонад, над'ячка, передміхурової залози та гіпоандрогенізація, знижувалися показники сперматогенезу. Після введення на тлі патології вітаміну D_3 відмічалось покращення морфологічної картини гонад. Сім'яні канальці мали нормальну гістологічну структуру. Статеві клітини розташовувалися концентричними рядами у відповідності до стадій розвитку, клітини Сертолі візуально були незміненими. Популяція клітин Лейдига візуально більш гетерогенна, ніж у контрольних тварин. Однак, іноді виявлялися сім'яні канальці з вогнищевим некробіозом статевих клітин та дистрофією клітин Сертолі, редукцією рядів статевих клітин. В цілому кількісні показники процесу сперматогенезу після введення вітаміну D_3 покращилися порівняно зі щурами з експериментальною гонадопатією, хоча і не досягали показників інтактного контролю. Введення на тлі гонадопатії комбінації

вітаміну D_3 та Трібестану потенціювало позитивний ефект кожного з компонентів при монозастосуванні. У щурів повністю відновлено мікроскопічний стан тестикулярної тканини. Сумісне використання вітаміну D_3 з препаратом Трібестаном нормалізувало масу гонад, їхніх придатків, значно зменшувало на гістологічних зрізах дистрофічно-деструктивні прояви у статевих клітинах у період росту і диференціювання, покращувало відносний рівень андрогенного статусу організму, позитивно впливало на сперматогенез у гонадах. Таким чином, нами встановлено, що комбіноване використання холекальциферолу та препарату Трібестан для корекції експериментальної гонадопатії проявляло більш ефективну дію, ніж використання одного із зазначених компонентів.

Ключові слова: *гістологічна будова сім'яника, гонадопатія, вітамін D, холекальциферол, сперматогенез.*

REQUIREMENTS FOR ARTICLES

For publication, scientific articles are accepted only in English only with translation on Ukrainian, which contain the following necessary elements: UDC code; title of the article (in English and Ukrainian); surname, name and patronymic of the authors (in English and Ukrainian); the official name of the organization (institution) (in English and Ukrainian); city, country (in English and Ukrainian); structured annotations (in English and Ukrainian); keywords (in English and Ukrainian); introduction; purpose; materials and methods of research; research results; discussion; conclusions; bibliographic references.

The title of the article briefly reflects its contents and contains no more than 15 words.

Abstract. The volume of the annotation is 1800-2500 characters without spaces. The text of an annotation in one paragraph should not contain general phrases, display the main content of the article and be structured. The abstract should contain an introductory sentence reflecting the relevance of the study, the purpose of the study, a brief description of the methods of conducting research (2-3 sentences with the mandatory provision of the applied statistical methods), a description of the main results (50-70% of the volume of the abstract) and a concise conclusion (1 sentence). The abstract should be clear without familiarizing the main content of the article. Use the following expressions: "Detected ...", "Installed ...", "Fixed ...", "Impact assessed ...", "Characterized by regularities ...", etc. In an annotation, use an active rather than passive state.

Keywords: 4-6 words (or phrases).

"Introduction"

The introduction reflects the state of research and the relevance of the problem according to the world scientific literature (at least 15 references to English articles in international journals over the past 5 years). At the end of the entry, the purpose of the article is formulated (contains no more than 2-3 sentences, in which the problem or hypothesis is addressed, which is solved by the author).

"Materials and methods"

The section should allow other researchers to perform similar studies and check the results obtained by the author. If necessary, this section may be divided into subdivisions. Depending on the research objects, the ethical principles of the European Convention for the protection of vertebrate animals must be observed; Helsinki Declaration; informed consent of the surveyed, etc. (for more details, see "Public Ethics and its Conflict"). At the end of this section, a "statistical processing of results" section is required, which specifies the program and methods for processing the results obtained by the automobile.

"Results"

Requirements for writing this section are general, as well as for all international scientific publications. The data is presented clearly, in the form of short descriptions, and must be illustrated by color graphics (no more than 4) or drawings (no more than 8) and tables (no more than 4), the information is not duplicated.

"Discussion"

In the discussion, it is necessary to summarize and analyze the results, as possible, compare them with the data of other researchers. It is necessary to highlight the novelty and possible theoretical or practical significance of the results of the research. You should not repeat the information already listed in the "Introduction" section. At the end of the discussion, a separate paragraph should reflect the prospects for using the results obtained by the author.

"Conclusion"

5-10 sentences that summarize the work done (in the form of paragraphs or solid text).

"Acknowlegements"

Submitted after conclusion before bibliographic references.

"References"

References in the text are indicated by Arabic numerals in square brackets according to the numerology in the list of references. The list of references (made without abbreviations) sorted by alphabet, in accordance with the requirements of APA Style (American Psychological Association Style): with the obligatory referencing of all authors, work titles, journal names, or books (with obligatory publication by the publishing house, and editors when they are available), therefore, numbers or releases and pages. In the Cyrillic alphabets references, give the author's surnames and initials in English (Cyrillic alphabet in brackets), the title of the article or book, and the name of the magazine or the publisher first to be submitted in the original language of the article, and then in square brackets in English. If available, doi indexes must be provided on www.crossref.org (at least 80% of the bibliographic references must have their own doi indexes). Links to online publications, abstracts and dissertations are not welcome.

After the list of references, it is necessary to provide information about all authors (in English, Ukrainian and Russian): last name, first name and patronymic of the author, degree, place of work and position, **ORCID number** (each of the authors of the ORCID personal number if absence - free creation on the official website http://www.orcid.org) to facilitate the readers of this article to refer to your publications in other scientific publications.

The last page of the text should include the surname, name and patronymic of the author, degree, postal address, telephone number and e-mail of the author, with which the editors will maintain contact.

Concluding remarks

The manuscript should be executed in such a way that the number of refinements and revisions during the editorial of the article was minimal.

When submitting the article, please observe the following requirements. The volume of the article - not less than 15 and not more than 25 pages, Times New Roman, 14 pt, line spacing - one and a half, fields - 2 cm, sheet A4. Text materials should be prepared in the MS Word editor (* .docx), without indentations. Math formulas and equations to prepare in the embedded editor; graphics - in MS Excel. Use the units of the International Measurement System. Tables and drawings must contain the name, be numbered, and references to them in the text should be presented as follows: (fig. 1), or (table 1). The drawings should be in the format "jpg" or "tif"; when scanned, the resolution should be at least 800 dpi; when scanning half-tone and color images, the resolution should be at least 300 dpi. All figures must be represented in the CMYK palette. The statistical and other details are given below the table in the notes. Table materials and drawings place at the end of the text of the manuscript. All elements of the text in images (charts, diagrams, diagrams) must have the Times New Roman headset.

Articles are sent to the editorial board only in electronic form (one file) at the e-mail address nila@vnmu.edu.ua

Responsible editor - Gunas Igor Valeryovich (phone number: + 38-067-121-00-05; e-mail: igor.v.gunas@gmail.com).

Signed for print 23.06.2023
Format 60x84/8. Printing offset. Order № 1107. Circulation 100.
Vinnytsia. Printing house “TVORY”, Nemyrivske shose St., 62a,
Vinnytsya, 21034
Phone: 0 (800) 33-00-90, (096) 97-30-934, (093) 89-13-852,
(098) 46-98-043
e-mail: tvory2009@gmail.com
http://www.tvoru.com.ua